Ryerson University
Digital Commons @ Ryerson

Theses and dissertations

1-1-2013

Techno-Economic Models For Integration Of Wind Energy

Chandrabhanu O.G. Kankanamalage
Ryerson University

Follow this and additional works at: http://digitalcommons.ryerson.ca/dissertations

 Part of the Electrical and Electronics Commons

Recommended Citation
Kankanamalage, Chandrabhanu O.G., "Techno-Economic Models For Integration Of Wind Energy" (2013). *Theses and dissertations.* Paper 2051.

This Thesis is brought to you for free and open access by Digital Commons @ Ryerson. It has been accepted for inclusion in Theses and dissertations by an authorized administrator of Digital Commons @ Ryerson. For more information, please contact bcameron@ryerson.ca.

TECHNO-ECONOMIC MODELS FOR INTEGRATION OF WIND ENERGY

By

Chandrabhanu Opathella Ganehi Kankanamalage

Bachelor of Science of Engineering, University of Moratuwa, Sri Lanka, 18 March 2004

Master of Engineering, Asian Institute of Technology, Thailand, 02 May 2008

A dissertation

presented to Ryerson University

in partial fulfillment of the

requirements for the degree of

Doctor of Philosophy

in the Program of

Electrical Engineering

Toronto, Ontario, Canada, 2013

©Chandrabhanu Opathella Ganehi Kankanamalage 2013

AUTHOR'S DECLARATION

I hereby declare that I am the sole author of this dissertation. This is a true copy of the dissertation, including any required final revisions, as accepted by my examiners.

I authorize Ryerson University to lend this dissertation to other institutions or individuals for the purpose of scholarly research.

I further authorize Ryerson University to reproduce this dissertation by photocopying or by other means, in total or in part, at the request of other institutions or individuals for the purpose of scholarly research.

I understand that my dissertation may be made electronically available to the public.

ABSTRACT

Dissertation Title: Techno-Economic Models for Integration of Wind Energy

Degree: Doctor of Philosophy

Year: 2013

Student Name: Chandrabhanu Opathella Ganehi Kankanamalage

Program: Electrical Engineering

University: Ryerson University

This thesis focusses on three specific areas of integrating wind energy with power systems: 1) technical modeling of wind generators for power flow analysis, 2) probabilistic modeling of wind generators for planning studies, and 3) economic modeling for integration of wind energy in electricity markets.

Wind generator output is a function of wind speed and 3-phase terminal voltages. Complete nonlinear three-phase models of wind generators are accurate but are computationally cumbersome and unsuitable for power flow analysis purposes. Intelligent models of wind generators are proposed for their accurate representation and use in power flow analysis algorithms. The main advantages of these intelligent models of wind generators are their mathematical simplicity, computational speed and numerical accuracy when the generators are connected to unbalanced three-phase distribution systems. These proposed intelligent models of wind generators were tested with the three-phase, unbalanced, IEEE 37-bus test system. The results show that the intelligent models of wind generators are computationally ten times faster than exact nonlinear models. In addition, simplicity of the proposed intelligent models of wind generators allows easy integration into commercial software such as PSS®E and PSS®SINCAL.

In the second study, a probabilistic model of wind generators was integrated with algorithm for distribution system analysis. The proposed probabilistic power flow analysis method for distribution systems takes into account the stochastic nature of wind generation and forecasted bus-wise peak load. Probability distribution functions for bus voltages are reconstructed. The proposed method is tested on a modified 70-bus distribution system and the results are reported.

Thirdly, an economic integration model for wind generators with electricity markets is proposed. The proposed model is in the form of a Wind Generators Cooperative (WGC). This proposed model overcomes challenges posed by uncertainty and intermittency of wind generation. The proposed cooperative model maximizes returns for wind generators by minimizing the effect of uncertainty by smoothing effect and using pumped-hydro facilities. A case study with actual data from Ontario (Canada) was completed. Analyses clearly demonstrate that the WGC increases returns to wind generators and reduces their exposure to uncertainty.

LIST OF PUBLICATIONS

1. C. Opathella, D. Cheng, B. N. Singh and B. Venkatesh, Intelligent Wind Generator Models for Power Flow Studies in PSS®E and PSS®SINCAL, IEEE Transactions on Power Systems, vol. 28, no. 02, pp. 1149-1150, May 2013.

2. C. Opathella, B. Venkatesh and A. Dukpa, Probabilistic Voltage Solution Method for Distribution Systems with Wind Electric Generators, The 9th International Power and Energy Conference (IPEC2010), pp. 220-223, Singapore, Oct. 2010.

3. C. Opathella and B. Venkatesh, Managing Uncertainty of Wind Energy With Wind Generators Cooperative, IEEE Transactions on Power Systems, Accepted for Future Publications (01 Dec. 2012).

ACKNOWLEDGEMENTS

I would like to express deep gratitude to Prof. Bala Venkatesh for his encouraging valuable advice throughout the period of study. Prof. Venkatesh was not only my supervisor but also a great inspiring friend during the last three and half years. Furthermore, he arranged all necessary financial assistance on time throughout the period of the study. Without his invaluable helps I would not have achieved this degree. My special thanks also go to Prof. B. N. Singh for his very important inputs for this dissertation. As a co-supervisor, his numerous inputs based on industrial expertise helped me to achieve this successful ending.

I would also like to thank Dr. Daniel Cheng and Dr. Alexandre Nassif for giving their important ideas and reviews. Their inputs helped to improve the quality of the research and publications.

Throughout the last three and half years Ryerson University and its staff provided me enormous support for the success of this thesis. I especially acknowledge the support given by Mr. Bruce Derwin and Ms. Lynda O'Malley. Without their valued support I could not have completed this thesis on schedule.

Because of the financial assistance provided by Hydro One Inc. and NSERC, this dissertation was completed successfully. Therefore I thank those organizations for their generous contributions.

I also recognize the moral support given by Dr. Andu Dukpa, Mr. Peng Yu, Mr. Reza Ghaffari, Dr. Travis Xu, Ms. Maryam Dadkhah, Mr. Kamran Masteri, Mr. Inderjeet Duggal, Mr. Inderpreet Singh, Mr. Inderdeep Singh and Mr. Amit Dadhania during last three and half years. Finally, I would like to thank my family members and various individuals and organizations whose names are not mentioned above for their various help.

TABLE OF CONTENTS

LIST OF TABLES

LIST OF FIGURES

LIST OF APPENDICES

Chapter 1

General Introduction

1.1 Introduction

Historically research in power systems is dominated by technological challenges in generation, transmission and distribution. Modern power system research focusses on a wider range of challenges as it relates to technology, as well as economics, environment and policy. The topics include electricity markets, smart grids, renewables, carbon foot print, etc. Interest in the last decade to reduce pollution has resulted in an impetus for renewables. This impetus has spurned research in wind energy for its technical and economic integration into power systems. A significant amount of research outcomes have been reported in literature. This thesis also attempts at solving techno-economic challenges in integration of wind generators with power systems.

1.1.1 Growth of Wind Energy

Wind energy is very attractive for several reasons. The most important is that it is a clean source of energy. Further, the cost of electricity generated from wind generators has decreased in the last few decades. The overall decreasing trend in cost is expected to continue during the next two decades [1]. These reasons have made wind energy one of the cheapest sources of renewable energy sources (Table 1.1). Rapid technological advancements such as variable speed wind generators, large turbine sizes, low wind speed operation capability, developments in offshore turbines, etc. have propelled a significant growth of wind electricity generation recorded in the past decade (Fig. 1.1). Further, this noticeable growth in wind energy was achieved with various economic incentives made available for wind power generation throughout the world.

Even though wind power penetration is increasing in many power systems, still in many markets, wind power has been shielded from true competition. As an example, Ontario (Canada) has a feed-in-tariff policy that gives wind generators a fixed price for their produced energy that is above the market rate, the average Hourly Ontario Energy Price (HOEP). Due to these favorable economic conditions, it is expected that considerable amounts of wind power will be connected to power systems in the future.

As wind energy becomes a significant portion of generation portfolio of power systems around the world, it would be expected that wind energy is competitively integrated into electricity markets and its technology is well tested. Significant research and development is required to address challenges associated with wind integration into the power system and achieve these aims.

Table 1.1. Levelized Costs of Electricity Generation of Renewable Energy Sources

Generation Technology	2010-2020 (2009 $ Per MWh)	2021-2035 (2009 $ Per MWh)
Hydro - large	94	95
Hydro - small	143	143
Biomass	131	126
Wind - onshore	85	65
Wind - offshore	101	74
Geothermal	52	46
Solar PV - large scale	280	157
Solar PV - buildings	406	217
Centralised solar power	207	156
Marine	281	187

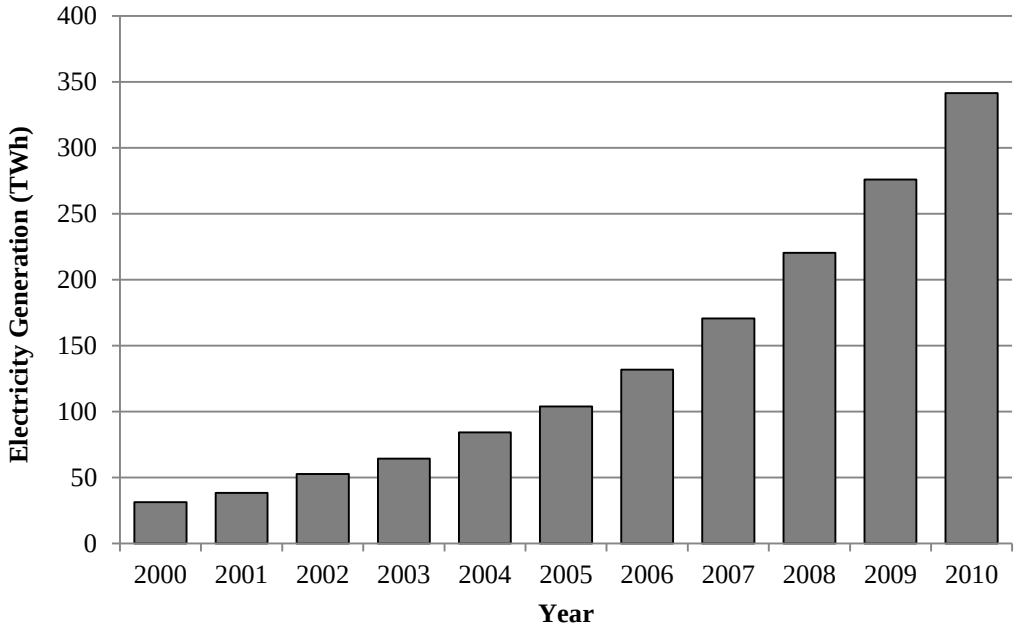

Fig. 1.1. Historical Trend of World Wind Electricity Generation [2]

1.1.2 Challenges of Wind Energy Integration

Wind energy integration into power systems creates a wide range of challenges. The key challenges include: 1) accurate modeling of wind generator in power flow analysis algorithms, 2) power system planning studies considering probabilistic behaviour of wind energy; 3) economic integration of wind energy in electricity markets with no subsidies. These three problems have been discussed in many recent research efforts.

Challenge 1: Technical Modeling

Unlike other conventional synchronous generators, variable speed wind generators are equipped with converters that mainly function to extract the maximum power from wind and supply the stipulated reactive power to the point of common coupling with the grid. It is common that simple models of wind generators assume balanced power output in power flow analysis. However, power output of wind generators are balanced only when terminal voltages are balanced.

North American distribution system lines are seldom transposed and hence distribution systems are inherently unbalanced. In addition, distribution systems are connected to several unbalanced loads. In these cases where distribution systems are unbalanced, accurate models of wind generators are required for accurate power flow analysis. In order to address these concerns, detailed research is being conducted to develop accurate models of wind generators for power flow analysis of distribution systems. A review of such studies is given later in this Chapter.

Challenge 2: Probabilistic Analysis Tool

Load forecasting and wind power prediction are critical for power system planning. Forecasters use complex models to predict wind power for long term planning studies

providing planners with statistical estimates of probable wind speeds and confidence values of such forecasts. Power systems analysis algorithms for planning studies consider such probabilistic information to compute probable line flows and bus voltages with corresponding confidence values. Probabilistic power flow is a key tool that has been used for several decades for this purpose. However, one might note that probabilistic distribution functions of long term load forecasts and long term wind speed forecasts are different. Hence their integration into algorithms for probabilistic power flow analysis becomes challenging. In this thesis, a survey of such methods is undertaken and then a discrete computing version of probabilistic power flow considering probabilistic distribution functions of both wind speeds and loads is proposed.

Challenge 3: Effective Integration of Wind Energy in Electricity Markets

Forecasted power output of wind generators are both uncertain and intermittent. Thus unlike other conventional power generation systems from fossil and nuclear fuels, wind energy is uncertain and intermittent. A power system requires an increased amount of reserves to counter this uncertainty and intermittency. These reserves are both for energy as well as for ramping capacity. These reserves should be able to react to ever changing wind power output. In the literature, technologies such as hydro power, pumped hydro power, flywheels, gas turbines, etc. are reported as fast reacting reserves. These reserves increase operating costs of power systems and hence should be investigated carefully. Therefore both uncertainty and variability of wind power output are widely discussed in literature in the context of power system planning.

In view of the above challenge, economic integration models for wind power with electricity market are investigated and a new model is proposed in this thesis.

1.2 Literature Review

This section of Chapter 1 reviews literature on various topics in relation to the three research objectives of this thesis as described later in Chapter 1.3. Reviews of wind generator models and distribution system power flow studies give background information for the first objective of this thesis. The necessary background information for the second objective is provided by a review of probabilistic models and probabilistic power flow studies. A review of strategies for economic integration of wind energy with electricity markets provides the required background for the third objective of this thesis.

1.2.1 Distribution System Power Flow Studies

Power flow analysis is used for planning, operation and control of the power systems. The results of power flow analysis consist of bus voltages magnitudes and phase angles, power flows in lines, and system losses. Several algorithms have been formulated to solve the bus power balance equations. The most popular ones are:

- Newton-Raphson Method Using Polar Coordinates
- Newton-Raphson Method Using Cartesian Coordinates
- Fast Decoupled Load Flow
- Ladder Iterative Technique
- Gauss-Seidel Method
- Jacobi Method
- Z-Matrix Method

Some of these algorithms are specific to radial distribution systems such as the ladder iterative technique. As mentioned in earlier sections of this chapter, the focus of research work reported in this thesis is to solve wind integration challenges in distribution systems and electricity markets. Therefore, further discussion on power flow studies is focused on distribution systems. The rest of the discussion presented here considers two types of power flow algorithms: (a) ladder iterative technique based algorithms, and, (b) network

matrices based algorithms. In both of these types of algorithms, radial topology of distribution systems is assumed. In the ladder iterative technique, bus-wise voltage computation or branch-wise power flow computation is performed in an orderly sequence following the radial topology of the network configuration. On the other hand, in network matrix based algorithms the radial topology of the distribution system is captured in network matrices. Therefore once the network matrices are formed, the solution can be achieved without referring to the network configuration.

Ladder Iterative Technique based Algorithms

The Ladder Iterative Technique [4] is the basis for a family of three-phase unbalanced load flow algorithms. When impedance parameters, voltages and currents of one side of a network component such as a three-phase transformer are known, voltages and currents of the other side of the network component can be estimated using simple Kirchhoff Voltage equations (Appendix A4). In the Ladder Iterative Technique, initially voltages at all buses are assumed to equal to the rated value. Then load currents at the end of lines are estimated using the assumed voltages and known loads. Considering basic circuit laws presented in Appendix A4 bus voltages and line currents are computed sequentially following the network configuration towards the substation. This is called the forward sweep. When the estimation process reaches the substation bus, the estimated voltages and substation voltages are compared. If the mismatch is more than the acceptable tolerance, a backward sweep is started assuming the actual substation voltage. Improved bus voltages are computed using line currents estimated in the forward sweep. This algorithm is applicable only for radial distribution systems. In some studies shunt charging admittances of the three-phase network component are neglected [6]. Power flow studies in Chapter 3 were completed using Ladder Iterative Algorithm.

An alternative modeling method was proposed in [7]-[8] and considers the shunt admittances as shunt current injections at each node, as shown in (1.1). Then the estimated shunt current is added to the load current. In this modeling technique, the series self and mutual impedances are modeled as series line elements.

$$[\mathrm{Ig}]_n = \frac{1}{2} \cdot [\mathrm{Yabc}]_{nm} \cdot [\mathrm{Vabc}]_n . \tag{1.1}$$

Ramos et al. [9] proposed a method to decouple the self and mutual components of all series impedances of network components. Firstly, the voltage drops or boosts due to the series mutual components are separated and then are considered as voltage sources. After the models are completed, the voltage sources are converted to current sources at both ends of the line components. With this modeling, the series mutual components disappear from network components. This modeling technique allows decoupling the three phases and hence studying the distribution system with conventional single line load flow techniques. When the admittances or mutual admittance are modeled as shunt bus currents they are dependent upon corresponding bus voltages. Therefore they should be updated when bus voltages are updated. This is one of the disadvantages of this modeling technique.

However, some other authors report studies that explore a different perspective to the aforementioned. In those cases, all the bus currents or loads are modeled as impedances. Then a ladder of shunt and series impedances is formed along the feeder. In this type of modeling the backward sweep can be simplified drastically. Backward sweep voltages are obtained by multiplying the forward sweep voltages by a correction factor [10]. If the load type is constant impedance, the ratio between the actual substation voltage and the

estimated substation voltage is considered as the correction factor for all the buses. This considerably simplifies the backward sweep.

Network Matrices based Algorithms

In the algorithms explained above, the system voltages are estimated sequentially along the radial topology of the distribution system. System topology is taken into account by the solution procedure in these algorithms. In contrast, in the category of power flow algorithms surveyed in this section, the network topology is captured by a network matrix. For large distribution systems, network matrices are extremely large and sparse. Once they are formed the solution techniques are robust. Several network matrix based methods are discussed briefly below.

The implicit Z_{bus} method has been proposed in [11] but very few applications can be found in recent studies. In this method the bus current injection [Iabc] is found using (1.2) with the most recent estimates of voltages and of the real and reactive power loads ([Pabc] and [Qabc]) at the buses. Subscript letters N and IT represent the bus number and the iteration count, respectively. No load bus voltages are assumed as the initial voltage estimates for all buses. The voltage deviation vector is estimated solving (1.3) and used to update the voltage at each bus for the next estimation of voltages (1.4).

$$[\mathrm{Iabc}]_{\mathrm{N}}^{\mathrm{IT}} = \left[\frac{[\mathrm{Pabc}]_{\mathrm{N}} + \mathrm{j}[\mathrm{Qabc}]_{\mathrm{N}}}{[\mathrm{Vabc}]_{\mathrm{N}}^{\mathrm{IT}}} \right]^{*}, \tag{1.2}$$

$$[\mathrm{Iabc}]^{\mathrm{IT}} = [\mathrm{Y}_{\mathrm{bus}}] \cdot [\mathrm{VDabc}]^{\mathrm{IT}}, \tag{1.3}$$

$$[\mathrm{Vabc}]^{\mathrm{IT}+1} = [\mathrm{Vabc}]^{1} + [\mathrm{VDabc}]^{\mathrm{IT}}. \tag{1.4}$$

The Y_{bus} matrix can be constructed based on either a single phase equivalent system or a three-phase system. A three-phase Y_{bus} matrix shown in Fig. 1.2 was developed in [11]-[12] and is similar to the conventional single phase matrix except that each network element has a 3X3 admittance matrix.

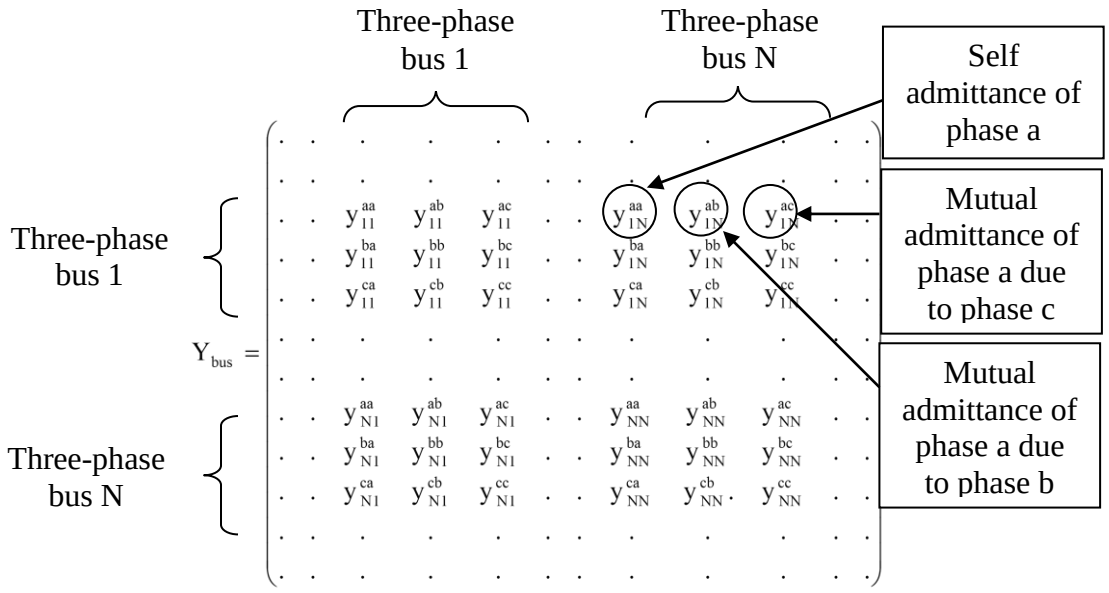

Fig. 1.2. Three-Phase Y_{bus} Matrix

Taking $[YB_{abc}]$ of dimensions 3X3 is an element of Y_{bus} the power balance equation is written as:

$$\left([\mathrm{Pabc}]_N + \mathrm{j}[\mathrm{Qabc}]_N\right) = [\mathrm{Vabc}]_N \left(\sum_{M=1}^{NB} [\mathrm{YBabc}]_{NM} [\mathrm{Vabc}]_M \right)^* . \quad (1.5)$$

Even though there are numerous power flow solution algorithms, the Newton-Raphson method is one of the most widely used algorithms to solve the single phase equivalent transmission system power flow problem. However in literature, it is mentioned that the Newton-Raphson method is not suitable for radial distribution systems. This is due to the numerical challenges of near singular Jacobian matrices of radial systems [3]. In [3], a modified accurate Newton-Raphson method is explained. This method is used for probabilistic power flow analysis in Chapter 4. The conventional Newton-Raphson method can be extended for three-phase power analysis. In this extended three-phase algorithm, the first order approximation of the Taylor series expansion is used for solving the nonlinear power balance equations (1.5) just as the same as its single-phase case. Three-phase systems are formulated either in polar or rectangular coordinates and the three-phase power balance equations are solved using the Newton-Raphson method. The Jacobian matrix is formed considering the first order derivatives. In the polar form, bus voltages are written with magnitudes and phase angles which is the common practice in single phase transmission system analysis. This allows decoupling the strong relationships of the real power to the voltage phase angles and the reactive power to the voltage magnitudes, respectively. This decoupling leads to the fast decoupled load flow algorithms [13]. In some studies the bus voltages are written considering Cartesian coordinates with their real and imaginary parts. It is also noted that the three-phase Newton-Raphson method for distribution system power flow analysis has poor performance due to a high R/X ratio of

distribution feeders that causes ill-conditioned Jacobian matrices [3]. In [14], it is proposed to process the Jacobian matrix by deleting rows with zero diagonal values and arranging off-diagonal entries. This overcomes the singularity issues of the Jacobian matrix.

A different form of the Newton-Raphson method has been reported in [15]. Instead of bus voltages, branch voltages are used as state variables. The current mismatch equations are solved considering the first order Newton-Raphson method. The main advantage of this method is that it has a diagonally strong Jacobian matrix, which can invert accurately.

Another type of power flow algorithm was proposed in [5][16][17]. In this method, the matrix Y_{bus} is not formed. The method, instead, forms two network topology matrices named Bus Injection to Branch Current (BIBC) and Branch Current to Bus Voltage (BCBV). All the line components are represented by three-phase impedance matrices. This method and the implicit Z_{bus} matrix method have very similar approaches.

1.2.2 Technical Models of Wind Generators

Steady state and dynamic models of wind turbines have been active subjects of many research studies. While dynamic models are used for simulation studies that analyze transients, steady state models are used for distribution system studies such as power flow analysis.

In [19]-[31] different accurate wind generator models incorporate the steady state behaviors of wind generators. There are three categories of wind energy conversion systems widely mentioned in literature. The first category (Type-1) has a fixed speed wind turbine connected to an induction generator through a gear box. The constant speed operation is achieved by using either stall control or pitch control. The second category (Type-2) is the semi-variable speed wind turbine connected to an induction generator, which has variable rotor resistance control. Pitch control and the rotor resistance control

allow semi-variable speed operation while maintaining constant frequency. The third category is the variable speed wind turbine generators which have two types: Type-3 and Type-4. They are: Doubly-Fed Induction Generator (DFIG, Type-3) and Full Converter Connected Generator (FCCG, Type-4). Both synchronous and induction generators are used for FCCG. The supply voltage and supply power are controlled by a converter bank placed between the generator and the power grid. In [20]-[22], buses with wind generators were modeled as constant power, constant power factor, or constant voltage nodes with required modifications to capture the characteristics of the wind generators. The authors of [19] and [23]-[31] model wind generators by cascading the turbine, the induction/synchronous generator and the power converter models. Research on this subject reveals that estimating the power output of a wind generator requires knowledge of seven parameters: the wind velocity, and the three wind generator terminal voltage magnitudes and respective three phase angles. The relationship between these parameters and the wind generator output power is highly nonlinear, as explained in [19] and [23]-[31]. In [30] and [31], the authors developed nonlinear models for Type-3 DFIG and Type-4 PMSG (Permanent Magnet Synchronous Generator) wind generators respectively by modeling each component of those wind generators. These two models have a three-phase representation of the wind generator that considers unbalanced distribution system voltage at the Point of Common Coupling (PCC).

The block diagram of the Type-3 DFIG wind generator's nonlinear model [30] and the corresponding mathematical model are given in Appendix A1. A complete mathematical model of Type-4 PMSG wind generator is given in Appendix A2 [31]. In general, these complete nonlinear mathematical models of any variable speed wind generator can be represented as (1.6) below using matrix equations where three-phase PCC voltage phasors

and wind speed are related to real and reactive net power injections from the wind generator into the connected bus.

$$0 = F(U, [V]_{abc}, [\delta]_{abc}, [P]_{abc}, [Q]_{abc}) \ . \tag{1.6}$$

where, U is wind speed, $[V]_{abc}$ is a vector of three-phase voltage magnitudes, $[\delta]_{abc}$ is a vector of three-phase voltage angles, $[P]_{abc}$ is a vector of three-phase real power output from the wind generator and $[Q]_{abc}$ is a vector of three-phase reactive power output from the wind generator. Here F(.) is a multi-dimensional matrix equation comprising a set of nonlinear equations. Generally these models (1.6) are nonlinear due to the nature of the machine. Therefore, the Newton-Raphson technique is popularly used to solve these models.

In detailed technical models, the relationship between inputs and outputs is established using fundamental equations. This is a common approach for modeling of electrical machines such as wind generators where fundamental equations can be established. However, in cases where fundamental equations cannot be established, various black-box models may be used. Modeling techniques such as Bayesian Networks, Machine Learning, Response Surface, Support Vector Machines, Artificial Neural networks, etc. can be used to build these empirical relationships. Once an appropriate model is built using any one of these techniques, the output of the black-box model should be close to the actual output but is unlikely to be 100% accurate. Most of these black-box models are used for probabilistic and prediction purposes. As an example, in [32] a prediction model has been built to forecast wind power generation. This literature survey did not find publications that propose black-box models for technical modeling of wind generators.

1.2.3 Distribution System Power Flow Studies with Wind Generators

The importance of accurate modeling of wind generators in power flow studies for distribution systems is explained in this section.

Power Flow Studies with Constant Power Wind Generator Models

It is common that the output of a wind generator is assumed as a function of wind speed only. Even though the output power of wind generator depends on the voltage at the Point of Common Coupling (PCC), in most power flow studies, wind generators were modeled as simple fixed power injections (independent of the terminal voltage) and only a function of wind speed alone [20][22]. This simplistic constant real and reactive power model was satisfactory in representing wind generators when a very few of them of small sizes were connected to a balanced three-phase distribution system. Hence simple (inaccurate) representation of wind generators using constant power values, as a function of wind speed without accounting for voltage unbalance at the point of connection, did not significantly influence power flow analysis results of a balanced distribution system.

Power Flow Studies with Nonlinear Wind Generator Models

With increased proliferation of large sized wind generators in distribution systems which have many such large machines on the same feeder, numerous instances are found where wind generators comprise a major portion of power flow in the distribution system and at times cause reverse power flow from the distribution system into the transmission system. The above-mentioned simple (inaccurate) representation of wind generators, using power values as a function of wind speed, is inadequate to provide accurate results for distribution system power flow analysis when several large machines are connected and the distribution system is considerably unbalanced. Further, it is important to note that low

voltage distribution systems in jurisdictions in North America such as Ontario (Canada) have three-phase lines that are not transposed and hence lead to severely unbalanced networks. In such cases, accurate modeling of wind generators becomes a must for accurate power flow analysis of distributions systems. In [19] and [23]-[31] different accurate wind generator models describe the steady state behavior of wind generators. These nonlinear accurate wind generator models have to be re-solved in each iteration of the power flow analysis. A flow chart for the modified ladder iterative power flow algorithm with an accurate wind generator model is shown in Fig. 1.3. The step-2 is solved in each power flow iteration. Due to the nonlinearity of these wind generator models, a separate iterative technique is needed to solve step-2 for all connected wind generators in the distribution system in each power flow iteration. Therefore, these nonlinear wind generator models, when integrated in a power flow algorithm, result in slow convergence and higher computing time [26].

Effect of Unbalanced PCC Voltages

Further, it may be noted that converters of wind generators try to operate the machines such that they extract maximum power from the wind. Excluding some losses, this power shall appear at the PCC as the sum of powers flowing from three phases. When the three-phase voltage at the PCC is balanced and at rated value, and the wind generator is at rated wind speed, the per phase power outputs are identical and equal to the rated power value. However, when the voltage magnitude drops, the phase currents increase and thus the total power loss in the wind generator also increases. Due to this effect, the drop in the PCC voltage magnitude reduces the total power supply to the PCC. Table 1.2 shows the estimates of power outputs of 1.5 MVA DFIG wind generators using the nonlinear three-phase model given in Appendix A1 and described in [30]. Furthermore, unbalanced PCC

voltage (voltage angle deviations) causes per phase power output to be unequal, while the sum of per phase powers to be equal to the mechanical power input from the wind turbine. These unequal power flows from the wind generator cause voltage regulation issues on the distribution system. As shown in Table 1.2 more than five times deviations can be expected between any two phases.

As was mentioned before, the distribution systems have unbalanced voltages. Reviewing DFIG output for an unbalanced case in Table 1.2, it is obvious that representing wind generators using balanced PQ values as a function of wind speed without accounting for voltage unbalances at the point of connection with the distribution system is highly inaccurate. Further, these deviations (between rated and actual) are compounded in long feeders with several wind generators. This is a typical case in Northern Ontario, Canada. Therefore it is important to accurately model wind generators considering the three phases, accounting for their power output relationship to the three-phase voltage at the PCC and wind speed.

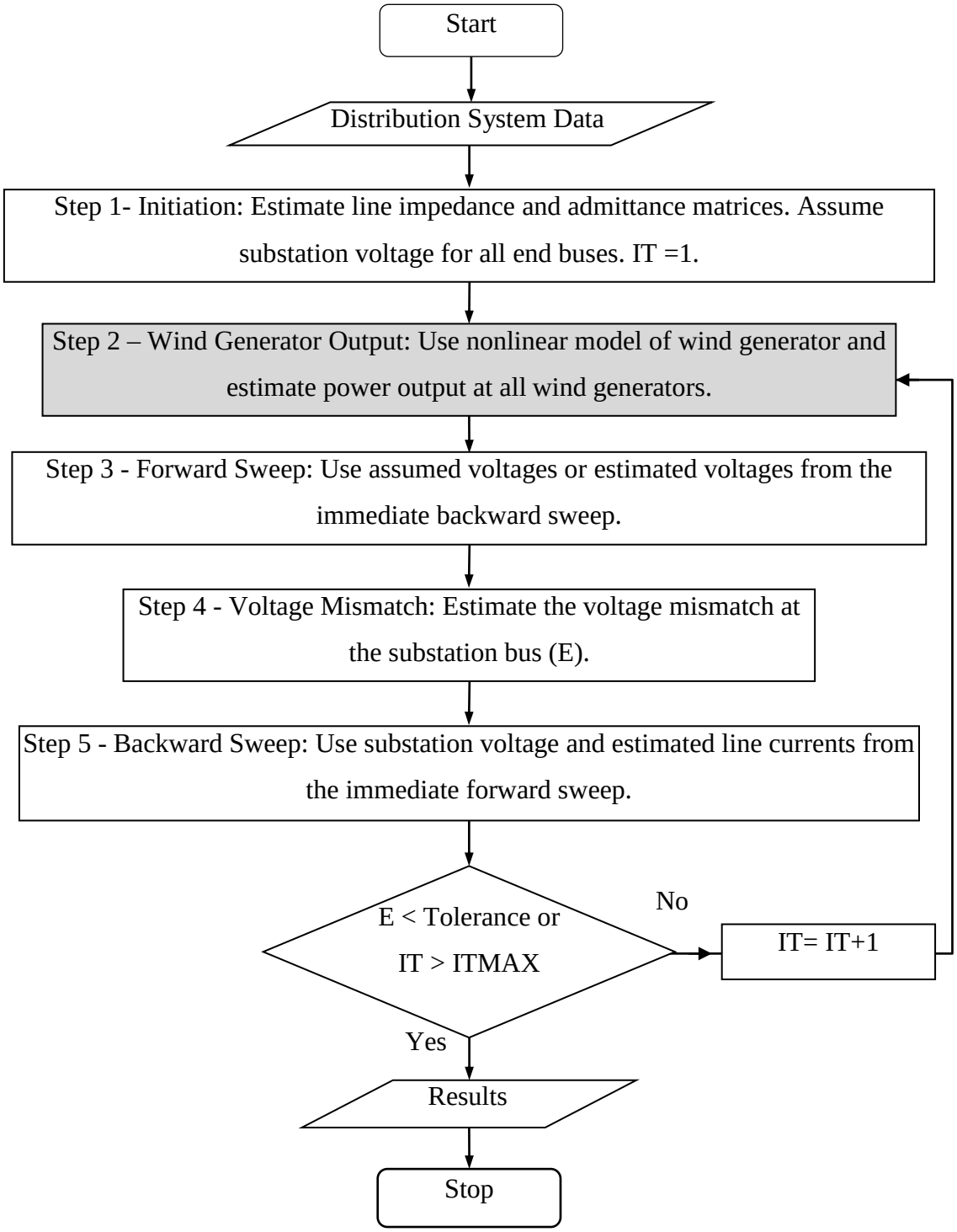

Fig. 1.3. Ladder Iterative Technique Power Flow Algorithm with a Wind Generator [4]

Table 1.2. Power Output Variations for Different PCC Voltages

	Phase a	Phase b	Phase c
Case: Balanced PCC Voltage			
Phase voltage at PCC	$0.94\angle 0^{o}$ pu	$0.94\angle -120^{o}$ pu	$0.94\angle -240^{o}$ pu
Phase Real Powers	0.8903 pu	0.8908 pu	0.8907 pu
Case: Unbalanced PCC Voltage			
Phase voltage at PCC	$0.99\angle 0^{o}$ pu	$1.06\angle -122^{o}$ pu	$0.94\angle -245^{o}$ pu
Phase Real Powers	0.2591 pu	1.0784 pu	1.3159 pu

Note: Rated per phase power output = 0.8917 pu

S_{base} = S_{base} of the Wind Generator / 3

1.2.4 Probabilistic Models of Wind Generators and Power Flow Studies

Studying the impact of uncertain parameters in the power system started a few decades ago. In the 1970s [34]-[35] described probabilistic behaviour of system parameters. In [34] probabilistic power flow study is explained considering probabilistic models for loads, generators and pump storage stations. A probabilistic model of an equivalent load is built by convolution of different components of the equivalent load. These components include: random component of the load, deterministic component of the load, random component of the generating unit outage and deterministic component of the generating unit outage. This technique is closely related to the conventional reliability analysis of generators. In [35] power inputs and outputs to the power system are assumed as independent random variables. Different probability distribution functions: normal, binomial and discrete etc. are used to model these inputs and outputs. A method is explained to find out probability distributions of other system parameters using the assumed probability distributions.

A probabilistic power flow technique is described in [36] using Monte Carlo simulation technique. In this study, it is assumed that system voltage magnitudes and power flows have Gaussian probability distributions. These assumptions are made in the probabilistic voltage solution method explained in Chapter 4. In the study explained in [36], linear dependency between system voltages and loads are assumed near the base case operating point. This allows creating the probabilistic voltage solution of the system. In [37] a similar study is described using Monte Carlo simulation technique for distribution system power flow analysis. Gaussian probability distribution is assumed for the loads in the distribution system. Photovoltaic generators are also modeled using appropriate probabilistic models. A probabilistic power flow analysis with wind generators is explained in [38]. In this study Weibull probability distribution is assumed for the wind speed and a derived discrete probability distribution is taken for the power output of wind farms. In the power flow

study with wind generators [39], a derived probability distribution and a Gaussian probability distribution are considered for wind generations and loads respectively. It was conducted without Monte Carlo simulation technique.

1.2.5 Economic Integration Models of Wind Energy

Wind generators receive special rates in most electricity markets [35]. Although such mechanisms exist in present day electricity markets, due to market forces and scale of economies, wind generators may have to competitively participate in electricity markets in the future. As briefly mentioned in Chapter 1.1.2 uncertainty and variability of wind power creates challenges in effective economic integration with electricity markets.

Amongst available conventional and non-conventional sources of energy, wind energy has a high degree of uncertainty. Uncertainty of wind power generation could cause uncertainty of other network parameters such as nodal prices [40]. Therefore, different electricity markets use various mechanisms to tackle uncertainty in supply [41]. In order to overcome uncertainty, a market operator has to incur an additional expense to forecast wind energy supply and carry increased online reserves. It is also noted that an increase in numbers of wind farms reduces the uncertainty [42]-[47] due to spatial smoothing effect. In some cases a 50% reduction of uncertainty (in terms of standard deviation) is observed due to the spatial smoothing effect [42]. In [43], high frequency and low frequency aggregation effects are discussed using an aerodynamic macro-model inside a wind farm. A study of smoothing effect on five planned wind farms distributed in the Atlantic Provinces of Canada is discussed in [44]. The study suggests that, if regional smoothing effect on wind power outputs is considered, the spinning reserve requirement and hence cost of integrating wind power can be reduced. However the benefit of smoothing effect is practically non-realizable to a single wind farm. Therefore in [47], coalition game theory

based collective operation of wind farms is proposed. According to [47], all wind farms get the benefit of smoothing effect though they are competitors in the market and no wind farm gets a higher profit by defecting from the coalition. A daily coalition profit sharing mechanism is explained and it is also mentioned that a negative profit can be expected based on the level of generation.

Apart from uncertainty, wind generator output varies continuously throughout the day. This variability causes a higher requirement of services such as Automatic Governor Control (AGC), ramp-rate, operational reserve and reserve capacity, which in turn causes a higher expense to the system operator. According to [48], at 20% wind penetration level these costs can be as high as $5.5/MWh. In [49], these costs have been reviewed from different previous studies. At present, wind generators are not required to pay these extra costs. However in a competitive market environment, wind generators would have to reduce variability in their output to mitigate such extra costs.

With rapid growth of wind power and the obvious integration challenges, many researchers have proposed energy storages, such as pumped-hydro storage systems, as a solution [50]-[54]. Energy storage systems give two different benefits: (a) reduce the effect of uncertainty, and, (b) energy arbitrage by enabling temporal shift of energy from low priced periods to high priced periods. In [50] optimal operation of a pumped-storage station and a wind farm is proposed to minimize the imbalance cost. A self-scheduling market operation of a generation company which owns a pumped-hydro storage and a wind farm is studied in [51]. From a case study in Spain, it is found that such a combined operation increases benefits for the generation company. Two studies of supplying islands' loads using wind-pumped-hydro hybrid power stations are explained in [52] and [53]. According to those studies, a hybrid power generation and storage operation facilitates an increase of wind power penetration of the island's grid and increases the combined firm

power capacity. Both output variations and output uncertainty of wind power are studied in [54]. The study achieved two goals: (a) increased profit of the wind farm and (b) smoothened output of the wind farm by the combined wind-pumped-hydro operation. Further, it is found that wind-pumped-hydro operation improves the market participation of the wind generator. It also gives an opportunity to deal with network restrictions. These studies [50]-[54] formulate short term optimization problems assuming wind power as a stochastic quantity. From previous research, it is clear that there are tangible benefits from combined operation of wind farms and pumped-storage stations. However, in practice, due to high capital cost, it is not economically attractive to have a pumped-storage system for each wind generator. Therefore, common pumped-storage systems are considered in government policies such as Ontario's Long-Term Energy Plan [55]. This allows harnessing the benefits of wind-pumped-hydro combined operation while sharing the burden of initial capital costs.

1.3 Objectives of this Thesis

As explained above, wind integration into the power system has two main challenges amongst several others. The first is the technical challenge of developing accurate engineering models of wind generators for planning and analysis of power systems. The second challenge is the need for economic models for competitive integration of wind energy into electricity markets. Therefore, the objectives of this PhD research focus on addressing these challenges.

First Aim (Chapter 2): Technical Models of Wind Generators (Analysis)

The first aim of this thesis is to develop an intelligent model of wind generators using artificial neural networks (ANN). This model should be suitable for modeling both Type-3

Doubly-fed Induction Generators (DFIG) and Type-4 Permanent Magnet Synchronous Generators (PMSG). Further, the model should be easily implementable in commercial power flow analysis software such as PSS®E and PSS®SINCAL.

Second Aim (Chapter 3): Technical Models of Wind Generators (Analysis)

The second aim of this thesis is to implement these intelligent models of wind generators in commercial software such as PSS®E and PSS®SINCAL.

Third Aim (Chapter 4): Probabilistic Models of Wind Generators (Analysis)

The third aim of this thesis is to model annual forecast of wind generator output and loads and incorporate them in power flow analysis studies for planning applications. This modeling technique should simplify the complexity of the probabilistic power flow study with several wind generators in the system.

Fourth Aim (Chapter 4): Economic Models for Integration of Wind Generators (Optimization)

The fourth aim of this thesis is to develop models for integration of wind generators with electricity markets. The aim is to ensure that wind generators competitively sell energy in electricity markets and do not depend on subsidies. The model should benefit from technical aggregation, smoothing effect, economic cooperation, etc.

1.4 Thesis Outline

This Chapter presents an introduction to the thesis and reviews literature related to wind power integration into the power system. It also gives introductions to different theoretical and mathematical concepts used in the study.

In **Chapter 2**, ANN based intelligent wind generator models are formulated. A method for generating epochs for training and selecting suitable ANN configurations for different wind generator models is presented. In this study several criteria were used for selecting the best ANN configuration. The findings of those detailed investigations about training and selection are given in Chapter 2. Two different wind generator models for: 1) a Doubly-Fed Induction Generator, 2) a Permanent Magnet Synchronous Generator are given in Chapter 2.

After building ANN wind generator models in Chapter 2, in **Chapter 3** the ANN wind generator models are implemented in three-phase unbalanced distribution system power flow algorithms in Matlab environment. The IEEE 37-bus unbalanced distribution system is used for this analysis. Two different power flow studies were completed for this purpose. Comparison of computation speed of power flow studies with ANN based wind generator models and with classical accurate models is given in this chapter. Then the ANN wind generator models are implemented in two commercial software packages, namely PSS®E and PSS®SINCAL. All details of these implementations are also given in Chapter 3.

In **Chapter 4**, a probabilistic voltage solution technique is explained for distribution systems. Probabilistic behavior of both loads and wind generators is considered for this study. Details of forming probabilistic event space are also presented. Results of a case study with IEEE 70-bus distribution system are given at the end of this chapter.

In **Chapter 5** a Wind Generators Cooperative (WGC) is proposed as an economic model for integration of wind generators with electricity markets. Both organizational structure and mathematical optimization formulation of the cooperative are given. After the formulating the WGC, it is tested with ten wind farms located in the southern Ontario grid. A detailed analysis of results of the base case and sensitivity cases are given at the end of Chapter 5.

Chapter 6 presents the conclusion of the thesis. Besides the summary of the complete study, contributions made by the study are also highlighted. At the end, future possible research opportunities are proposed.

1.5 Chapter Summary

This chapter provided an introduction to the challenges faced in the integration of wind generators with power systems, both technical and economic. A survey for those challenges was presented. Thereafter, three specific technical and economic challenges were identified. Research aims in this thesis were also identified and presented. Finally, a chapter wise summary was provided.

Chapter 2

Artificial Neural Network Wind Generator Models

2.1 Introduction

Wind generators are versatile and complex machines. Accurate models are important for technical studies such as power flow analysis. Historically, with a few wind generators on the distribution system, their approximate representation was adequate to complete a near-accurate engineering analysis. However, their increased use has necessitated their accurate representation. The reasons for requiring accurate representation are outlined below. It must be noted that work scope in this thesis is limited to Type-3 DFIG and Type-4 PMSG wind generators.

Unbalanced Distribution Systems: North American distribution systems, specifically that in Ontario (Canada) are unbalanced as the low voltage lines are not transposed and loads are not balanced. This leads to the terminal voltage being unbalanced in both magnitudes and angles for wind generators.

Unequal Power Output in Phases: When the terminal voltages at the wind generator are unbalanced (voltage angles), the mechanical power supply from the wind turbine shaft and correspondingly its electrical output is not equally distributed in the three phases. Table 1.2 in Chapter 1 shows this change in phase power outputs as voltages change from a balanced case to an unbalanced case. This case of unbalanced power outputs in phases aggravates imbalance of voltages in the distribution system. Hence it is imperative to model wind generators accurately for accurate distribution system analysis.

Effect of Change in Voltage Magnitude from Rated Value: Conventional power models of wind generators use wind speed curves to compute power output. This model assumes that terminal voltages are at the rated value and balanced. Accordingly, the shaft power is divided into three equal parts for the three phases. However, when the mechanical shaft power input is constant and the terminal voltage is changed, currents in phases change leading to a change in real power losses. Accordingly, with declining terminal voltages, losses in wind generators increase and power outputs reduce.

Accurate Model Integration with PSS®E and PSS®SINCAL: From literature surveyed in Chapter 1, it is clear that Wind generator models calculate the power output of wind generators using the three-phase system voltage and wind speed. Wind generator models established a mathematical relationship between the input variables (three-phase system voltage and wind speed) and output variables (three-phase real and reactive power generations). Conventionally, this relationship is established by cascading all the governing mathematical models of the turbine, generator and converters (Appendix A1, Appendix A2). The challenge is that these models form a set of nonlinear equations that must be solved using iterative techniques such as the Newton-Raphson technique. They are required to be solved in every iteration of the power flow algorithm. Accordingly, power flow analysis algorithms become very slow. Also, these models cannot be directly integrated by the user into commercial software such as PSS®E and PSS®SINCAL.

These challenges of using accurate representation and integrating it with software such as PSS®E and PSS®SINCAL can be solved using artificial neural network (ANN) models. ANN models can be trained to represent nonlinear relationship mapped by the accurate models of wind generators. On training, ANN offers a simple set of matrix relations. These

relations can be easily implemented in the common commercial software such as PSS®E and PSS®SINCAL.

In this chapter, proposed ANN models of wind generators, both Type-3 DFIG and Type-4 PMSG, are presented.

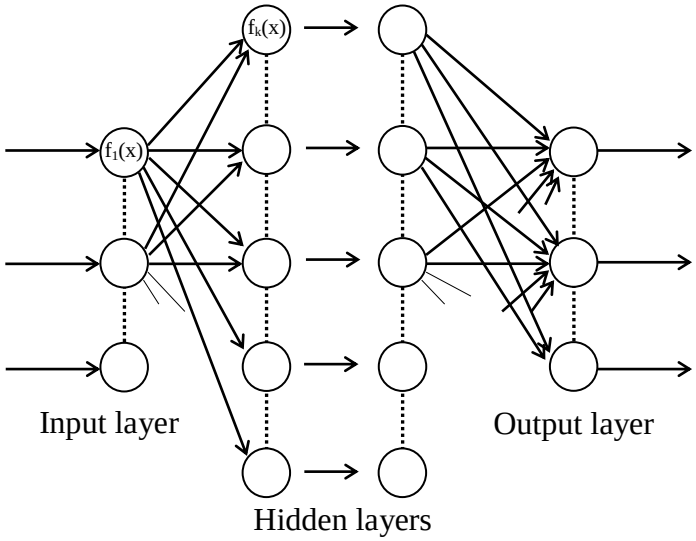

Fig. 2.1. Multi-Layer Feed Forward Artificial Neural Network

2.2 Introduction to Artificial Neural Networks

An Artificial Neural Network (ANN) can be used to map a function by establishing a relationship between its input and output domains. The ANN uses series of functional elements to establish this relationship. This mapping is carried out without reference to the actual physical relationship between input and output domains. Therefore, for cases where such physical relationships using fundamental equations cannot be built, ANNs are widely used. An excellent example is econometric studies. In econometric studies, relationships are established by regression techniques which are particularly useful for sensitivity analysis and elasticity studies in economics. Similarly, ANNs that build a relationship by extensive training are particularly useful for prediction purposes and therefore, they are preferably used for such purposes instead of econometric models. In [32] an ANN model is proposed to predict wind power output. The model describes the wind power output of a wind generator as a function of wind velocity and wind direction. An ANN is capable of mapping complex nonlinear relationships with remarkable accuracy. Similar to econometric studies, training an ANN model requires a considerable effort. There are two methods of training an ANN: supervised training and unsupervised training. In the supervised training, the target output is known and error signals are created comparing the target output and the estimated output. These error signals are used for training the network. In the unsupervised training, an adaptation rule is used for training the network. More details of building ANNs can be found in [33]. Once an ANN model is built, its execution is simple and fast.

A simple form of multi-layer feed forward ANN is shown in Fig. 2.1. Circles represent functional elements with a mathematical input and output relationship called the "activation function". A functional element with incoming links and an output link forms a neuron. The input layer has as many neurons as required for representing input variables.

These input variables are connected to the neurons of output layer through one or more hidden layers. All the combining links have weights that determine the contribution from each input to the output. The output layer has output neurons each representing an individual output. The number of hidden layers and the number of neurons in each hidden layer are determined at the training stage by experimenting with different configurations.

2.3 ANN Models for Wind Generators

ANNs establish complex mathematical relationships using series of simple mathematical operations. A well trained ANN model consistently gives an accurate set of outputs for a set of inputs. This is accomplished by means of extensive training of the ANN model. The use of Artificial Neural Networks (ANNs) in wind power is not new but in most cases ANNs are deployed for forecasting wind power [32]. In such studies, econometric models are replaced by ANNs. In contrast, this study proposes three-phase wind generator models using Artificial Neural Networks to replace the existing nonlinear mathematical wind generator models.

Building an artificial neural network involves several important steps. They are:

1. Identify the correct inputs and outputs and then generate sufficient number of data sets of these inputs and outputs. One data set of inputs and outputs is called an epoch. These epochs are used to train an ANN. Epochs for training an ANN can be generated by using an accurate nonlinear mathematical model of a wind generator or can be obtained from measured input-output data.

2. Use the prepared epochs to train several configurations of ANN and select the ANN configuration which has the best performance. The performance of ANN configurations is measured by its output accuracy. In this chapter, output accuracy was measured using

Average Root Mean Square Error (ARMSE), Average Absolute Error (AAE) and Maximum Absolute Error (MAE). The ANN configuration that has smallest ARMSE, AAE and MAE is selected for the modeling the corresponding three-phase wind generator because it produces the most accurate output values.

3. The selected ANN configuration is further trained to improve the accuracy of the output. After this extensive training, the ANN can be used to compute output for any given set of inputs.

This process of building an ANN model of a wind generator is explained in the rest of the chapter. Sections 2.3.1, 2.3.2 and 2.3.3 illustrate the ANN training algorithm and configuration selection criteria. Section 2.3.4 explains the process of generating epochs for training an ANN. Sections 2.4 and 2.5 give details of two ANN models of wind generators built for this study. The first model is for a Doubly Fed Induction Generator (DFIG) and the second model is for a Permanent Magnet Synchronous Generator (PMSG). The two ANN models developed in this Chapter are used later in Chapter 3. A summary of the Chapter is given in section 2.7.

2.3.1 The ANN Architecture

Each input parameter is fed to a neuron in the input layer of the ANN. Therefore, the number of input neurons in the input layers is decided by the number of input parameters of the wind generator model. Similarly each output parameter represents the output of a neuron in the output layer of the network. Therefore, the number of output neurons in the output layer is also decided by the number of output parameters of the wind generator model. Between the input and output layers there can be many hidden layers in the

network. A typical feed-forward neural network model, adapted to be used as a wind generator model, is shown in Fig. 2.2.

2.3.2 The ANN Training Algorithm

In this section, k is used as a notation for the k^{th} layer of an ANN. There can be m_k neurons in the k^{th} hidden layer. The number of neurons in the input and output layers are determined by the number of input and output parameters respectively. The number of hidden layers and the number of neurons in each hidden layer are determined by experimenting with different ANN configurations. This experimentation process and the selection criterion for identifying the best configuration are explained in section 2.3.3.

A neuron is formed by one or more inputs, a functional element and an output. Fig. 2.3 shows a neuron and its notation as employed in this study. The back propagation technique explained from (2.1) to (2.5) [33] was used for training ANN models of wind generators developed in this study.

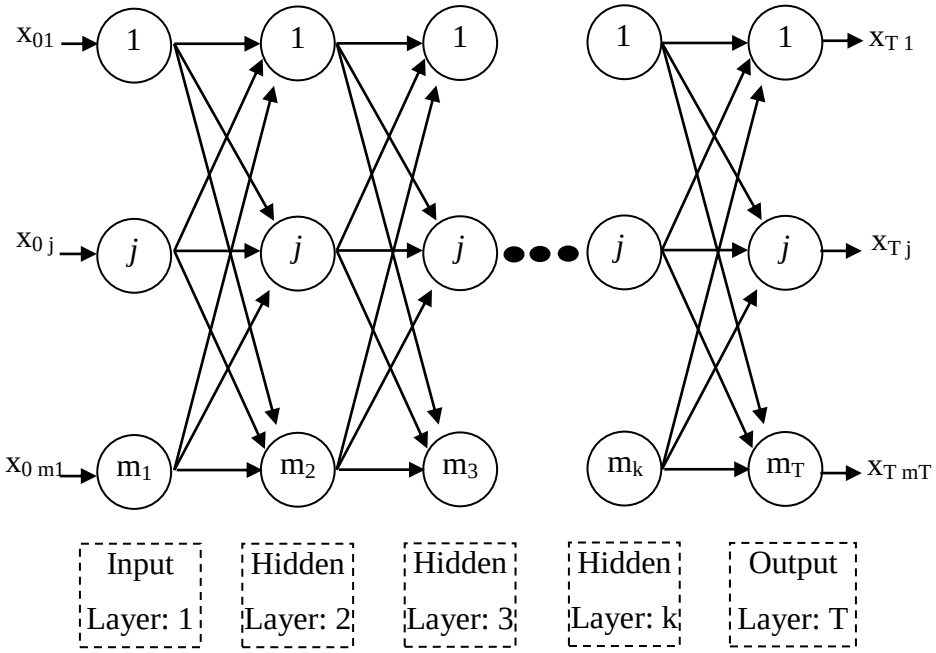

Fig. 2.2. An ANN-Based Wind Generator Model.

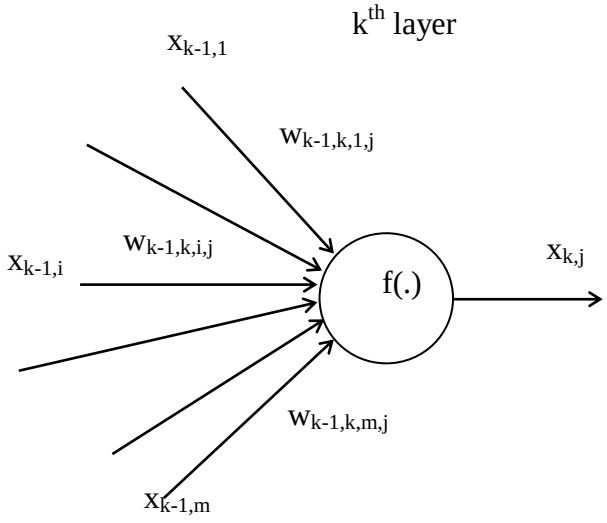

Fig. 2.3. A Neuron and Its Notation in an ANN Model

In this notation, $w_{k-1,k,i,j}$ represents the weight of the link between the i^{th} neuron in $(k-1)^{th}$ layer and the j^{th} neuron in k^{th} layer. $w_{k-1,k,0,0}$ represents the bias value of layer k. The output of the neuron i in layer (k-1) is denoted by $x_{k-1,i}$. The total input signal into the j^{th} neuron of layer k is the net-stimulus ($ns_{k,j}$) and is the weighted summation of outputs of m_{k-1} neurons in the layer (k-1) as below:

$$ns_{k,j} = w_{k-1,k,0,0} + \sum_{i=1}^{m\,k-1} w_{k-1,k,i,j} \cdot x_{k-1\ i} \tag{2.1}$$

The output of the neuron j in layer k is written as:

$$x_{k,j} = f_{k,j}\left(ns_{k,j}\right) = \frac{1}{\left(1+e^{-ns_{k,j}}\right)} \tag{2.2}$$

The sigmoid activation function of the neuron j in layer k is denoted by $f_{k,j}(.)$. The feed-forward ANN (Fig. 2.2) is completely estimated using the values of input parameters, (2.1) and (2.2). When the normalised inputs are fed to the input layer (no functional elements are assigned for the neurons in the input layer), the error ($Er_{T,j}$) of the j^{th} neuron in output layer (T) compared with the normalised target output (y_j) is estimated as:

$$Er_{T,j} = \left.\frac{\partial f_{T,j}(x)}{\partial x}\right|_{ns_{T,j}} \left(x_{T\,j} - y_j\right), \tag{2.3}$$

The propagated errors of the hidden layers are estimated as:

$$Er_{k-1,i} = \left.\frac{\partial f_{k-1,i}(x)}{\partial x}\right|_{ns_{k-1,i}} \sum_j w_{k-1,k,i,j} \cdot Er_{k,j} \tag{2.4}$$

The weights are updated in order to minimise the error at the output layer. The formula for updating weights is given in (2.5).

$$w_{k-1,k,i,j}^{n+1} = w_{k-1,k,i,j}^{n} - \eta \cdot Er_{k,j}^{n+1} \cdot x_{k-1\,i}^{n+1}, \tag{2.5}$$

where n is the ANN training cycle count and η is the learning rate.

Each neuron in the ANN has an activation function $f_{k,j}(.)$. In this study sigmoid function (2.2) was used as the activation function of all neurons. Output of the sigmoid function varies from 0 to 1. Input for the function can be varied from $-\infty$ to $+\infty$. However it has greater output variation for the inputs near zero. Considering these facts Min-Max data normalisation (2.6) was adapted for this study assuming the minimum of the normalised parameter (x_{Min_Rage}) is 0 and the maximum of the normalised parameter (x_{Max_Rage}) is 1.

$$x = x_{Min\_Range} + \frac{\left(X - X_{Min\_Epoch\_Set}\right)}{\left(X_{max\_Epoch\_Set} - X_{Min\_Epoch\_Set}\right)} \times \left(x_{Max\_Range} - x_{Min\_Range}\right) \tag{2.6}$$

$$X \in \left(U, V_a, V_b, V_c, \delta_a, \delta_b, \delta_c, P_a, P_b, P_c, Q_a, Q_b, Q_c\right)$$

2.3.3 Training Algorithm Convergence Criteria

The Average Root Mean Square Error (ARMSE) (2.7) was estimated considering target outputs (Y_j) and the ANN outputs ($X_{T\,j}$).

$$ARMSE = \sum_{j=1}^{Nout}\left(\sum_{e=1}^{Ne}\frac{\left(X_{T\,j}-Y_j\right)^2}{Ne}\right)\Big/ Nout \tag{2.7}$$

where, e is an index to denote epochs, Ne is number of epochs and Nout is the number of neurons in the output layer

The ARMSE was the primary criterion to check the performance of an ANN's configuration. The ANN configurations with low ARMSE have output values closer to the target outputs. However, due to averaging and squaring, ARMSE does not give a complete assessment of the performance of an ANN. As an example, when the output error of one neuron is high and the output errors of all other neurons are low, a low ARMSE value can result. This is not desirable because the ANN model should be accurate for all output parameters. Therefore, Maximum Absolute Error (MAE) (2.8) was also recorded considering outputs of all neurons in the output layer at each training cycle.

$$MAE = \max\left|X_{T\,j}-Y_j\right| \qquad \forall \;\; e, j \tag{2.8}$$

Upon training, if the ARMSE value was low and MAE value was also low, the ANN configuration was selected.

The convergence of weights was investigated by evaluating Average Absolute Error (AAE) (2.9) using outputs.

$$AAE = \sum_{j=1}^{Nout}\left(\sum_{e=1}^{Ne}\frac{\left|X_{T\,j} - Y_j\right|}{Ne}\right)\Big/ Nout \tag{2.9}$$

By plotting the AAE against the number of training cycles, the level of training of the selected ANN configuration was monitored.

ANN training algorithm (2.1)-(2.5) was used for building ANN models of wind generators. Training data (Epochs) were normalised as given in (2.6). The convergence criteria explained in (2.7)-(2.9) were used for selecting the best ANN configurations. Details of the ANN wind generator models built in this chapter are explained in the sections below.

2.3.4 Generating Epochs

In order to build an ANN model of a wind generator, it is necessary to identify input and output parameters of a wind generator. Seven parameters are needed to estimate the power output of a wind generator (Fig. 2.4). They are: Wind speed, three voltage magnitudes and three voltage angles at the point of common coupling (PCC). The outputs of the ANN consist of six parameters comprising the three phase real and reactive powers outputs of the wind generator at the PCC. Measured input and output data can be used as epochs for building ANN wind generator models. Otherwise the inputs and outputs estimated using an available wind generator ([19]-[31]) model can also be used for this purpose. In this study, epochs were created using accurate nonlinear models of wind generators reported in Appendix A1 [30] and Appendix A2 [31].

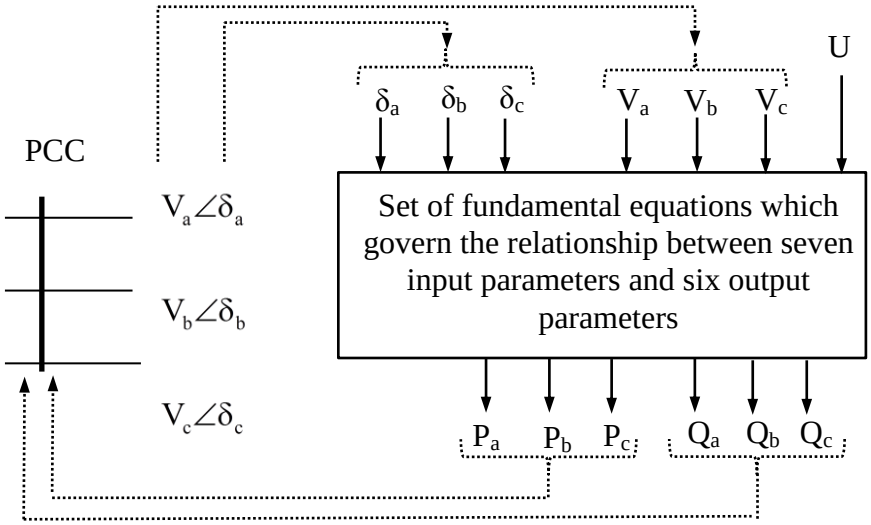

Fig. 2.4. Three-Phase Power Estimation of Wind Generator

(PCC: Point of Common Coupling)

2.4 ANN Model of a Type-3 DFIG Wind Generator

Training Data (Epoch Set 1): The input data of an epoch comprises: wind speed (U), voltage magnitudes of phases a, b and c (V_a, V_b, V_c), and voltage angles of phases a, b and c (δ_a, δ_b, δ_c). A series of ten thousand random numbers between 4 m/s and 20 m/s was chosen as wind speed data for ten thousand epochs. Three series of ten thousand random numbers between 0.94 pu and 1.06 pu were created for voltages magnitudes (V_a, V_b, V_c) for ten thousand epochs. Three more series of ten thousand random data points were chosen in the range of -5º to 5º for voltage phase angles of phases a, b and c (δ_a, δ_b, δ_c) for ten thousand epochs. These seven series of ten thousand numbers were collated to form input portion of the set of ten thousand epochs. For each Epoch in this set of 10,000 Epochs, a corresponding output has to be determined. The output has six parameters representing the three-phase real and reactive power output of the wind generator. These output parameters for each Epoch are computed using the accurate Type-3 Doubly Fed Induction Generator model given in Appendix A1 [30]. Solving the model once for every set of input parameters of each Epoch using the Newton-Raphson technique yielded corresponding output parameters for ten thousand Epochs consisting of P_a, P_b, P_c, Q_a, Q_b and Q_c.

Using the Epoch Set 1 and the training algorithm explained above, the ANN model for the Type-3 DFIG wind generator (Appendix A1) was built. The nonlinear mathematical model of the generator needs seven input parameters (U, V_a, V_b, V_c, δ_a, δ_b, δ_c) for estimating the output. The reactive power output of the generator is maintained at zero by the controllers of the generator. Therefore reactive power output parameters are zero at all phases. Therefore three reactive power series (Q_a, Q_b and Q_c) are set as zeros in Epoch Set 1. Given this fact, only real power series (P_a, P_b and P_c) of Epoch Set 1 were generated for building the ANN model of the wind generator. Therefore, the input layer and the output

layer of the ANN for this generator model have seven and three neurons respectively. Many network configurations of the hidden layers are considered for the study. The best network configuration was selected based on the criteria above (2.7)-(2.9).

2.4.1 Effect of ANN Configuration on Accuracy of DFIG Output Estimation

MAE was plotted to select the best ANN configuration. Fig. 2.5 shows the MAE (2.8) of different ANN configurations. The same learning rate (η=0.7) and tolerance (0.0001) were used for all configurations.

2.4.2 Effect of ANN Configuration on Training Time

Apart from the accuracy of ANNs, the time taken for the convergence was also recorded. Fig. 2.6 shows convergence time required with different ANN configurations. Generally, when the ANN configuration is complex (many hidden layers and neurons) the convergence time is higher. However, there are exceptional larger configurations that train faster than smaller sized configurations.

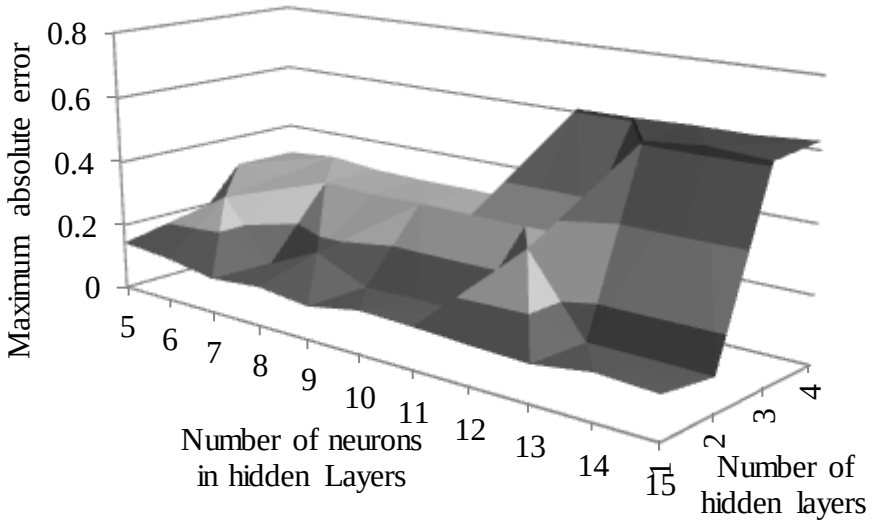

Fig. 2.5. MAE of Different ANN Configurations – Type-3 DFIG Wind Generator Model

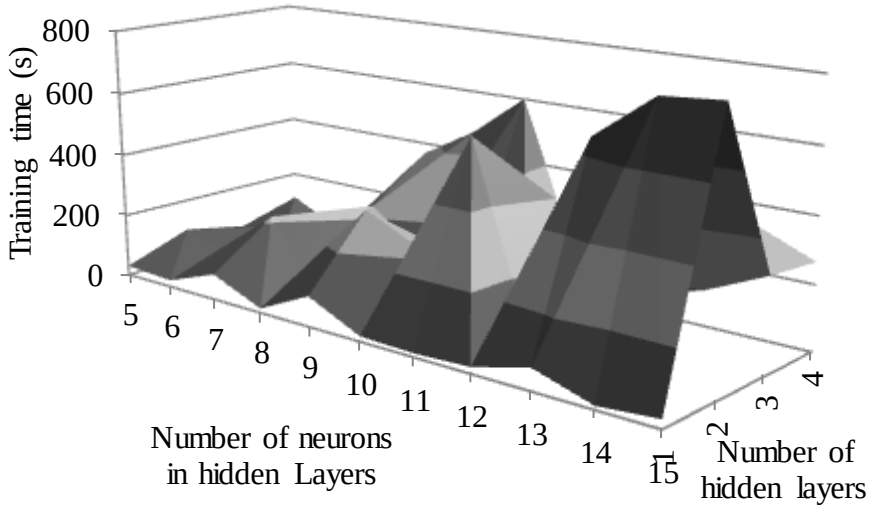

Fig. 2.6. Convergence Time of Different ANN Configurations of Type-3 DFIG Wind Generator

2.4.3 Selected ANN Model for Type-3 DFIG Wind Generator

The smallest ARMSE was found to be 0.0138 for an ANN consisting of four-layers i.e. two-hidden layers plus input and output layers. The configuration consisted of seven neurons in the input layer (three-phase voltages phasors and the wind speed), ten neurons in the first hidden layer, ten neurons in the second hidden layer and three neurons in the output layer representing the three-phase real power output of the wind generator. As mentioned above, reactive power outputs were not considered because they were zero at all phases. The bias values at each layer were 0.0, -0.5, -1.0 and -1.8, respectively. The variation of AAE (2.9) for this ANN configuration is shown in Fig. 2.7. It shows reduction in the AAE with training. It also shows that it is fully trained for 10,000 epochs within 1000 training cycles and the deviation from the nonlinear model (Appendix A1) is minimal.

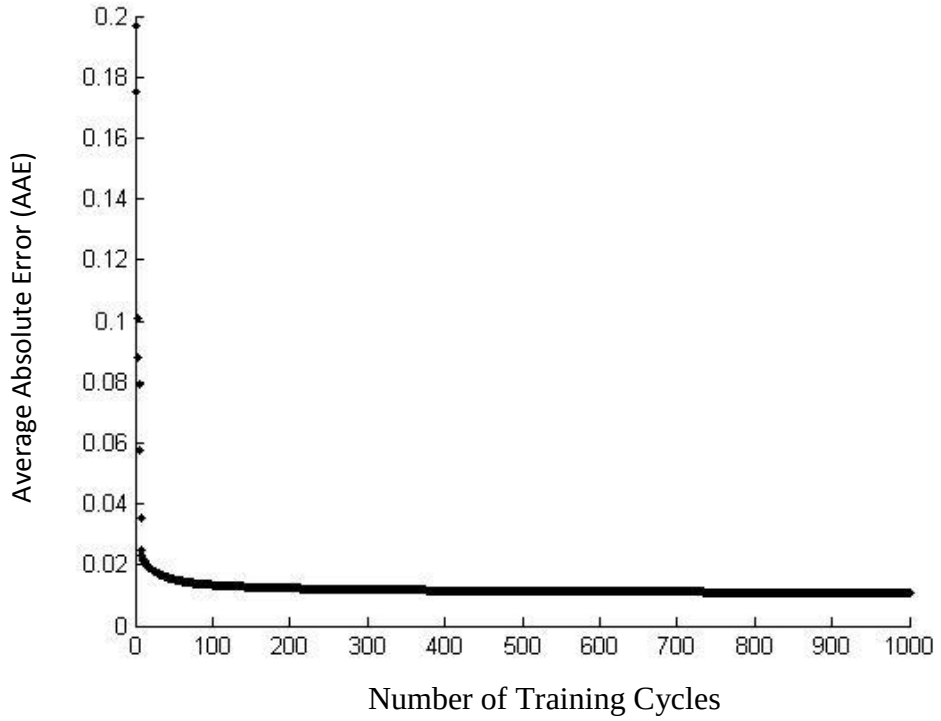

Fig. 2.7. Reduction of Absolute Error over the Number of Training Cycles

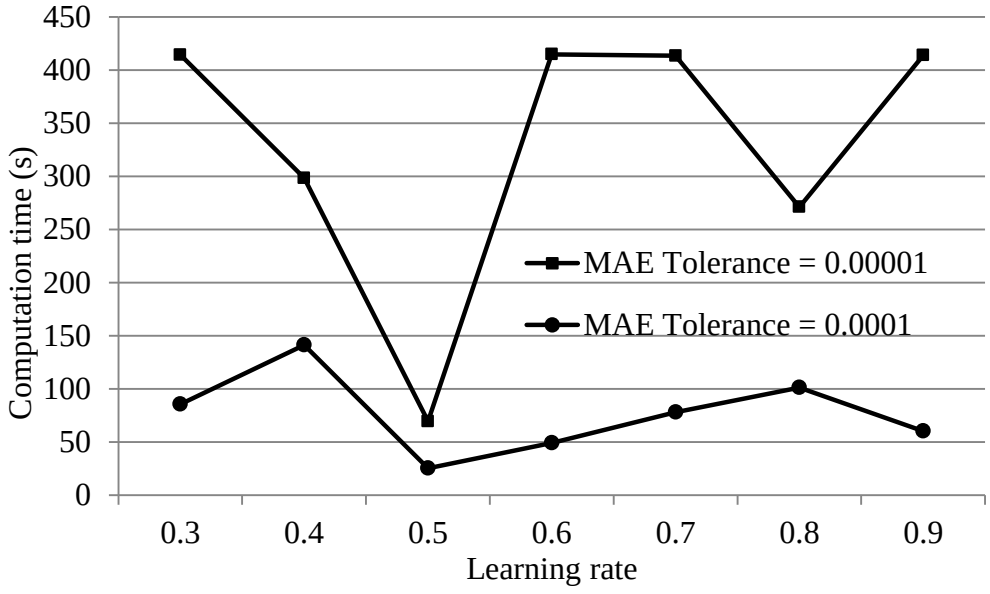

Fig. 2.8. Convergence Time of the Selected ANN Configuration of Type-3 DFIG Wind Generator for Different Learning Rates and Convergence Criteria

2.4.4 Effect of Learning Rate on Training Time

The learning rate (η) and the MAE tolerance have a direct relationship to the training time of an ANN. In order to investigate this relationship, the selected ANN configuration (2 hidden layers with 10 neurons each) was trained with different learning rates and tolerance criteria. The results of this study are given in Fig. 2.8. From this analysis, it is clear that when the optimal learning rate (0.5) is selected, this ANN configuration can be trained considerably faster, even for a tighter convergence criterion.

2.5 ANN Model for Type-4 PMSG Wind Generator

Training Data (Epoch Set 2): Using the same input data of Epoch Set 1, 10,000 corresponding output sets for PMSG were created and included in Epoch set 2. The relevant Type-4 PMSG model used for this work is given in Appendix A2 [31]. The Newton-Raphson technique was used to solve this accurate model considering input data set of each Epoch and generate the corresponding output data set comprising P_a, P_b, P_c, Q_a, Q_b and Q_c.

The training algorithm presented in Chapter 2.3.2 was used for building the ANN model for Type-4 PMSG wind generator given in Appendix A2. Epoch Set 2 was used for building this ANN model. Similar to the DFIG model, reactive power output of the wind generator was set to zero by means of the controller action. Therefore only three real power outputs of the wind generator were considered for ANN modeling. This ANN model has seven input parameters representing wind speed, three-phase voltage magnitudes and angles. The outputs of the ANN model are real powers of three phases. Therefore input and output layers have seven and three neurons respectively. The number of hidden layers and hidden neurons were decided via experimentation with different configurations. The detailed process is given below.

2.5.1 Effect of ANN Configuration on Accuracy

In order to select the best ANN configuration for Type-4 PMSG wind generator model, MAE was plotted against various ANN configurations. Fig. 2.9 shows the MAE of different ANN configurations. According to Fig. 2.9, the ANN configuration with two hidden layers and 10 neurons in each hidden layer has the lowest MAE.

2.5.2 Effect of ANN Configuration on Training Time

Fig. 2.10 shows convergence time required with different ANN configurations. Training convergence was decided with a MAE tolerance of 0.0001 and a learning rate 0.7. A trend of higher training times was observed with increase in the size of the network. However, some large sized networks train faster than smaller network configurations. Because ANN training is done once, training time was not considered as a criterion for selecting the best network configuration.

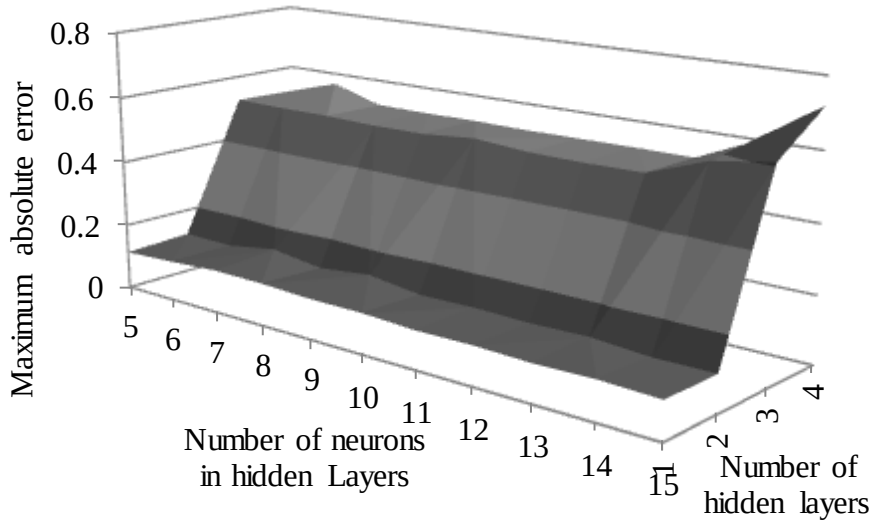

Fig. 2.9. MAE of Different ANN Configurations – Type-4 PMSG Wind Generator Model

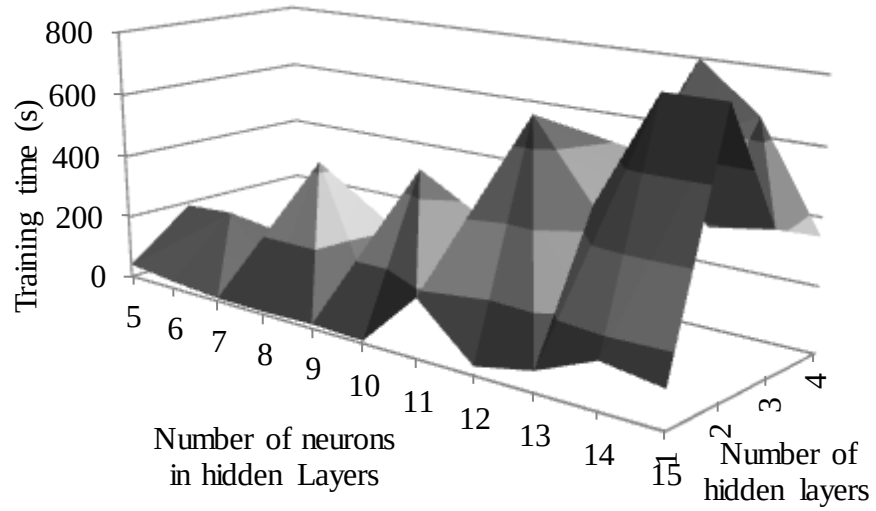

Fig. 2.10. Convergence Time of Different ANN Configurations of Type-4 PMSG

2.5.3 The Selected ANN Model of Type-4 PMSG Wind Generator

After training several ANN configurations, the configuration with the lowest ARMSE (2.7) with a value of 0.0014 was selected. The selected configuration of ANN model for Type-4 PMSG wind generator has four layers i.e. two hidden layers plus input and output layers. The input layer and the output layer have seven and three neurons respectively. Both hidden layers have ten neurons each. The variation of AAE (2.9) of the selected ANN configuration during the training process is shown in Fig. 2.11. The graph shows that the ANN model of Type-4 PMSG wind generator is fully trained for the 10,000 epochs within 1000 training cycles and the deviation from the nonlinear model (Appendix A2) is minimal.

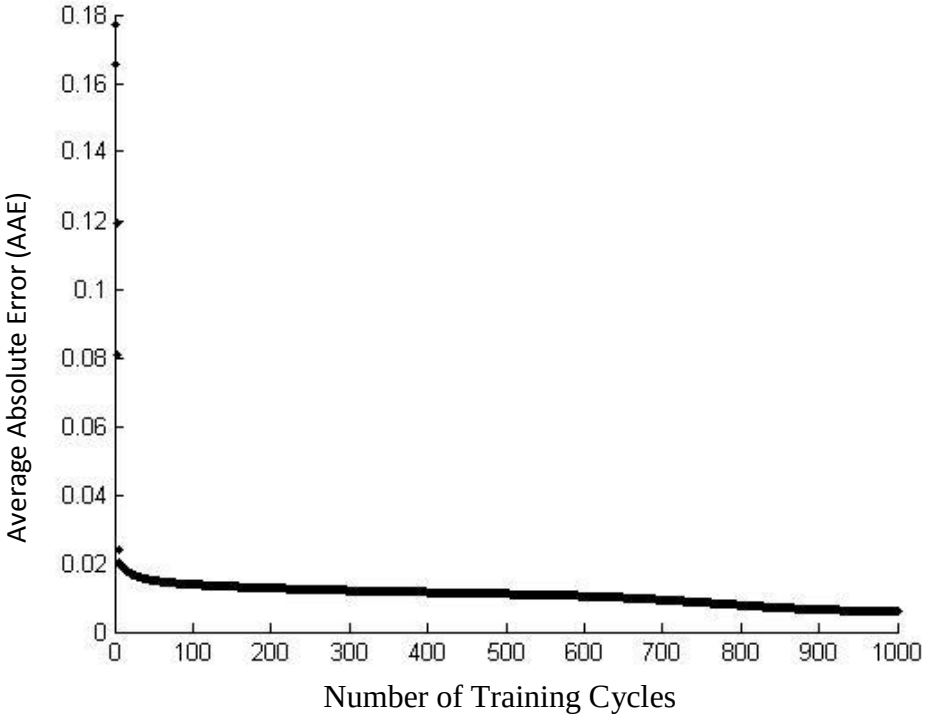

Fig. 2.11. Reduction of Absolute Error over the Number of Training Cycles

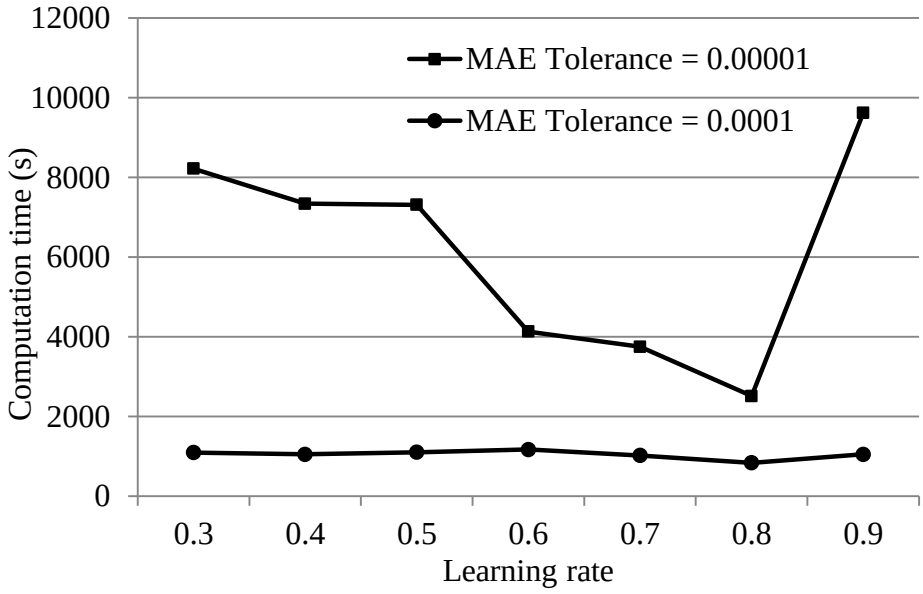

Fig. 2.12. Convergence Time of the Selected ANN Configuration of Type-4 PMSG Wind Generator for Different Learning Rates and Convergence Criteria

2.5.4 Effect of Learning Rate on Training Time

The learning rate (η) and the MAE tolerance have a direct relationship to the training time of ANNs. In order to investigate this relationship, the selected ANN configuration (2 hidden layers with 10 neurons each) was trained with different learning rates and tolerance criteria. The results of this analysis are given in Fig. 2.12. According to the analysis, it is clear that when the optimum learning rate (0.8) is selected, this ANN can be trained considerably faster, even for a tighter convergence criterion.

In this study, it was noticed that as the number of epochs increases, the mapping of solution space has a finer resolution. This improvement is achieved while the ANN size remains invariant. Further, the ANN model of a wind generator provides continuous mapping as it interpolates its training epoch set.

2.6 Summary

ANN models for wind generators were proposed in this chapter. ANN models establish complex mathematical relationships using series of simple mathematical operations. Therefore, as explained in the chapter the input-output relationships of wind generators are established using ANN models. Each wind generator, for which the ANN model needs to be built, should have a proper Epoch Set prepared for ANN training. Epoch sets can be generated by solving the accurate model in the form of a set of nonlinear equations representing wind turbine, generator, and power electronic controllers (Appendix A1 and Appendix A2). If those accurate models are not available, measured input and output data of a wind generator can also be used to form a set of Epochs. Using this set of Epochs, ANN models of wind generators are built using a back propagation training algorithm presented in this chapter. The training algorithm is common for any type and size of wind generator. During this ANN training process, a method to select the best ANN

configuration for a wind generator was guided by parameters such as ARMSE, MAE and AAE.

Details of two wind generator models (Type-3 DFIG and Type-4 PMSG) built in this study were also presented in the chapter. On successful training, these new ANN wind generator models accurately compute output of actual wind generators using series of simple mathematical operations.

Chapter 3

Artificial Neural Network Wind Generator Model Implementations

3.1 Introduction

Chapter 2 shows that the proposed ANN models accurately map nonlinear models of Type-3 DFIG (Appendix A1) and Type-4 PMSG (Appendix A2) wind generators. This chapter presents integration of ANN wind generator models with a power flow analysis algorithm and integration with commercial software such as PSS®E and PSS®SINCAL. Performance of the proposed ANN wind generator models in power flow analysis algorithms is assessed.

The power flow analysis is a study wherein bus power balance equations are solved and bus voltages at all buses are determined using an algorithm such as the ladder iterative technique (see section 1.2.1). This power flow analysis algorithm is iterative and in each iteration, it determines an improved voltage solution. Since wind generator models are functions of terminal voltages, their outputs are recomputed in each iteration. In the past [30][31], those nonlinear accurate models were resolved in every iteration with an improved voltage solution. However, solving those nonlinear models was time consuming and slowed the power flow algorithm significantly. Further, as the number of wind generators increased, nonlinear models of each wind generator were resolved in each power flow algorithm iteration. Thus, an improvement made in wind generator models, which are executed in each iteration, gives a computational improvement in the overall power flow analysis. If many wind generators are modeled in the power flow study, a huge reduction of execution times can be expected.

This Chapter presents power flow analysis with wind generators using the Ladder Iterative Technique [4]. Even though the Ladder Iterative Technique was selected in this

study, these proposed ANN models are equally suitable for use with other methods of power flow analysis. Accuracy of power flow results with the proposed ANN wind generator models are explained in Chapter 3.3 and Chapter 3.4. The main advantage of ANN models is the improvement of execution time and easy integration with commercial power flow analysis software such as PSS®E and PSS®SINCAL. Both accuracy and computational speed of proposed ANN models are compared with those of nonlinear models while using in the Ladder Iterative Technique for power flow analysis. Two separate power flow analysis: (1) with a Type-3 DFIG in Chapter 3.3 and (2) with a Type-4 PMSG in Chapter 3.4 were completed for this assessment. Results of these power flow analysis studies are presented in detail in this chapter.

Another benefit of proposed ANN models of wind generators is the simplicity in computation. After training, ANN models of wind generators provide simple relationship between inputs and outputs. In this case, input comprises wind speed and terminal voltage phasor values. Output comprises real power output values from three phases. This enables easy implementation of ANN models in commercial software. Details of two implementations in PSS®E and PSS®SINCAL are given at the end of this chapter.

3.2 Power Flow Studies with Wind Generators

The IEEE 37-bus test distribution system [56], (Appendix A3) shown in Fig. 3.1, was used to demonstrate the performance of the proposed ANN models of Type-3 DFIG and Type-4 PMSG wind generators. This test system is an unbalanced, three-phase distribution system with unbalanced loads and underground cables. The power balance equations were solved using the ladder iterative technique [4] (Fig. 1.3). All the unbalanced network components were modeled accurately considering their mutual couplings and capacitance elements of all three phases. The three-phase π model has been formulated to represent

series and shunt elements [4]. Appendix A4 provides a detailed model of a network component between node N and M. Relevant [a][b][c][d][A][B] parameter matrices are also given in Appendix A4. These relationships of three-phase voltages and current are used for three-phase power flow studies in this Chapter.

In accurate three-phase power flow studies, wind generators have to be modeled accurately considering all three phases. In order to check performance of different wind generator models, two separate distribution system power flow studies (Study 1 and Study 2) were completed in Matlab considering Type-3 DFIG wind generator and Type-4 PMSG wind generator models respectively. In each power flow study, the proposed ANN wind generator models were compared with corresponding fixed PQ wind generator models and with corresponding accurate nonlinear models (Appendix A1 and Appendix A2) to assess the accuracy of the proposed models and solutions. In both studies it is assumed that a wind generator is connected to bus 775 and that the rating of the transformer XFM-1 (Appendix A3) connected between bus 775 and 709 was modified to match the power generation from the wind generator. In order to magnify the effects of the wind generator, a 1.0 MW per-phase pure active power load was added at buses 730 and 731. These assumptions are similar to those of [30] and [31]. Both ANN models and the nonlinear wind generator models that compute power output are functions of wind speed and three-phase PCC voltage phasors. For fixed PQ models, the power output is estimated externally using the power output curves supplied by the wind generator manufacturer for operating wind speeds and is not a function of PCC voltage. For these power flow studies, the wind speed was assumed equal to 14 m/s for all models.

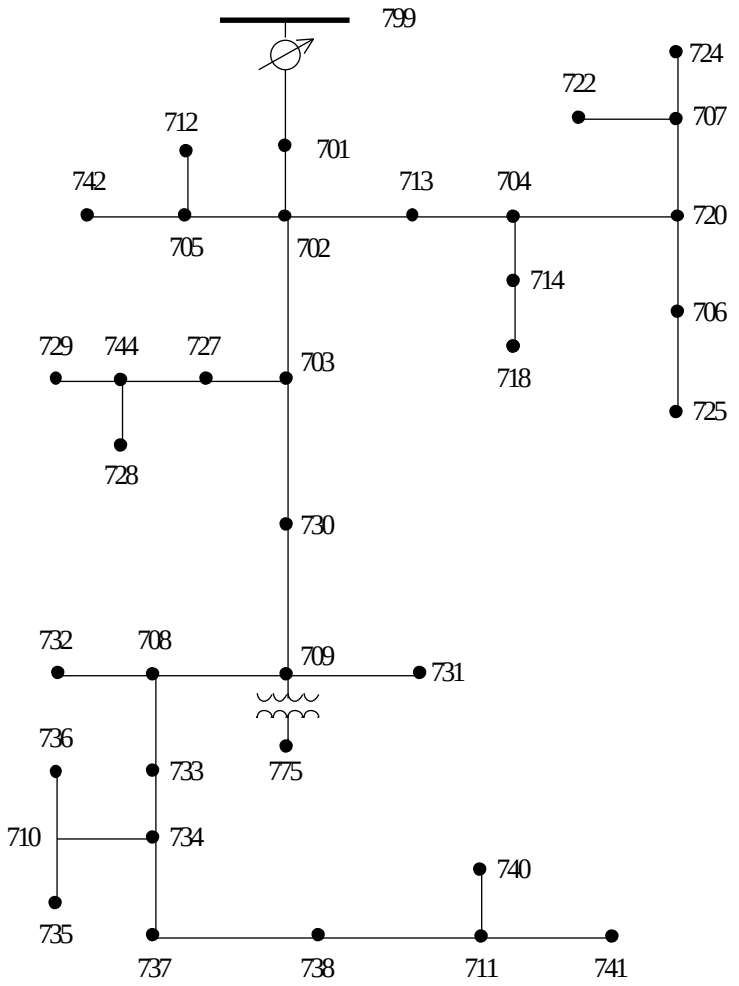

Fig. 3.1. Wind Generator Connection to the IEEE 37-Bus Three-Phase Distribution System

3.3 Study 1: IEEE 37-Bus System with Type-3 DFIG Wind Generator

The details for this power flow study include: (1) the capacity of the transformer XFM-1 was taken as 1.5 MVA (0.5MVA in original IEEE 37-bus test system) (Appendix A3) and the same was considered as the system MVA base, (2) the transformer low voltage side is taken to be 2.4 kV (0.48 kV in original IEEE 37-bus test system). This data is the same as that used in [30]. Three cases with different Type-3 DFIG wind generator models were considered:

Case 1 is a power flow analysis using the accurate nonlinear DFIG wind generator model described in (Appendix A1) and [30]. The wind generator is assumed to operate at unity power factor.

Case 2 is a power flow analysis using a fixed PQ model where generation is treated as a negative real power load of 0.8916 pu for all three phases. Reactive power injection was assumed zero for all three phases.

Case 3 is a power flow analysis using the proposed ANN Type-3 DFIG wind generator model presented in Chapter 2. This ANN model maps unity power factor operation of the nonlinear model [30].

Except for the wind generator models, all other values were the same in all three cases. Wind speed is 14 m/s for all three cases. The nonlinear wind generator model (i.e. model used in Case 1) is considered accurate [30]. Therefore, Case 1 was used as the basis for comparison with the other two cases. The accuracy of the power flow solution using the proposed ANN model was compared with Case 1, revealing a close match of results. Fig. 3.2 shows the deviations of voltage solutions of Cases 2 and 3 of power flow study 1 compared to the voltage solution of Case 1. From the graph, it can be clearly noted that power flow study results of Case 3, using the ANN model of DFIG wind generator, are in very good agreement with those of Case 1 with the nonlinear wind generator model. In

contrast, Case 2 with the fixed PQ model gives the larger error as compared to Case 1. The fixed PQ model has the highest real power output errors compared with the real power output of the nonlinear model. They are 10%, 2% and 6% in P_a, P_b, and Pc respectively. This clearly shows that even though the errors in the voltage solution are small, the corresponding real power solution is significantly inaccurate in the fixed PQ model.

The observed real power output estimation errors in the ANN wind generator model are 0%, 2%, and 0% in P_a, P_b, and P_c respectively. The main advantage of the ANN-based approach is its high accuracy which is comparable to that of the nonlinear models, while it greatly surpasses the nonlinear models in computational speed. The computational speed was obtained on a Window 7 computer with an Intel core 2 duo E7500 processor of 2.93 GHz and 4GB RAM. Table 3.1 shows that the fixed PQ models have the fastest execution times because the power flow program reads those models by loading a simple data file with no further computation. While the ANN model of Type-3 DFIG wind generator has the second best execution time, the nonlinear models have the slowest execution time. Comparing the execution times, it is noted that the ANN model of Type-3 DFIG wind generator is twelve times faster than the nonlinear model. This leads to a much faster execution of the power flow analysis algorithm. In this power flow study, the total execution time was improved by about 40% when the ANN model is used instead of the nonlinear model. Even though the improvement seems to be moderate in absolute terms for this simple system with one wind generator, the improvement will be significant when solving power flow problems of large systems with several wind generators.

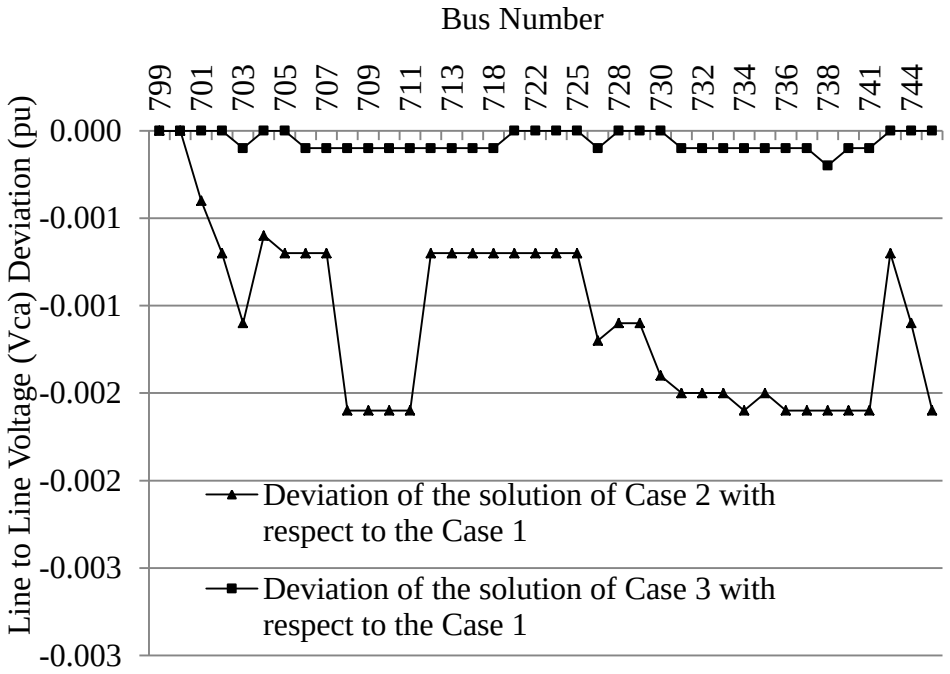

Fig. 3.2. Study 1: Case 2 (PQ Model) & Case 3 (ANN Model) Bus Voltage Deviations from the Voltage Solution of Case 1 (Accurate Nonlinear Model)

Table 3.1. Execution Times with Type-3 DFIG Wind Generator Models

	Fixed PQ	Nonlinear	ANN
Time taken for executing the model once (ms)	0.0020	59.9713	4.9915
Number power flow iterations	10	11	10
Average execution time taken for the LIT power flow study (s)	0.9831	1.8789	1.1302

3.4 Study 2: IEEE 37-Bus System with Type-4 PMSG Wind Generator

The details of this power flow study are as follows (same as given in [31]): (1) the capacity of the Type-4 PMSG wind generator, system power base and the rating of XFM-1 are 2 MVA, (2) the generation voltage is 575 V (the low side voltage rating of XFM-1). Similar to the previous comparison, three cases were considered with different Type-4 PMSG wind generator models and the results are compared. Wind speed is 14 m/s for all three cases below.

Case 1 is a power flow analysis using the accurate nonlinear wind generator model described in [31]. Reactive power output is assumed zero for all three-phases.

Case 2 is a power flow analysis using a fixed PQ model where generation is treated as a negative real power load of 1.0 pu for all three-phases. Reactive power injection was assumed zero for all three phases.

Case 3 is a power flow analysis with the proposed ANN Type-4 PMSG wind generator model given in Appendix A2. This ANN model maps the unity power factor operation of the nonlinear model of [31].

Fig. 3.3 shows the deviations of voltage solutions of Cases 2 and 3 in power flow study compared to the voltage solution of Case 1, which is the most accurate solution. It can be clearly seen that power flow analysis results of Case 3 using ANN model of Type-4 PMSG wind generators is in very good agreement with accurate results of Case 1 using the nonlinear wind generator models (Fig. 3.3). In contrast, Case 2 with the fixed PQ models gives the larger error as compared to Case 1.

Real power output estimation errors in P_a, P_b, and P_c (compared with the nonlinear model) are: 6%, 4% and 2% respectively for the fixed PQ model, and 2%, 1% and 1% for the ANN wind generator model. On making execution-time based performance comparison, the proposed ANN model for Type-4 PMSG wind generator is much faster

than the corresponding nonlinear model (Table 3.2). The computational speed was obtained on a Window 7 computer with an Intel core 2 duo E7500 processor of 2.93 GHz and 4GB RAM.

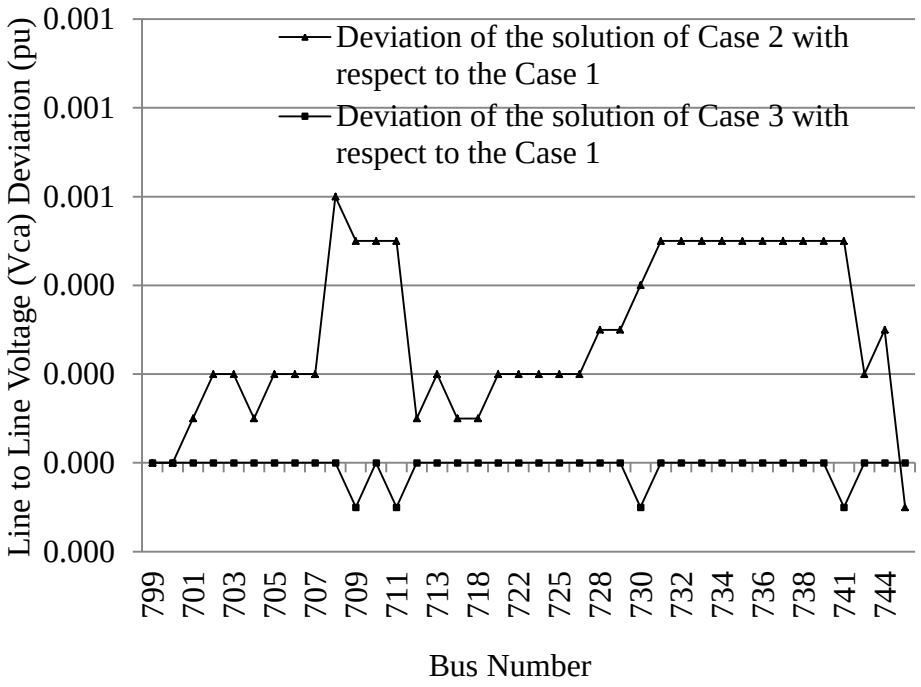

Fig. 3.3. Study 2: Case 2 (PQ Model) & Case 3 (ANN Model) Bus Voltage Deviations from the Voltage Solution of Case 1 (Accurate Nonlinear Model)

Table 3.2. Execution Times with Type-4 PMSG Wind Generator Models

	Fixed PQ	Nonlinear	ANN
Time taken for executing the model once (ms)	0.0020	66.5356	3.4714
Number of power flow iterations	10	10	10
Average execution time taken for the LIT power flow study (s)	1.0023	1.8443	1.0286

3.5 ANN Model Implementation in PSS®E and PSS®SINCAL

From Fig. 3.2 and Fig. 3.3, and Table 3.1 and Table 3.2, it is clear that the ANN models of Type-3 DFIG and Type-4 PMSG wind generators are as accurate as nonlinear models and much faster than the nonlinear models. Further, as shown in Chapter 2, the ANN model can be built for any type or size of wind generator without extra effort. The only requirement is the complete data set presented and illustrated in Chapter 2.

An important benefit of the proposed ANN models is their ready integration into popular commercial power system analysis software. To investigate the flexibility of implementation in commercial power flow software, the ANN model of Type-3 DFIG wind generator explained in Chapter 2 was coded using python script language in Power System Simulator for Engineers (PSS®E) software. The PSS®E is a transmission system planning tool which calculates network states assuming the single line equivalent network. But the ANN Type-3 DFIG wind generator model described in Chapter 2 was built considering a three-phase system. To overcome this incompatibility a positive sequence phasor system was generated using the voltage solution of PSS®E power flow iteration. Then the generated positive sequence voltage phasor system was fed to the ANN model of Type-3 DFIG wind generator. At end of each power flow iteration, bus voltages are updated and hence the power output from the wind turbine is updated (Fig. 3.4). The ANN model of Type-3 DFIG wind generator described in Chapter 2 was implemented in a hypothetical test system which signifies the effect of wind generator. This implementation was verified by establishing identical results in the Matlab environment using the ANN model of Type-3 DFIG wind generator. Fig. 3.5 shows variations in the output of the ANN model of Type-3 DFIG wind generator with PSS®E voltage solution. The power flow solution process converged and the ANN model of Type-3 DFIG wind generator stabilized at 0.8908 pu as its active power output.

The same ANN model of Type-3 DFIG wind generator was implemented in PSS®SINCAL, which can solve three-phase unbalanced distribution system power balance equations. The ANN model of Type-3 DFIG wind generator was coded as a Windows Script macro in PSS®SINCAL. The real power output mismatch of the ANN model of Type-3 DFIG wind generator at the end of each power flow iteration is shown in Fig. 3.6 . When the voltage solution converges, the outputs of the ANN model also stabilizes. These implementations are possible because the ANN model does not require any complex solvers or optimization techniques to estimate the power outputs. The same cannot be accomplished using the accurate nonlinear models of Type-3 DFIG presented in Appendix A1 or Appendix A2

These implementations proved the simplicity of adopting the ANN models of wind generators for any practical power flow study. It further revealed that the ANN model of Type-3 DFIG wind generator can be adapted to any system, even for those where actual manufacturer data is not available. In that case the ANN model is built using the measured inputs-outputs of the wind generator and integrated into the power flow analysis software using simple programming code.

Further, it is important to point out that, on testing the proposed ANN wind generator model, it has not caused any algorithmic stability issues with the Ladder Iterative Technique or other power flow solution techniques including the Newton Raphson and Gauss-Seidel methods used in PSS®E and PSS®SINCAL.

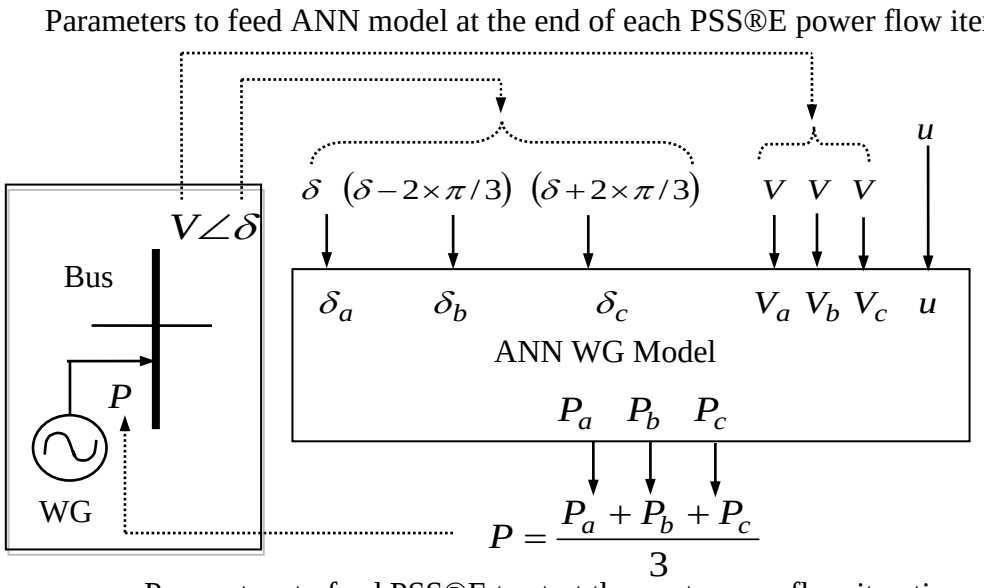

Fig. 3.4. Snapshot of Each PSS®E Power Flow Iteration

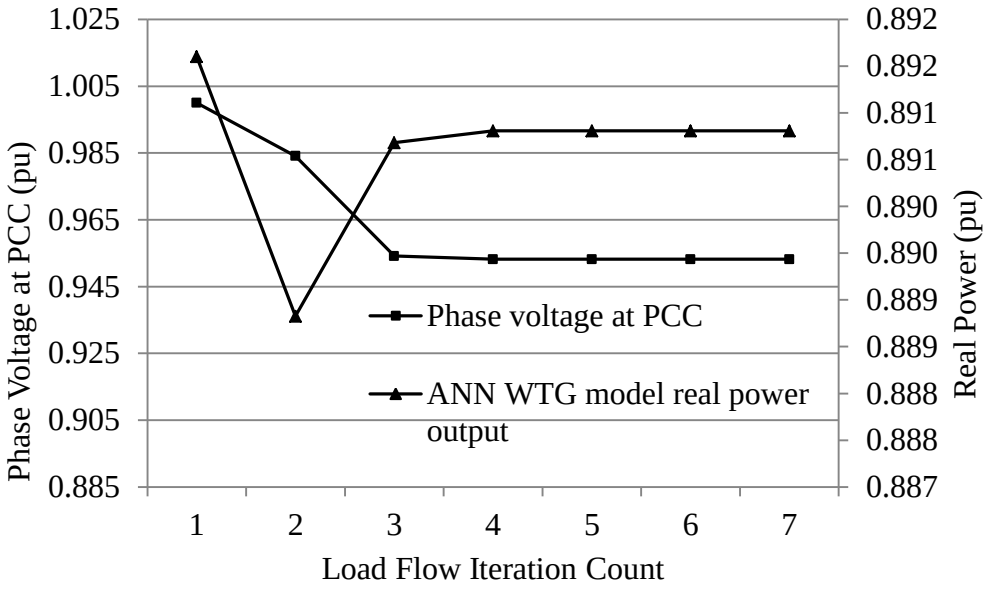

Fig. 3.5. Variation of Real Power Output of ANN Wind Generator Model in PSS®E

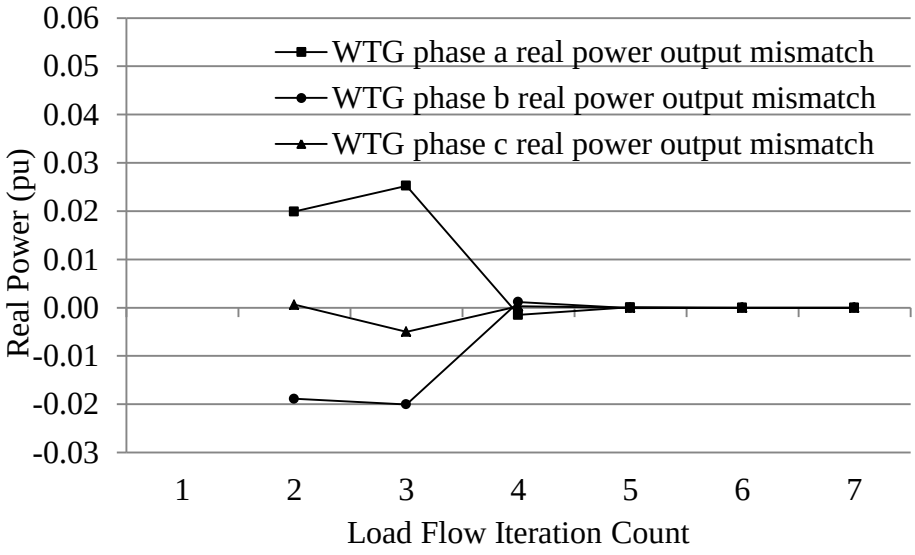

Fig. 3.6. Variation of Three-Phase Real Power Output Mismatch of ANN Wind Generator Model in PSS®SINCAL

3.6 Summary

This Chapter reports the performance of ANN wind generator models and demonstrates their ready integration into popular commercial power system analysis software. These ANN models are: (1) three-phase models as accurate as the true nonlinear models that are functions of wind speed and terminal voltage phasors, (2) suitable for unbalanced three-phase systems, (3) much faster than conventional nonlinear models, (4) universal hence they can be trained to model any type or size of wind generators and (5) readily extendable to model wind generators without nonlinear models using measured data.

The ANN models presented in Chapter 2 are implemented in power flow algorithms in Matlab, PSS®E and PSS®SINCAL. Comparing accuracy of results of the power flow studies with fixed PQ models that are a function of wind speed, nonlinear accurate models and ANN models, it can be seen that ANN models give very accurate solutions that are very close to those of the nonlinear models. Furthermore, ANN wind generator models are computationally ten times faster than nonlinear wind generator models. The fast execution of ANN wind generator models improves the overall execution time of the power flow algorithm by at least 40%, as demonstrated when testing with a small distribution system with one wind generator. This improvement will be very significant for larger systems with several wind generators.

Further, these ANN wind generator models have been demonstrated to be easily implemented in commercial software packages such as the PSS®E and PSS®SINCAL which only require minimal integration effort entailing only a few lines of coding.

Chapter 4

Probabilistic Voltage Solution Method for Distribution Systems with Wind Electric Generators

4.1 Introduction

Forecast of loads and wind power are probabilistic. These forecasts comprise a mean value and a probabilistic distribution function. In power system planning exercises, *probabilistic power flow* plays an important role by determining probabilistic estimates of voltages and line flows considering these probabilistic models of loads and wind power. With significant integration of wind power with distribution systems, probabilistic power flow assumes importance.

In this Chapter uncertainty in the distribution system voltage is considered as dependent upon the uncertainty of loads and wind generation in the distribution system. Thus probabilistic distribution functions of loads and wind generation are used to generate a probable event space. With this approach, the complete event space is considered for estimating the probability distribution of voltage solutions of all buses. This approach is presented in this Chapter.

4.2 Probabilistic Modeling of System Loads

Variations of load at bus N (PD_N) are modeled assuming a normal probability distribution function with respective mean values and variance values. Standard deviation (σ_N - square root of variance) is the same for all the load buses. This is a reasonable assumption considering the geographical proximity of load buses in a distribution system. The Probability Density Function (PDF) of PD_N at bus N is defined below (4.1):

$$\rho_N(PD_N) = \frac{1}{\sqrt{2\pi\sigma_N^2}} . e^{-(PD_N - \hat{PD}_N)^2 / 2\sigma_N^2} \quad (4.1)$$

where $\rho_N(PD_N)$ is the value of probability density for a real power demand PD_N with the mean value of $\hat{PD}_N$. The PDF of PD_N within the interval of $PD_N \pm 3.\sigma_N$ has a probability of 0.997. This interval is divided into ND sections having equal widths. The probability and the average power demand of section ψ are $pd_{N\psi}$ and $PD_{N\psi}$ respectively. Considering ND number of pairs ($PD_{N\psi}$, $pd_{N\psi}$) approximately represents the PDF of the load at bus N. When load buses are in the same distribution system loading activities are similar in all buses. As an example, the type of loads in the distribution system could be households. When ND and σ_N are the same for PDFs of all the load buses, the probability of ψ^{th} section of any two buses N and M are equal ($pd_{N\psi} = pd_{M\psi}$). Then, in general, it can be denoted as pd_ψ. This allows modeling of PDFs of all loads using ($PD_{N\psi}$, pd_ψ) pairs for ψ varying from 1 to ND and N varying from 1 to NLB (number of load buses). Fig. 4.1 gives a graphical view of the above formulation.

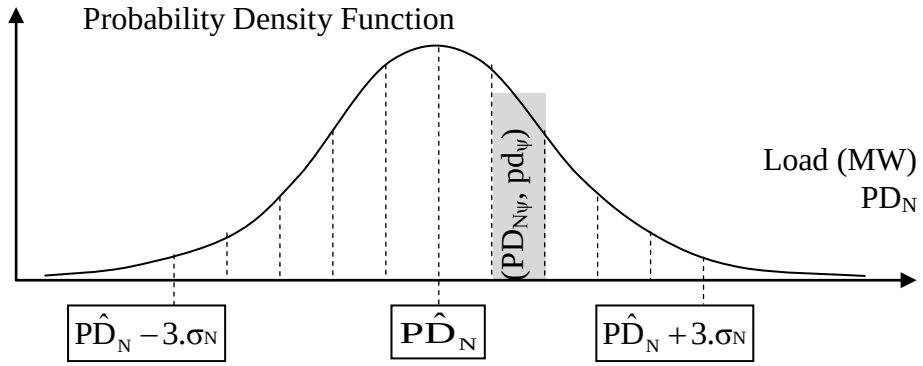

Fig. 4.1. Probability Density Functions of the Annual Load Demand (Standard Normal Distribution)

4.3 Probabilistic Modeling of Wind Generators

The annual wind speed varies randomly having Weibull probability distribution function (4.2) [57] as shown in Fig. 4.2

$$\rho_N(U_N) = \left(\gamma / \beta_N{}^{\gamma}\right) U_N^{\gamma-1} . e^{-(U_N/\beta_N)^{\gamma}} \tag{4.2}$$

where U_N is the wind speed in m/s. The shape and scale parameters are γ and β_N respectively, defining the shape of the probability distribution. The peak of the probability distribution occurs at its mean speed $\hat{U}_N$. The shape parameter is the same for all buses due to the geographical proximity among buses. Scale parameter β_N is determined for the wind generator connected to the N^{th} bus. Considering the variance of U_N (ξ_N), the interval [0 to $(\hat{U}_N + 3.\sqrt{\xi_N})$] is divided to NW sections as shown in Fig. 4.2. The area of q^{th} section represents the probability (pw_{Nq}) that wind speed lies within the speed range of this section. The mean wind speed of the range is denoted as U_{Nq}. This notation allows modeling the Weibull distribution of wind speed by NW pairs (U_{Nq}, pw_{Nq}). The shape parameters of probability distributions are the same for geographically close wind generators. The scale parameters are the same for all the turbines when they are identical. Due to this reason the areas of q^{th} section of PDFs at bus N and bus M are same. Therefore, in general the pair of values is written as (U_{Nq}, pw_q).

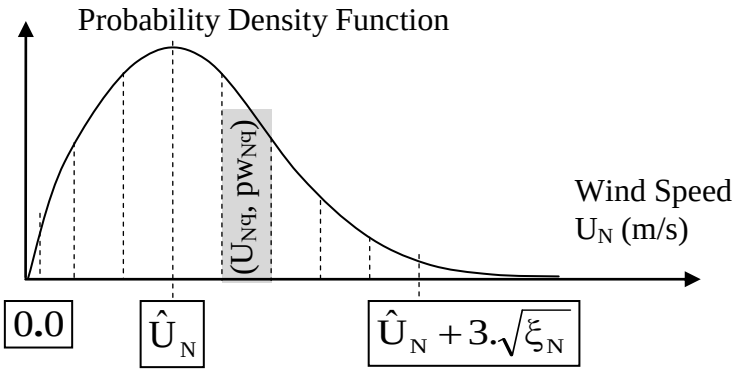

Fig. 4.2. The Probability Density Function of Annual Wind Speed Variations (Weibull Distribution).

The cubic relationship between wind power generation and the wind speed is used to estimate the wind power generation PG_N for any wind speed U_N. Wind power supply at N^{th} bus is considered as a negative load at bus N. It is considered that wind generators have their own reactive power sources and hence the net reactive power supply from any wind generator is zero. With this formulation probabilistic wind power generation of N^{th} bus is modeled as NW pair of ($-PG_{Nq}$, pw_q).

4.4 Joint Probabilistic System Model

Considering the ψ^{th} section of PDFs of all buses, the common probability of occurrence is pd_ψ with each bus having its own load. This can be represented by the data set: {($PD_{1\psi}$, $PD_{2\psi}$, $PD_{3\psi}$, ….. $PD_{NLB\psi}$), pd_ψ}. Setting SPD_ψ equal to the set of bus-wise loads in the whole system with a probability of pd_ψ, SPD_ψ = ($PD_{1\psi}$, $PD_{2\psi}$,….. $PD_{NLB\psi}$). In order to capture full probabilistic nature ψ varies from 1 to ND.

Similarly considering the q^{th} segment of PDFs for all the wind generator outputs, they can be represented by the data set: {($-PG_{1q}$, $-PG_{2q}$, $-PG_{3q}$,…. $-PG_{NGq}$), pw_q} where q varies from 1 to NW. Setting SPG_q equal to the set of wind generator outputs in the whole system with a probability of pw_q, SPG_q = ($-PG_{1q}$, $-PG_{2q}$, $-PG_{3q}$,…. $-PG_{NGq}$).

Now consider the ND occurrences of bus-wise loads and NW occurrences of wind speeds as independent probabilistic events. It gives rise to ND x NW combinations of loads and generations. For the occurrence of ψ^{th} load and q^{th} generation segments, the probability equals: (pd_ψ.pw_q). Thus $(\psi,q)^{th}$ event, $E_{(\psi,q)}$, has a load/generation data set of ($PD_{1\psi}$, $PD_{2\psi}$, $PD_{3\psi}$,…, $PD_{NLB\psi}$, $-PG_{1q}$, $-PG_{2q}$, $-PG_{3q}$,…, $-PG_{NGq}$) and a probability of (pd_ψ. pw_q). The summation (pd_ψ.pw_q) over ψ and q gives the total probability of the joint distribution and it is equal to unity. Therefore, the joint event space covers the total sample space.

It is common that the variations of loads over a year are expressed using Load Duration Curves (LDC) as shown in Fig. 4.3 for the load at bus N. This LDC considers NH segments in its model. At any given time in a segment, the Load Factor (LF) is defined as the ratio between the actual load delivered and the mean forecasted load at the bus.

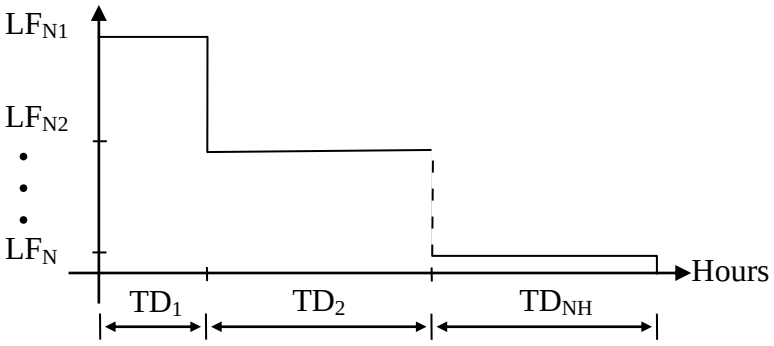

Fig. 4.3. Forecasted Load Duration Curve at N^{th} Bus.

Considering the mean forecasted real power demand $\hat{PD}_N$ and load factor in t^{th} period (LF_t), the average real power demand in t^{th} period can be written as below:

$$LF_t \cdot \hat{PD}_N \tag{4.3}$$

The average real power demand for any period t ($LF_t \cdot \hat{PD}_N$) is forecasted using historical load patterns. The real power demand ($\hat{PD}_N$) varies in its neighborhood and that is defined by the variance of forecasted load. In a planning exercise, the reactive power demand is assumed to be proportional to PD_N and the constant power factor is assumed to be equal to PF.

For the LDC segment #1 (t=1), ND x NW probabilistic combinations exist. Referring to Fig. 4.4, each of these combinations relate to a cube in the top most layer. The two horizontal axes (ψ = 1 to ND and Ψ = 1 to NW) account for these ND x NW combinations. Effecting the LDC factors of LF_1, LF_2, …, LF_{NH}, NH layers with each layer having ND x NW combinations of loads/generations are created. A visual image of these load/generation combinations totaling to ND x NW x NH is shown in Fig. 4.4.

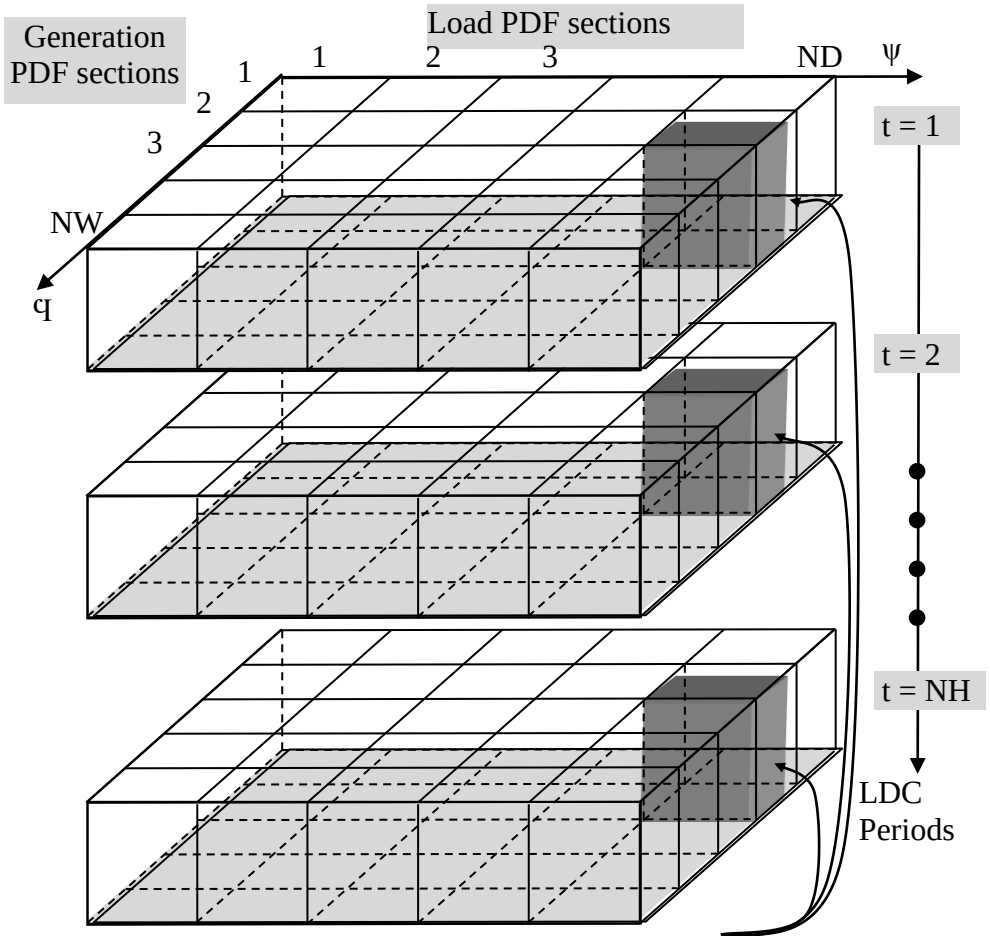

Shaded cubes represent $(\psi,\mathrm{Ч})^{th}$ event (ψ=5, Ч=2) of load and generation with a probability of (pd_5 . $pw_{2)}$ for all the LDC periods.

Fig. 4.4. Event Space of Joint Probability Distribution.

4.5 Distribution System Model

Power distribution system model proposed in [3] has a set of 3(NB-1) equations and the solution algorithm [3] converges to an accurate solution. For the event $E_{t\ (\psi,\varphi)}$ corresponding to the t^{th} segment of the LDC and (ψ,φ) PDF sections, the system of equations can be written as below (4.4)-(4.6).

Voltage equation:

$$F\Lambda(\Lambda_{t\ (\psi,\varphi)}, P_{t\ (\psi,\varphi)}, Q_{t\ (\psi,\varphi)}) = 0_{(NB-1)x1} \quad (4.4)$$

Power balance equations for real power (4.5) and reactive power (4.6):

$$FP(\Lambda_{t\ (\psi,\varphi)}, P_{t\ (\psi,\varphi)}, Q_{t\ (\psi,\varphi)}) = LF_t \,.\, SPD_\psi - SPG_\varphi \quad (4.5)$$

$$FQ(\Lambda_{t\ (\psi,\varphi)}, P_{t\ (\psi,\varphi)}, Q_{t\ (\psi,\varphi)}) = LF_t \,.\, PF \,.\, SPD_\psi \quad (4.6)$$

where: $\Lambda_{t\ (\psi,\varphi)}$ is a vector of square of magnitude of bus voltage ($V_{t\ (\psi,\varphi)}$), $P_{t\ (\psi,\varphi)}$ is the vector of real power injections from buses and $Q_{t\ (\psi,\varphi)}$ the vector of reactive power injections from buses relevant to $E_{t\ (\psi,\varphi)}$.

This system of equations (4.4) – (4.6) is solved using first order Newton-Raphson technique [3]. This formulation gives an accurate solution for the system of power balance equations and was tested with a test system as reported in the next section. It is used to determine the voltage solution to each cube in Fig. 4.4. Correlating those voltage solutions with probabilities of occurrence, the PDF of bus voltages is recreated in the next section.

4.6 Estimation Procedure – Voltage Distribution

For a given LF_t value, the t^{th} layer of Fig. 4.4 has ND x NW cubes each representing a load and generation combination. The $(\psi,\Psi)^{th}$ cube with a probability of pd_ψ x pw_Ψ ($E_{t\ (\psi,\Psi)}$ event) can be analysed by solving (4.4) – (4.6). Taking square roots of $\Lambda_{t\ (\psi,\Psi)}$ the voltage solution relevant to $(\psi,\Psi)^{th}$ cube for all buses is estimated. The probability of the voltage solution of $E_{t\ (\psi,\Psi)}$ is given by (pd_ψ x pw_Ψ). Collating all the ND x NW solution for a given t^{th} LDC segment gives a probabilistic voltage solution. This process of collation is explained below.

Considering N^{th} bus in the t^{th} LDC segment, there are ND x NW voltage values. If several of those voltage values are equal, their probability values are added. Otherwise a unique voltage solution and respective probability is considered as a section of the PDF of voltage. The pair of solutions for the PDF section ϑ is ($V_{N\,t\,\vartheta}$,$pv_{N\,t\,\vartheta}$). These probabilities are then converted to PDF values by dividing by the corresponding section widths (4.8). These section widths are estimated using the mid points of voltages of PDF sections. Fig. 4.5 shows this process.

$$\rho_{N\,t}(V_{N\,t}) = \frac{pv_{N\,t\,\vartheta}}{wd_\vartheta} \tag{4.8}$$

A standard normal curve is fit to the resultant PDF, minimizing root mean square (RMS) errors at all PDF points. This gives the probabilistic voltage solution for bus N in the t^{th} segment of the LDC. Similarly probabilistic solutions of bus power injections ($P_{N\,t}$ and $Q_{N\,t}$) are also estimated for all buses. Through the above procedure, they are collated into normal distributions that yield mean values and standard deviations.

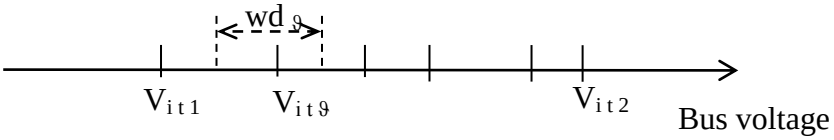

Fig. 4.5. Event Space of Joint Probability Distribution

4.7 Test System and Results

With this formulation, a 70-bus distribution system [58] (Appendix A5) was solved. The system data were altered in order to accommodate necessary wind generators and the LDC. Five wind turbines having 500 kW capacities each were connected to buses: 15, 25, 31, 42 and 62. The net reactive power supply by these wind generators was zero. The LDC had three periods with LF values of 1.0, 0.625 and 0.42. The system load and wind generation were modeled with ten probability states for both ND and NW. The variance of the system load was 10% of the average forecasted load in the 70-bus data set. The value of the shape parameter was taken as 2.0, complying with the range of values estimated in [59]. The scale parameter was 6.006.

Following the procedure outlined in Chapter 4.2, Chapter 4.3 and Chapter 4.4, data sets were created and solved. The procedure in Chapter 4.6 was used to create the solutions' PDF parameters.

Table 4.1 shows mean and standard deviation values of fitted normal curves for all buses considering a three-segment LDC. Fitted three PDFs for $\hat{V}_N$ of voltage solutions V_N give the complete variation of bus voltage at bus N. Similarly, the complete variations of P_N and Q_N are obtained using fitted PDFs. From the case study it was found that normal probability distributions can be fitted to the estimated PDFs with minimal deviations. This finding matches with the assumption of Gaussian probabilistic distribution for system voltage and power flows in [36].

Table 4.1 shows $\hat{V}_N$, $\hat{P}_N$, $\hat{Q}_N$ and respective standard deviations for the selected set of buses at all three LDC periods. Buses which are closer to the substation (such as bus 30, 40 and 50) have lesser variation of bus voltages. This phenomenon is intuitively expected as the high voltage bus of a distribution substation generally exhibits stable voltage condition.

Therefore standard deviation of voltage is low at buses along a feeder closer to the substation compared with other buses. It can also be validated from the standard deviation results given in Table 4.1.

Table 4.1. Mean Values and Standard Deviations of V, P and Q for Selected Buses

Bus	$\hat{V}_N$	σ_{VN}	$\hat{P}_N$	σ_{PN}	$\hat{Q}_N$	σ_{QN}
t=1, LF_1 = 1.0						
10	0.964	0.019	1.410	0.690	1.410	0.064
20	0.925	0.059	0.439	0.326	0.439	0.021
30	0.999	0.002	0.274	0.324	0.274	0.013
40	0.999	0.001	0.358	0.325	0.358	0.017
50	0.993	0.001	0.457	0.017	0.457	0.017
60	0.897	0.031	1.979	0.321	1.979	0.092
69	0.957	0.026	0.034	0.001	0.034	0.001
t=2, LF_2 = 0.625						
10	0.984	0.017	0.582	0.656	0.582	0.039
20	0.967	0.056	0.133	0.324	0.133	0.013
30	1.000	0.002	0.030	0.324	0.030	0.008
40	1.000	0.001	0.083	0.324	0.083	0.010
50	0.996	0.000	0.291	0.011	0.291	0.011
60	0.948	0.027	1.182	0.340	1.182	0.057
69	0.982	0.024	0.021	0.001	0.021	0.001
t=3, LF_3 = 0.42						
10	0.990	0.018	0.136	0.642	0.136	0.026
20	0.990	0.055	-0.036	0.323	-0.036	0.009
30	1.000	0.002	-0.105	0.323	-0.105	0.005
40	1.000	0.001	-0.070	0.323	-0.070	0.007
50	0.997	0.000	0.194	0.007	0.194	0.007
60	0.967	0.028	0.660	0.326	0.660	0.038
69	0.989	0.025	0.014	0.001	0.014	0.001

4.8 Summary

This study presents a simple probabilistic technique to evaluate the probabilistic variation of bus voltages and power flows in a planning exercise. Further, it explains the process of converting PDFs to probability values considering the area of the PDF section. Due to the formulation of probabilistic sections with the same probability values at all buses, complexity is largely reduced. It reduces the event space and hence the number of power flow computations. After estimating the probability values and system parameters for each event, the PDFs of the solution are derived. The case study demonstrates the simplicity of the proposed method. Further, it is observed that the standard normal distributions can be approximated successfully for probabilistic system solutions. Mean values and standard deviations can be estimated for all the buses.

Chapter 5

Economic Models for Integration of Wind Energy - Wind Generators Cooperative

5.1 Introduction

Uncertainty and intermittency of wind power poses both technical and economic challenges. The last chapter addressed technical challenge associated with uncertainty of wind power. This chapter addresses economic challenges posed by uncertainty and intermittency of wind power.

This chapter proposes a cooperative model for wind generators that can be used to minimize effects of uncertainty and intermittency of wind power output while maximizing economic returns from the sale of wind energy. The proposed model is named the Wind Generator Cooperative (WGC) model. By this model a market operation mechanism is proposed to realize the benefits of coalition of wind farms which was explained in the context of game theory in [47]. The proposed WGC model aims to provide three main benefits to the participating wind farms:

Minimized effect of uncertainty: Uncertainty in availability of wind energy decreases the ability of wind generators to bid correct amounts of energy into competitive electricity markets and exposes them to risks from potential failure to deliver the bid amounts of energy. The WGC model aggregates output of its wind farms and the resultant **smoothing effect** tends to reduce the net uncertainty of the WGC's power output. Further, the WGC model collectively uses a few pumped-hydro energy storage systems to minimize uncertainty.

Energy arbitrage: Availability of wind energy is a function of nature (usually high at night in Ontario) whereas electricity demand occurs on desire in a 24-hour period (usually high in the day time). As demand correlates with marginal price, in the proposed model,

wind energy generated during low price (night) hours is stored in pumped-hydro stations and is released during high price (day) hours. The collective ability of a WGC to procure energy storage services is more.

Capacity credit (minimize effect of intermittency): Due to the combined operation of many wind farms, as a WGC, a percentage of power capacity is always available (firm capacity). The remaining non-firm portion of power output is intermittent. Wind generators get the benefit of this firm power capacity. These benefits are achieved by operating wind farms cohesively and with pumped-hydro storage facilities.

In the proposed WGC model, return from the sale of energy will come from: (a) sale of the variable (intermittent) power component, and, (b) sale of the firm power component. Further, costs shall be incurred due to use of: (a) storage, (b) use of transmission system, and, (c) costs of administering the WGC. The proposed model is for a year, where forecasted wind energy is taken as the input, and the output of the WGC and energy storage systems are optimized to maximize profits of the WGC and its constituent wind farms.

A test study of the WGC model comprising a set of ten wind farms based on southern Ontario (Canada) is described in a later section of this chapter. The test study reveals that the WGC model is economically profitable, practical and an attractive market model that incentivizes voluntary participation of wind farms. In order to check the validity of the test study results, sensitivities to four important parameters were studied. These parameters include: expected uncertainty, smoothing effect, electricity market price and cost of storage systems (pumped-hydro). Results of the sensitivity studies prove the validity of the proposed WGC model.

5.2 The WGC Model and Its Operation

A WGC, comprised of many wind farms, aims to minimize uncertainty and variability by collective operation. All wind farms have the same contract with the WGC that defines their operational role inside the WGC. The WGC purchases reserves to be shared among its participants. These reserves may be procured from any type of reserve service provider such as thermal generators, pumped-hydro companies, etc. In this study, it is assumed that the WGC purchases reserves from pumped-storage companies to manage uncertainty due to their attractive benefits mentioned in Chapter 1.2.5. The WGC contracts with pumped-storage companies by considering hydro usage, storage capacity limits and other operational aspects. In this study, a generic formulation of the WGC model is presented irrespective of the number of participating wind farms and the number of contracted pumped-hydro storage companies. In this study, it is assumed that wind generators and pumped-hydro stations are existing elements of a power system and are feasibly connected to the power network. The cost of any connection-related network infrastructure is already included in their contracts with the WGC. A schematic diagram of the proposed WGC model is shown in Fig. 5.1.

The operating principle of the WGC is as follows: the WGC optimally schedules the total energy from all the wind farms to sell a portion to the market and store the rest into its contracted energy storage (pumped-hydro) systems. Optimization also considers uncertainty of wind forecast and retains a reserve in the storage for underproduction (stored energy) and overproduction (capacity to store). This helps to overcome uncertainty in wind power output. The WGC model optimizes the output from the WGC, energy stored in the pumped-hydro systems, the portion of energy sold as firm supply (PCF) with revenue RVCF and the portion of energy sold as variable supply (PCV) with revenue RVCV. The model considers costs associated with storage/retrieval of energy (CST), cost of

transmission (CT) and cost of administration (CA) during optimization. The financial cash flow mechanism is shown in Fig. 5.2.

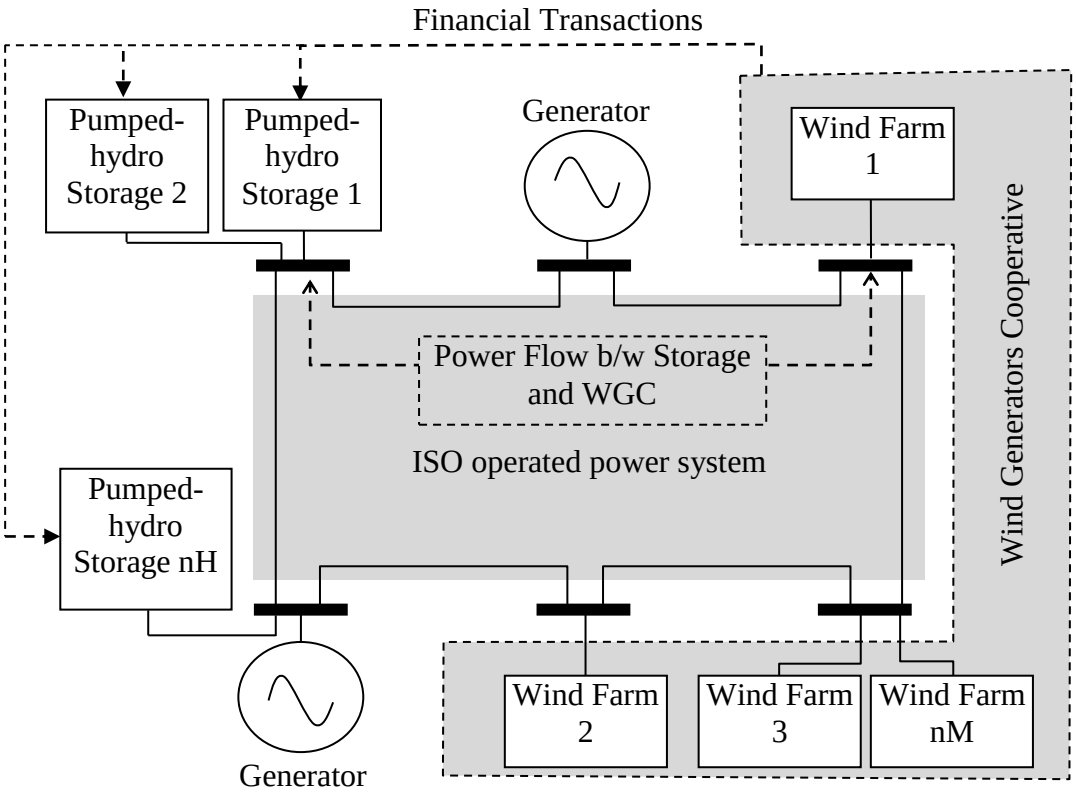

Fig. 5.1. Wind generators Cooperative Model Showing the Power Flows

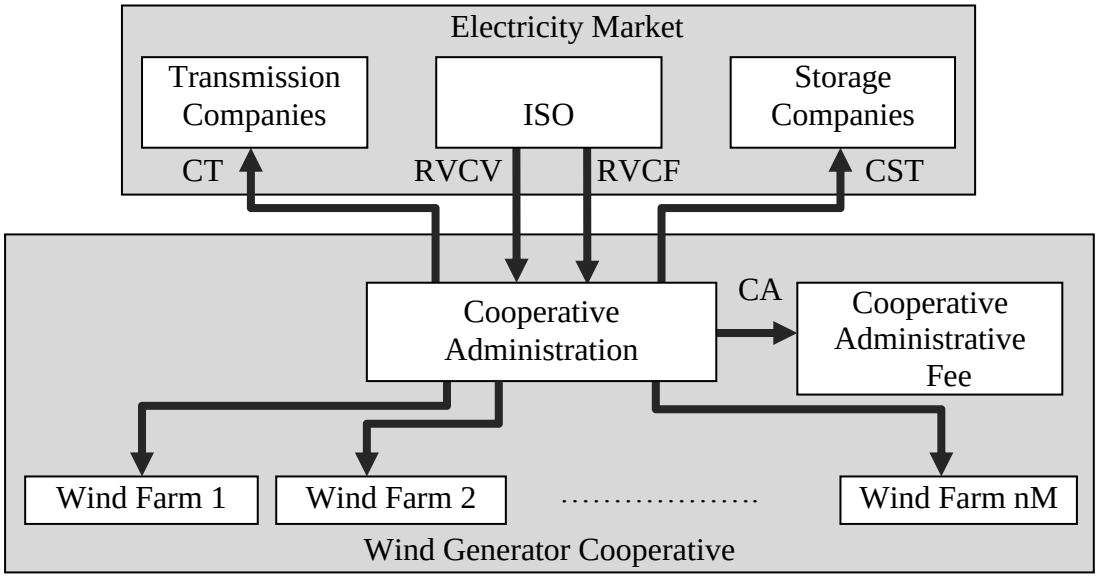

Fig. 5.2. Wind Generators Cooperative Model Showing the Funds Flow

5.2.1 Firm and Variable Power Components

By forming a WGC, the benefit of capacity credit of wind farms is harnessed as follows: owing to the uneven wind conditions and spatial distribution of wind farms, a part of the WGC wind power capacity has high availability. The probability of having zero outputs in all wind farms simultaneously is very small. Even in such a situation, contracted pump-storage systems can make up any shortfall to meet the required generation capacity. As a result, a percentage of power capacity of the WGC is always available irrespective of the wind availability. The rest of the generation capacity varies with time. The firm generation (always available) capacity is capable of attracting better revenue.

However, producing high amount of firm power may be costlier compared with variable power because it requires the operation of pumped-storage facilities. Therefore, the optimum amount of firm power needs to be determined. The WGC model formulation optimizes these values over a year such that the net revenue for the WGC and thus participating wind farms is maximized.

The complete mathematical formulation of the optimization problem and the methodology of sharing costs and benefits are given in Chapter 5.3.

5.3 Mathematical Model Formulation

5.3.1 Optimization Problem

The problem is formulated for a year with nS seasons, nDs days for each season ‘s’, and nT hours for each day (24 hours).

The net average water flow (excluding pumped-up water) into the storage (WFA), reserve storage capacity (WSR), uncertainty of the WGC (σ_{WGC}), sum of firm power bids (PCF) and their prices (BF) are seasonal parameters. All other parameters are expressed for each bidding period.

Objective: Maximize the returns from sale of energy (variable component: RVCV and fixed component: RVCF) to the electricity market while minimizing cost of storage (CST):

(RVCV+RVCF-CST) =

$$\sum_{s}^{nS}\sum_{d}^{nDs}\sum_{t}^{nT} PCV_{s,d,t} \cdot BV_{s,d,t} + \sum_{s}^{nS}\left(PCF_{s} \cdot \sum_{d}^{nDs}\sum_{t}^{nT} BF_{s,d,t} \right) - \sum_{s}^{nS}\sum_{d}^{nDs}\sum_{t}^{nT} CST_{s,d,t} \quad . \tag{5.1}$$

Constraints:

Power bid capacities are restricted to a percentage of hourly system load:

$$PCV_{s,d,t} \leq PLoad_{s,d,t} \quad \forall\, t,d,s \ . \tag{5.2}$$

Power balance of the WGC: $PCV_{s,d,t} + PCF_{s} = PS_{s,d,t} + PWT_{s,d,t} \quad \forall\, t,d,s \ .$ (5.3)

Total wind generation forecast: $PWT_{s,d,t} = \sum_{m}^{nM} PW_{m,s,d,t} \quad \forall\, t,d,s \ .$ (5.4)

Power from pumped-storage stations: $PS_{s,d,t} = KWP_{h} \cdot WF_{s,d,t} \quad \forall\, t,d,s \ .$ (5.5)

Energy (water) balance equations of storage reservoirs:

$$WS_{s,d,t,h} = \sum_{l=1}^{s}\sum_{k=1}^{d}\sum_{j=1}^{t}\left(WFA_{l,h} - WF_{l,k,j,h}\right) + WSI_{h} \ \forall\, h,t,d,s \ . \tag{5.6}$$

Capacity limits of pumped-storage reservoirs:

$$WSR_{s,h} \le WS_{s,d,t,h} \le WS_{max,\,h} - WSR_{s,h} \quad \forall\, h,t,d,s \tag{5.7}$$

Max/Min flow limits of pumped-storage stations:

$$-WF_{min,\,h} \le WF_{s,d,b,t,h} \le WF_{max,\,h} \quad \forall\, h,t,d,s \quad . \tag{5.8}$$

Storage reserve capacity requirement as a function of wind energy uncertainty:

$$\sum_{h}^{nH}\left(WSR_{s,h} \cdot KWR_{h}\right) \ge 3 \cdot \sigma_{WGC,\,s} \quad \forall\, s \ . \tag{5.9}$$

Reserve capacity should be convertible to power and subject to reservoir flow limits:

$$-WF_{min,\,h} \le WSR_{s,h} \le WF_{max,\,h} \quad \forall\, h,s\,. \tag{5.10}$$

Aggregate uncertainty of WGC: $\sigma_{WGC,s} = (1 - KSM) \times \max_{d,t}\left\{\sum_{m}^{nM} \sigma_{m,s,d,t}\right\} \quad \forall\, s \quad .$ (5.11)

Costs for storage (CST) = Storage costs (CSS) + Reserve capacity cost (CSR):

$$CST_{s,d,t} = \sum_{h}^{nH}\left(rWS_{h} \times \sum_{l=1}^{s}\sum_{k=1}^{d}\sum_{j=1}^{t}\left(-WF_{l,k,j,h}\right)\right) + \sum_{h}^{nH}\left(rWC_{h} \cdot WSR_{s,h}\right) \qquad \forall\, h,t,d,s \ . \tag{5.12}$$

In the optimization problem $PW_{m,s,d,t}$, $PWT_{s,d,t}$, $\sigma_{WGC,s}$, $WSR_{s,h}$, KWP_h , KWR_h , KSM, $WS_{max,h}$, rWS_h , rWC_h , $WF_{min,h}$, $WF_{max,h}$, WSI_h , $WFA_{s,h}$, $PLoad_{s,d,t}$, $BV_{s,d,t}$, $BF_{s,d,t}$ are known quantities.

The mathematical model is optimized to determine $PCV_{s,d,t}$, PCF_s , $WS_{s,d,t,h}$, $WF_{s,d,t,h}$, $WSR_{s,h}$, $PS_{s,d,t}$, $CSS_{s,d,t}$, $CSR_{s,d,t}$. In other words, these are decision variables of the optimization problem. Most importantly the output of this optimization problem gives the WGC's amount of seasonal firm power capacity bids (PCF_s) and hourly variable power bids ($PCV_{s,d,t}$).

This optimization formulation may be solved using a commercial optimization software. In this case, the formulation was optimized using a linear optimization tool in Matlab. The distribution of revenues and costs among participating wind farms is given below.

5.3.2 Distributing Costs and Benefits

Revenue of the WGC from sale of the variable component of energy to the market operated by ISO:

$$RVCV_{s,d,t} = PCV_{s,d,t} \cdot BV_{s,d,t} \quad \forall\, t,d,s\,. \tag{5.13}$$

Revenue of the WGC from sale of the firm component of energy to the market operated by ISO:

$$RVCF_s = \left(PCF_s \cdot \sum_{d}^{nDs} \sum_{t}^{nT} BF_{s,d,t} \right) \times \frac{1}{nDs \cdot nT} \quad \forall\, s\,. \tag{5.14}$$

The WGC's revenue from the sale of the variable component of energy must be fairly apportioned amongst all the wind farms. While there are several ways, in this study, we propose to compute average locational marginal prices at all the wind farms and apportion revenues as a function of average locational marginal price at the bus connecting the wind the farm and power output of the wind farm. This fair revenue distribution argument results in the following expression:

$$RVGV_{m,s,d,t} = \frac{PW_{m,s,d,t} \cdot ALMP_m}{\sum_{m}^{nF} \left(PW_{m,s,d,t} \cdot ALMP_m \right)} \cdot RVCV_{s,d,t} \; \forall t, d, s, m \,, \tag{5.15}$$

$$\text{where,} \quad ALMP_m = \frac{1}{8760} \cdot \sum_{s}^{nS} \sum_{d}^{nDs} \sum_{t}^{nT} LMP_{m,s,d,t} \; \forall m \quad . \tag{5.16}$$

In a similar manner, it is proposed in this study to apportion revenue from the sale of the firm component of energy on the basis of ALMP. The firm power capacity of the WGC depends on the total capacity of the WGC. Therefore, fair distribution of the firm revenue component among wind farms is proposed as a function of PWC and ALMP as below:

$$RVGF_{m,s} = RVCF_s \cdot \frac{PWC_m \cdot ALMP_m}{\sum_{n}^{nM} \left(PWC_n \cdot ALMP_n \right)} \; \forall t, d, s, m \;. \tag{5.17}$$

The cost of storage (CST) to the WGC must also be apportioned rationally amongst wind farms. The contribution to the total storage cost from each wind farm is derived from two considerations. Firstly, the reserve storage requirement of a wind farm is proportional to its uncertainty. Secondly, the cost of energy arbitrage is proportional to the power output

generated from a wind farm. Therefore storage cost is prorated considering the standard deviations and the generation contributions from wind farms:

$$CS_{m,s,d,t} = \frac{\sigma_{m,s,d,t}}{\sum_{m}^{nM} \sigma_{m,s,d,t}} \cdot \frac{PW_{m,s,d,t}}{\sum_{m}^{nM} PW_{m,s,d,t}} \cdot CST_{s,d,t} \quad \forall\, t,d,s,m \ . \tag{5.18}$$

Transmission cost component of a wind farm can be computed by:

$$CT_{m,s,d,t} = rT_{m} \cdot PW_{m,s,d,t} \quad \forall\, t,d,s,m \ . \tag{5.19}$$

Final hourly payment to Wind farms =

(1) Revenue component from sale of variable energy +

(2) Revenue component from sale of firm energy –

(3) Cost of storage –

(4) Cost of transmission –

(5) Cost of administration :

$$RT_{m,s,d,t} = RVGV_{m,s,d,t} + RVGF_{m,s} - CS_{m,s,d,t} - CT_{m,s,d,t} - CA/(8760 \times nM) \ \forall\, t,d,s,m \, . \tag{5.20}$$

These values are computed after optimization.

5.4 Case Study of Ontario

The proposed WGC model was tested by considering a scenario in the southern Ontario power grid. At present, Ontario incentivizes wind energy through its attractive Feed-in-Tariff. Currently wind energy receives about five times the Hourly Ontario Energy Price

(HOEP) [60]. This high level of subsidy is economically sustainable at low levels of wind energy participation. In the year 2010, wind energy accounted for 2% of total energy production from all sources in Ontario. However, Ontario plans to increase its renewable energy portfolio (excluding large hydro) to 15.5% by the year 2030, mainly through rapid integration of wind energy [55]. As wind energy participation exceeds 5% in the next few years, the present feed-in-tariff structure will become economically unsustainable. In April 2012, Ontario lowered its feed-in-tariff rates to reflect reduction in renewable energy equipment costs. In this context the proposed WGC model would be an important idea for the future Ontario electricity market. Details of the case study are given below.

5.4.1 Data

Ten wind farms (1,144.5 MW) were considered to create a WGC. Fig. 5.3. shows spread of wind farms in southern Ontario and their planned capacities. Wind farms included in the WGC model are Amaranth I & II, Gosfield, Kingsbridge, Kruger Energy Chatham, Port Alma (Kruger), Port Burwell, Ripley South, Spence, Underwood and Wolfe Island. Hourly wind generation output statistics of 2011 [61] were taken as the wind generation forecast (mean values). The uncertainty of hourly wind generation forecast is defined by standard deviation and expressed as a percentage of the mean wind power forecast. In [62], Ontario winter wind power uncertainty has been reported as 18% of installed capacity. For this study, uncertainty of the wind forecast was assumed to be 21% of the mean power output of wind farms. After analysing historical variation of wind power output in Ontario, the smoothing effect arising from combined operation of wind farms, is taken as 20%. It means that $\sigma_{WGC,s}$ is 80% (KSM = 0.8) of the sum of standard deviations (σ_m) of individual wind power forecasts of wind farms.

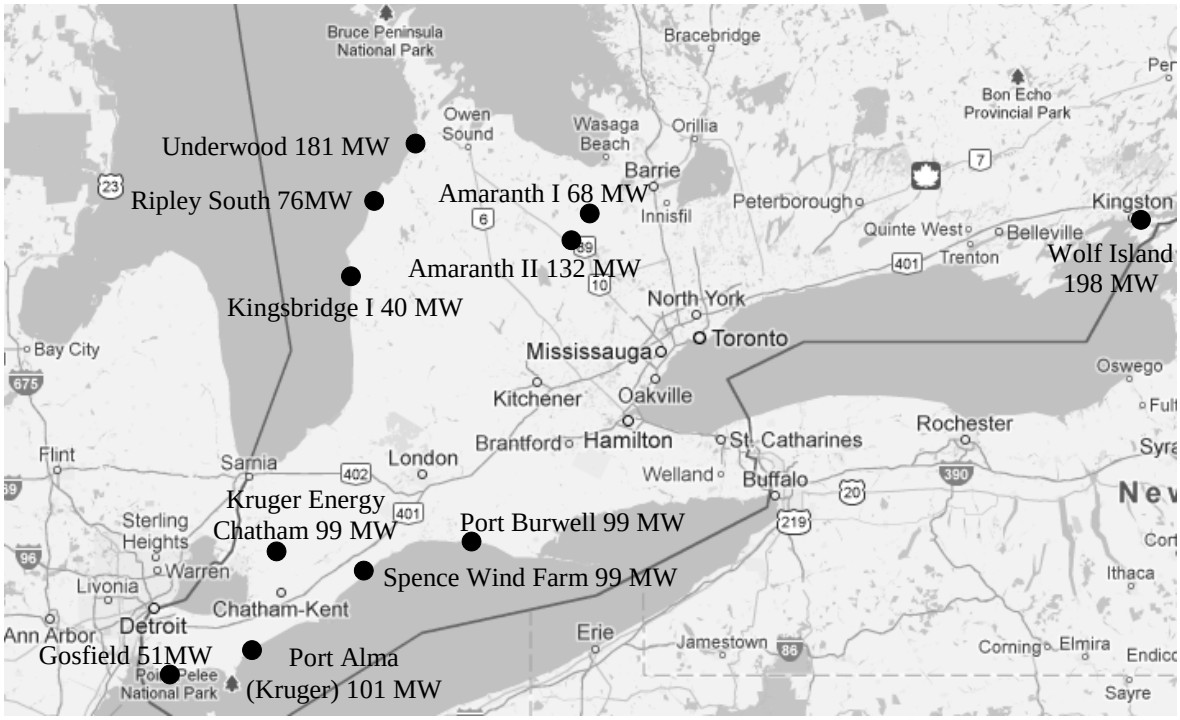

Fig. 5.3. Wind Farms in Southern Ontario

In order to restrict a single supplier's market power, the maximum output of the WGC is limited to a percentage of hourly total system demand that varies throughout the day. During peak load periods (5 hours of a day), the WGC output is limited to 1,500 MW. During the intermediate load periods (10 hours of a day), the WGC output is restricted to 1,100 MW. The WGC output is restricted to 700 MW in the base load periods (9 hours in every day). These limits are lower than the largest nuclear power station capacity in the Ontario grid.

After investigating historical wind generation statistics, five seasons were considered for the study. These seasons are:

(1) high wind season from January to the end of April,

(2) moderate wind season of May,

(3) low wind season from June to August,

(4) moderate wind season from September to October, and,

(5) high wind season from November to December.

Southern Ontario has 2187.7 MW of hydro power capacity connected to the power grid. Out of that, only 174 MW is pumped-storage facilities. This capacity is not enough for the proposed WGC model. Therefore, two hydro pumped-storage power stations, (storage 1 of 2,000 MW and storage 2 of 1,600 MW) were assumed for the study. Pumped-storage reservoir maintains a reserve capacity as: (1) stored water to counter wind power under-production, and (2) as empty capacity to counter over-production of wind power. Therefore, maintaining reserve capacity (water and empty capacity) occupies the reservoir as twice actual water storage. Therefore rate of rent for reserve capacity (rWC) is taken as twice of rate of rent of actual water storing (rWS). All the other related assumptions of pumped-storage systems are given in Table 5.1. Wind farms and the pumped-storage stations are in five different zones and hence their locational marginal prices are different

from each other. Recorded zonal marginal prices in the year 2011 were considered as the price forecast for this study [61]. Extreme price variations due to the system contingencies were replaced by the local average zonal marginal prices. The transmission rent (rT_m) (wheeling rates) were estimated using the zonal price differences and assumed as the rates for estimating cost of transmitting power from wind farms to pumped-storage station. The firm capacity bid price (BF) is the zonal marginal price at the pumped-storage station 1. The price of WGC's variable power (BV) equals the locational marginal price at the pump-storage station 1 minus the costs for additional expenses such as additional AGC, ramping and reserve requirements. Based on the review in [49], 20% of bid price was assumed for all those costs. Therefore, BV is taken as 80% of BF.

Table 5.1. Ontario Base Case Data

	Parameter	**Assumption**
Wind Farms	$PW_{m,s,d,t}$	Historical wind generation output in 2011 [61]
	$\sigma_{m,s,d,t}$	21%, Defined as a percentage of $PW_{f,s,d,t}$
Pumped-Storage Company 1	$WS_{max,\ 1}$	500 million m^3
	WSI_1	250 million m^3
	rWS_1	\$800 per million m^3 per hour
	rWC_1	\$1600 per million m^3 per hour
	$WF_{min,\ 1}$	-277.8 m^3 per second
	$WF_{max,\ 1}$	277.8 m^3 per second
	$WFA_{s,\ 1}$	0 m^3 for all seasons
	KWP_1, KWR_1	500.0 seconds per million m^3 (for 2,000 MW)
Pumped-storage Company 2	$WS_{max,\ 2}$	300 million m^3
	WSI_2	150 million m^3
	rWS_2	\$1000 per million m^3 per hour
	rWC_2	\$2000 per million m^3 per hour
	$WF_{min,\ 2}$	-694.4 m^3 per second
	$WF_{max,\ 2}$	694.4 m^3 per second
	$WFA_{s,\ 2}$	0 m^3 for all seasons
	KWP_2 ,KWR_2	500.0 seconds per million m^3 (for 1,600 MW)
WGC bid prices	BF	Hourly energy price at Niagara falls [61]
	BV	0.8 x BF (20% reduction from BF due to increased ramping and AGC requirements)

In addition to the base case study, four sensitivity analyses were completed to check the model validity considering variations of four key parameters.

5.4.2 Results of the Base Case

The optimization formulation (5.1)-(5.12) was coded in Matlab R2012.a and solved using Mosek optimization solver version 6. A summary of the base case results is given in Table 5.2. For comparison purposes, parameters relevant to independent operation of wind farms (WF: wind farms participate separately in the market without the WGC) are also given in Table 5.2.

The cost of avoiding uncertainty in independent operation of wind farms is conservatively estimated assuming that each wind farm spends the same rental which the WGC pays for the pumped-storage company 1 (rWC_1). Furthermore, when wind farms operate independently they have enough reserve capacity to purchase at the aforementioned cheaper rate of rent. In other words, it is conservatively assumed that wind farms have a cheaper option of purchasing their total reserve requirements than the WGC. It is further assumed that only 90% of the reserve requirements have to be carried by the wind farms when they operate independently. This is to recognize that a wind farm's marginal contribution to the system uncertainty is lesser than its uncertainty in isolation. Additionally, it may be noted that according to the assumed parameters in Table 5.1, pumped-storage Company 1 is comparatively cheaper but has a tighter water flow limit compared to pumped-storage Company 2. Due to these differences, both storage companies 1 and 2 are utilized by the WGC for energy arbitrage and maintaining reserves.

5.4.3 Results for the WGC

According to the results, when wind farms are in the WGC, the total revenue from energy sales increases by 45.2% over their total revenue when they operate independently. The total final payment to wind farms is increased by 32.1% when they are in the WGC.

Table 5.2. Base Case Results of the WGC Based on the Assumptions in Table 5.1

Wind farms independent operation (WF)		
RVCV	Total revenue from variable generations	$61,345,156
CSR	Cost of avoiding uncertainty	$17,496,491
RVCV-CSR	**Total of final payments to wind farms**	**$43,848,665**
WGC operation		
RVCV	Total revenue from variable generations	$77,871,072
RVCF	Total revenue from firm power generations	$11,220,886
CSS	Cost energy (water) storage	$9,532,608
CSR	Cost of reserve storage capacity	$ 15,936,546
CT	Cost of transmitting power	$2,705,383
CA	Administrative cost	$3,000,000
RVCV+RVCF-CSS-CSR-CT-CA	**Total final payments to wind farms**	**$ 57,917,421**

5.4.4 Results for a Participating Wind Farm

This increased final payment is converted to hourly payments to each wind farm. The relevant revenue distribution formulation is detailed in Chapter 5.3.2. Results for the 11th hour of September 19th for Kruger Energy Chatham wind farm (t = 11, d = 19, s = 4, m = 4) are given in Table 5.3. For this wind farm in the considered hour, $PW_{4,4,19,11}$ = 96 MW, PWC_4 = 101.2 MW, rT_4 = 0.34 $/MWh. For season four, the assumed uncertainty of Kruger Energy Chatham wind farm ($\sigma_{4,4,19,11}$) is 20.6 MW. The total power output of wind farms for the considered hour ($PWT_{4,19,11}$) and the sum of standard deviations ($\sum_{m=1}^{10}\sigma_{m,4,19,11}$) are 664 MW and 231.4 MW respectively. The generations from other wind farm for the consider hour are: Amaranth I & II = 51.0 MW, Gosfield = 42.0 MW, Kingsbridge = 29.0 MW, Port Alma (Kruger) = 92.0 MW, Port Burwell = 70.0 MW, Ripley South = 62.0 MW, Spence = 68.0 MW, Underwood = 68.0 MW and Wolfe Island = 86.0 MW. In the case of independent operations, it is assumed that all wind farms have marginal smoothing effect of 10% when they are independently connected to the system which requires matching 90% of its reserve requirement. For Kruger Energy Chatham wind farm, it is 55.6 MW. For season four, optimal firm power from WGC (PCF_4) is 29.44 MW.

The Kruger Energy Chatham wind farm gets $77.97 per hour during September and October irrespective of its power output due to firm power contracts. With the WGC, for the considered hour, the Kruger Energy Chatham wind farm receives 70% increased final payment versus its independent operation.

Table 5.3. Base Case Results of Kruger Energy Chatham Wind Farm Based on the Assumptions in Table 5.1

Wind farms independent operation (WF): Kruger Energy Chatham		
$RVGV_{9,4,19,13}$	Total revenue from variable generations	$2,682.62
$CS_{9,4,19,13}$	Cost of avoiding uncertainty	$177.81
$RVGV_{9,4,19,13}$ -$CS_{9,4,19,13}$	**Total of final payment to Kruger Energy Chatham wind farm**	**$2,504.81**
WGC operation: **Kruger Energy Chatham**		
$RVGV_{9,4,19,13}$	Revenue from variable generations	$4,400.85
$RVGF_{9,4,19,13}$	Revenue from firm power generations	$77.97
$CS_{9,4,19,13}$	Cost storing water and avoiding uncertainty	$162.00
$CT_{9,4,19,13}$	Cost of transmitting power	$32.64
CA/(8760x10)	Administrative cost	$22.83
$RT_{9,4,19,13}$	**Total final payment to Kruger Energy Chatham wind farm**	**$4,261.35**

From Table 5.3, one may clearly see that a wind farm benefits by being a part of the WGC, However it is required to check whether all wind farms get similar benefits. Fig. 5.4 shows additional final payments received by all wind farms in the considered hour. As mentioned above, the Kruger Energy Chatham wind farm receives the highest payment when it has the highest generation in the considered hour as a part of WGC. The hourly revenue distribution depends on individual power output, ALMP and capacity of the wind farm (5.15)-(5.17). However, the annual final revenue distribution to a wind farm is proportional to its annual generation Fig. 5.5. The biggest wind farm, Wolfe Island receives the highest final revenue while the smallest wind farm, Kingsbridge, has the lowest final revenue. From Fig. 5.5, it is evident that every wind farm benefited by entering the WGC.

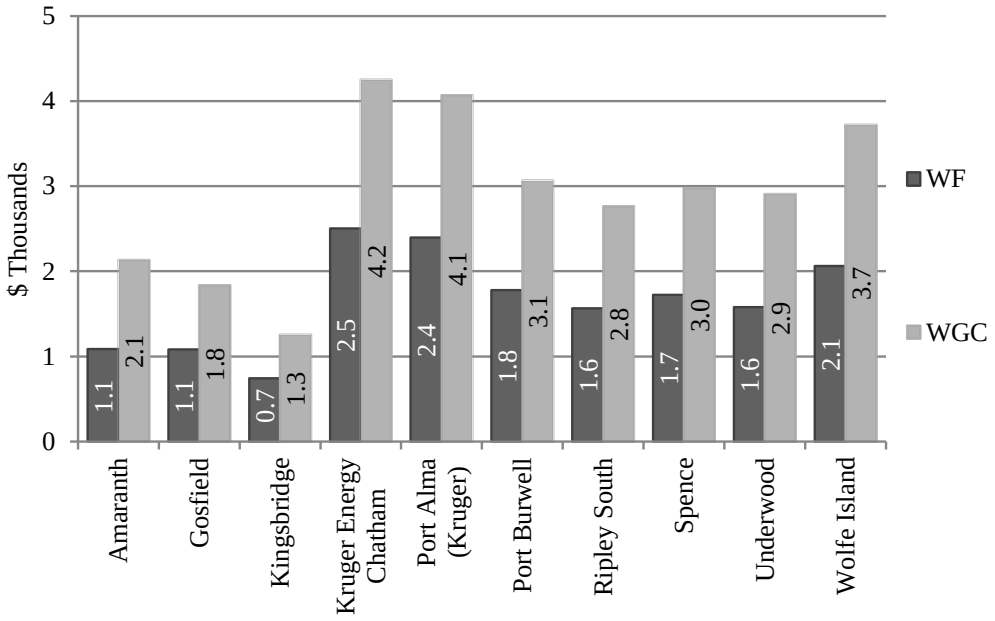

Fig. 5.4. Final Payments for All Wind Farms in the WGC and Independent Operation of Wind Farms (WF) in the Eleventh Hour of September 19th.

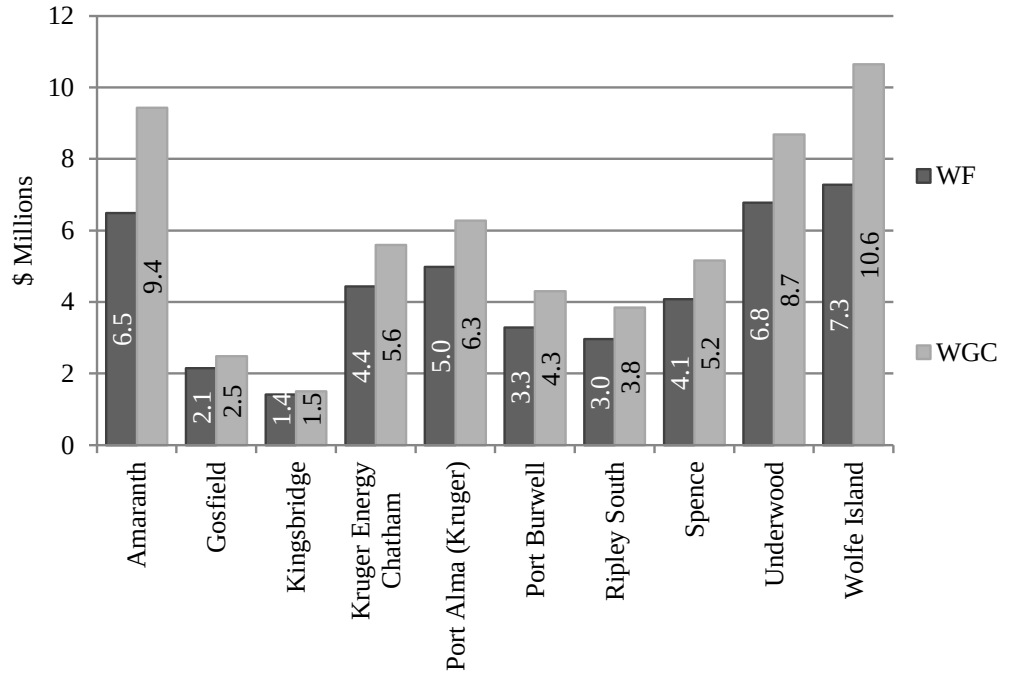

Fig. 5.5. Total Final Payments during the Year to All Wind Farms in the WGC and Independent Operation of Wind Farms (WF).

5.4.5 Sensitivity to Uncertainty

The uncertainty of the wind generation forecast is represented by standard deviation at a wind farm (σ_m) and it is expressed as a percentage of the mean wind generation forecast. This sensitivity study considers five σ_m values of 7%, 14%, 21%, 28% and 35%. Each is expressed as a percentage of the mean wind forecast. Fig. 5.6 shows the variation of total revenue of wind farms. When the uncertainty of the forecast increases (higher σ_m), the total revenue of wind farms reduces. Comparing operation of the WGC and independent wind farms, at uncertainty of 35%, the WGC receives 40% more total revenue than when wind farms operate independently.

As mentioned in Chapter 5.1, this increased benefit of the WGC model consists of three components. The first noticeable component is the minimized effect of uncertainty. In all cases, cost of avoiding uncertainty (CSR) for WGC is less than that for WF. Due to energy arbitrage, the total revenue is increased considerably for WGC as compared with WF. The third benefit (Capacity Credit) is seen as the firm revenue (RVCF) of the WGC.

5.4.6 Sensitivity to the Smoothing Effect

From an analysis of the historical wind generation of the above mentioned wind farms, it is noticed that combined output of wind farms (WGC output) has less percentage variation than individual wind farms. This is due to the smoothing effect on uncertainty of wind farms in a WGC. As an example, in second season, sum of maximum standard deviations of wind farms is 229.74 MW but the standard deviation of total output of WGC is 207.9 MW. It is a 10% reduction of standard deviation (5.11) (KSM = 0.10). However, the standard deviations are estimates and accordingly the smoothing effect is also an estimate. In the base case, a smoothing effect of 20% was considered for the WGC. In order to study the effect of this smoothing effect, standard deviation reductions of 10%,

15%, 20%, 25% and 30% were considered for the WGC in five sensitivity cases. Relevant KSM values were 0.1, 0.15, 0.2, 0.25 and 0.3 respectively. Fig. 5.7 shows the results of this study.

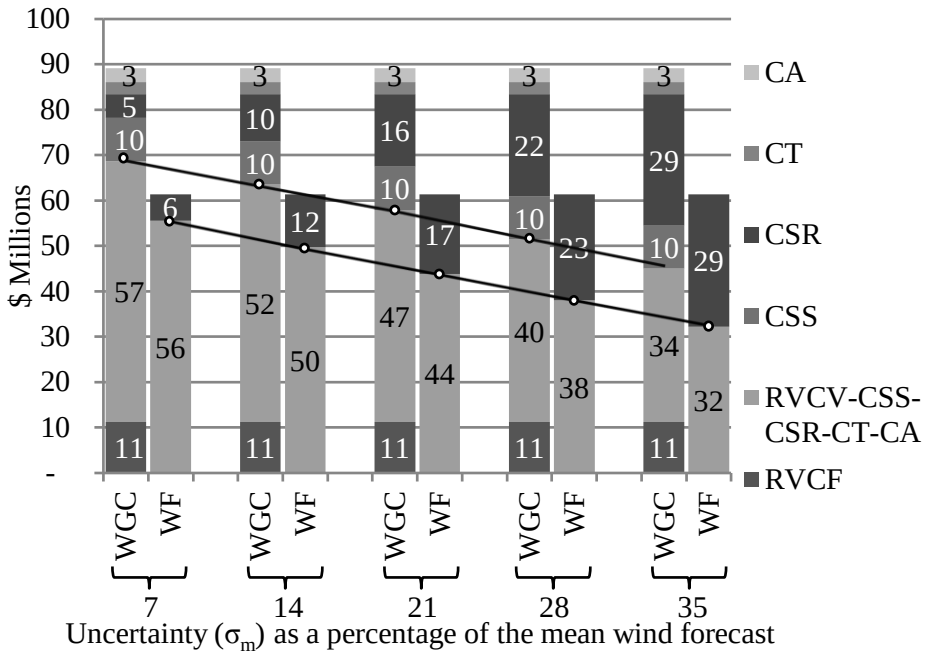

Fig. 5.6. Revenue and Cost Components of the WGC Operation and Independent Operation of Wind Farms (WF) Considering Different Wind Power Forecast Uncertainties

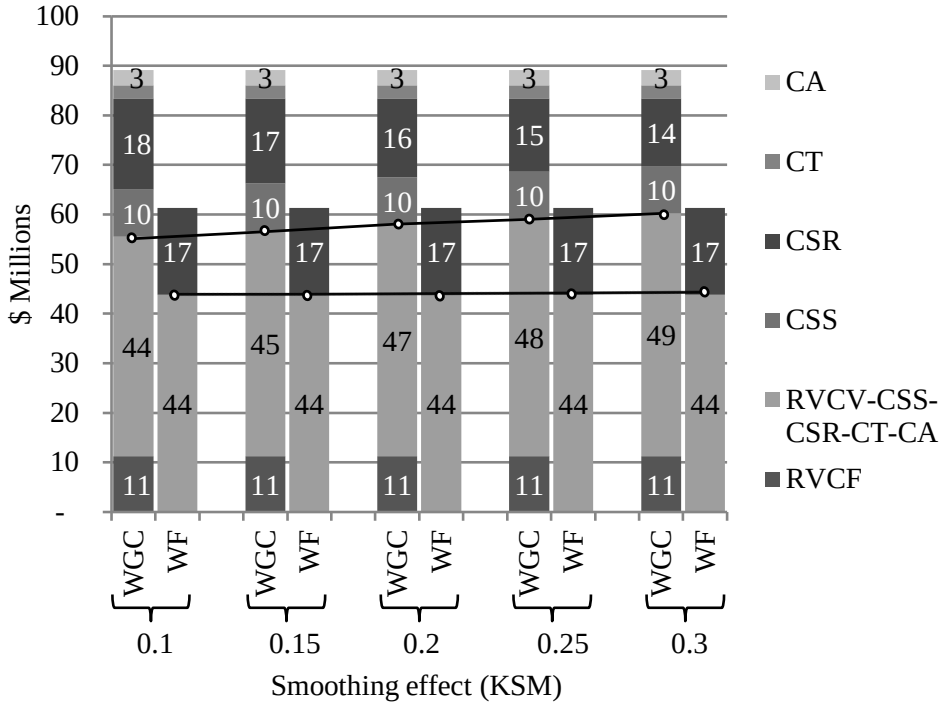

Fig. 5.7. Revenue and Cost Components of the WGC Operation and Independent Operation of Wind Farms (WF) for Different Smoothing Effect Values

As mentioned in Chapter 5.4.1, when wind farms operate independently they have 10% flat smoothing effect recognized by the system operator. Therefore, their revenue is the same irrespective of the variation of combined wind farms smoothing effect. In all cases of this sensitivity study, there is no significant variation in the benefit from energy arbitrage for WGC. However, if the WGC has a low KSM value, the cost of minimizing uncertainty (CSR) is considerably high. Therefore, the total final variable payments from the WGC to wind farms (RVCF+RVCV−CT−CSS−CSR−CT−CA) are low. The firm revenue component of WGC (RVCF) does not vary with the smoothing effect. For the cases with higher smoothing effects (high KSM values), the total benefit of the WGC is increased.

The sensitivity analysis explained above and shown in Fig. 5.7 assumed that when wind farms operate independently, 90% of the reserve requirement should be matched by wind farms. The grid assumes that 10% of reserve is not required due to the collective smoothing effect of the whole power system. However, the best assumption is that each wind farm should carry a reserve capacity to match marginal increase of the reserve requirement of the system due to the connection of the wind farm. Even though this is the most accurate method of handling reserve purchases, it should be noted that the marginal reserve requirement varies from one system condition to another. Therefore, in the base case it is assumed that each wind farm needs to match 90% of its reserve requirement. However this assumption is very critical to the financial attractiveness of the WGC. Therefore, a separate sensitivity analysis studying the effect of smoothing on independent operation of wind farms was completed. In this sensitivity analysis, the percentage of reserves purchased by wind farms was varied from 100% to 80%. Results of the sensitivity analysis are given in Fig. 5.8. It is also assumed that all wind farms have enough pumped-hydro reserves to be purchased at the lowest rate (rWC_1= \$1600 million m^3 per hour), which the WGC would pay to hydro power storage company 1. From the results, it is clear

that even when wind farms have the same smoothing effect, the WGC gives a higher overall benefit.

5.4.7 Sensitivity to the Market Price Bandwidth

The major portion of the WGC revenue is from shifting energy from low priced periods to high priced periods. The bandwidth between the lowest price and the highest price is the key factor influencing shifting of energy and hence the revenue of the WGC. Therefore in this sensitivity study, five cases of different price scenarios with different price variation bandwidths were considered. In two sensitivity cases, price bandwidths were reduced by 20% and 40% from that of the base case. In the other two cases, price bandwidths were increased by 20% and 40% from that of the base case. The fifth case is the base case. However, in all cases, average of the price and the pattern of price variation are the same.

According to Fig. 5.9, the market price bandwidth has a significant direct impact on the revenue of the WGC. When the wind farms operate independently, a slight decrease of revenue is expected with an increase of market price bandwidth. However, when wind farms are in the WGC, with an increase in market price bandwidth, pumped-storage reservoirs are used extensively to shift energy from the low priced hours to the high priced hours. Therefore, the revenue from shifting energy increases significantly. However, there is no observable variation of uncertainty related cost (CSR) with the variation of market price bandwidth.

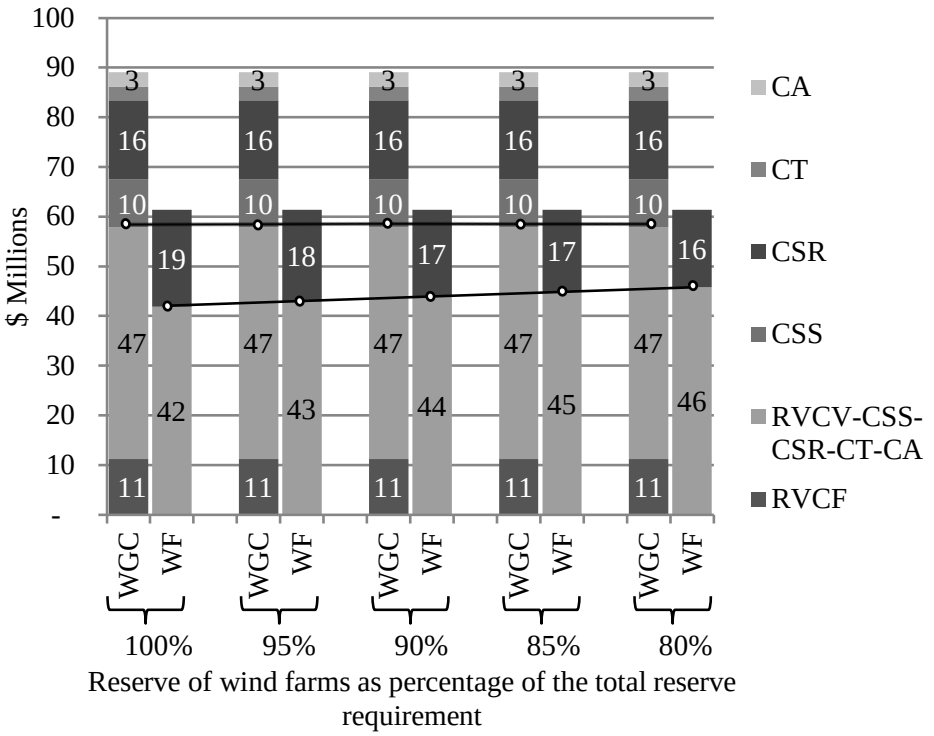

Fig. 5.8. Revenue and Cost Components of the WGC Operation and Independent Operation of Wind Farms (WF) for Different Smoothing Effect values

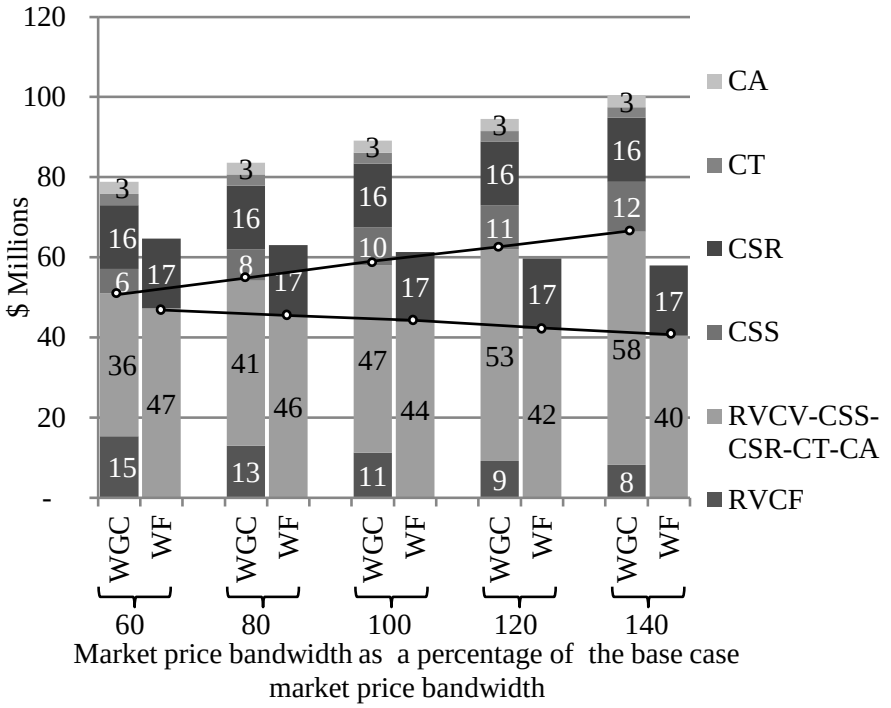

Fig. 5.9. Revenue and Cost Components of the WGC Operation and Independent Operation of Wind Farms (WF) for Different Values of Market Price Bandwidth

5.4.8 Sensitivity to Storage Costs

As formulated in (5.12) the cost of storage consists of two components. The rate of rent (rWC) for reserve storage capacity (WSR) is assumed to be twice the rate of rent (rWS) for actual usage of the reservoir (Table 5.1). The viability of the WGC model is very much dependent on these rent rates. Therefore, in this sensitivity study, these two rates were varied. Five sensitivity cases were defined with rate pairs (rWS, rWC) (Table 5.4). In all cases the ratio between rWS and rWC is 2 for both pumped hydro companies. Except rWS and rWC all other parameters are same for all cases. The results of the sensitivity study are shown in Fig. 5.10.

Table 5.4. Sensitivity Cases for Storage Cost Rates

	Case I	Case II	Case III	Case IV	Case V
(rWS_1,rWC_1)	(400,800)	(600,1200)	(800,1600)	(1000,2000)	(1200,2400)
(rWS_2,rWC_2)	(400,800)	(700,1400)	(1000,2000)	(1300,2600)	(1600,3200)

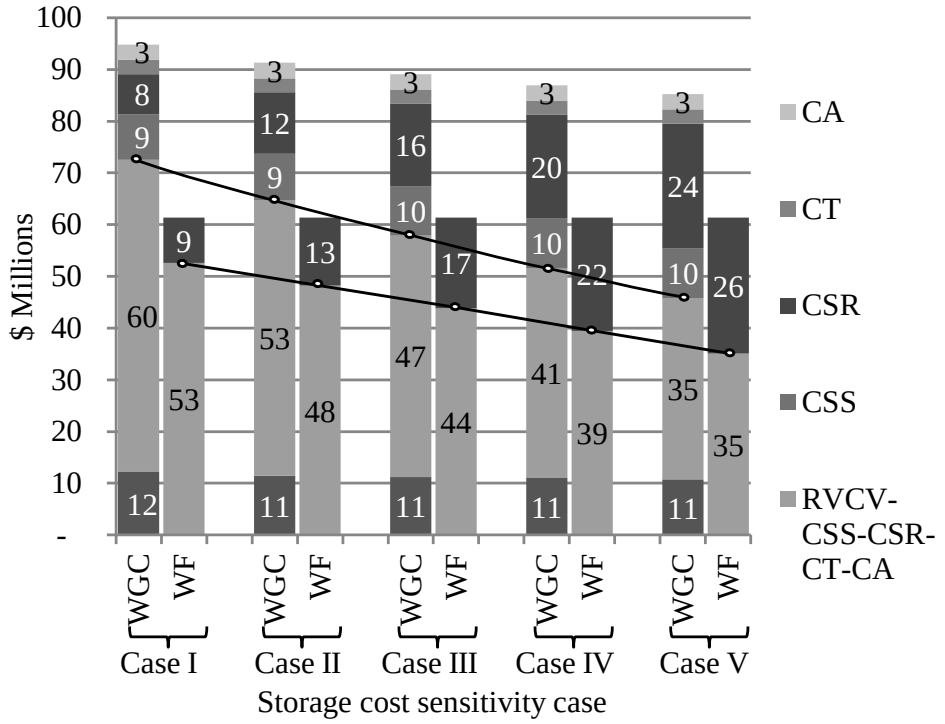

Fig. 5.10. Revenue and Cost Components of the WGC Operation and Independent Operation of Wind Farms (WF) for Different Values of Storage Cost

As the cost of storage increases, payment to wind farms decreases. This is a combined result of two phenomena. The first is the higher uncertainty related cost (CSR). However, in all cases, it is lower than the uncertainty avoiding costs of independent wind farms. Secondly with higher rWS rates, use of pumped-storage facility is reduced. Both RVCV and RVCF revenue components are reduced as well.

As mentioned above, the cost of storage has two components: cost of reserve and cost of actual water being stored. Each component has its rate of rent. In all cases considered above, the rate of rent of reserve is twice the rate of rent of actual water storage. Even though these reservoir activities decide the total cost and they have less impact on the overall ratio between the cost and benefit of the WGC, it is important to clarify the effect of the ratio between these rates of rents. Therefore, another five sensitivity cases were defined varying the ratio between the rent rate of reserve (rWC) and the rate of rent of storage (rWS) (Table 5.5). The ratio of rWC/rWS is varied from 4 to 0.5. However, in order to maintain a stable price level among all cases, the mid-point between rWC and rWS is kept same in all cases for both storage companies. As shown in Fig. 5.11, the WGC generates a higher total final payment in all five cases. When rWC decreases, reserve related cost component (CSR) is decreased. It is the same for both the WGC and independent operation of wind farms (WF). On the other hand at low rWS rates, cost of storing water is low and hence a higher amount of water is stored for energy arbitrage. However, variation of benefit of energy arbitrage is relatively low even for doubling rWS rates. In Case X, where rWS is twice as rWC, the WGC gives 12.4% higher final benefits to participating wind farms than their independent operation.

Table 5.5. Sensitivity Cases for the Ratio of Storage Cost Rates

	Case VI	Case VII	Case VIII	Case IX	Case X
(rWS_1,rWC_1)	(500,2000)	(600,1800)	(800,1600)	(1200,1200)	(1600,800)
(rWS_2,rWC_2)	(600,2400)	(750,2250)	(1000,2000)	(1500,1500)	(2000,1000)
(rWC/rWS)	4.0	3.0	2.0	1.0	0.5

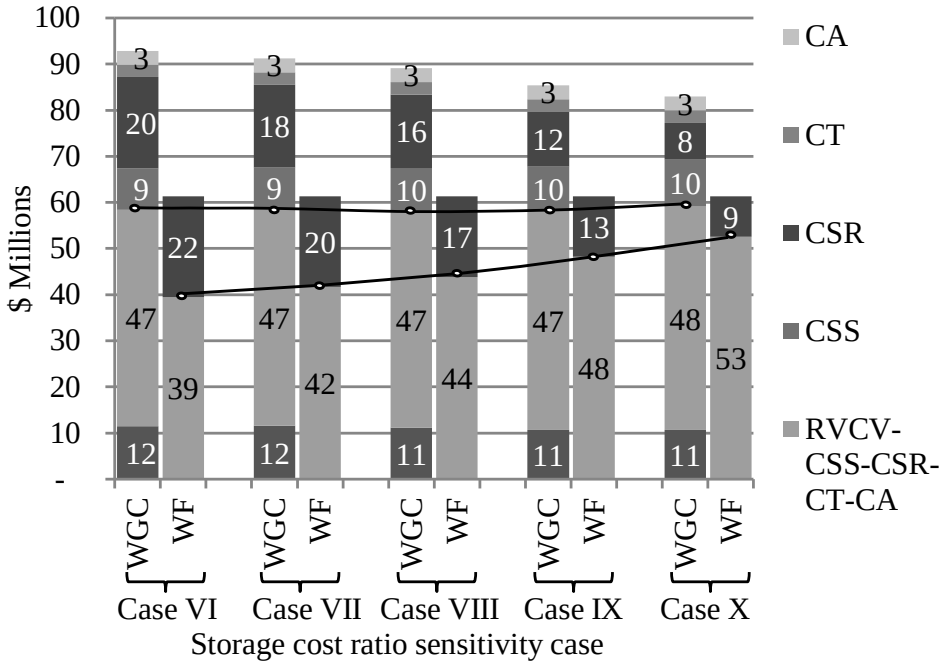

Fig. 5.11. Revenue and Cost Components of the WGC Operation and Independent Operation of Wind Farms (WF) for Different Values of Storage Cost Ratio

5.5 Summary

This study proposes a Wind Generation Cooperative (WGC) model to trade in wind energy, in a collective manner, on behalf of a set of wind farms that are geographically dispersed. A formulation to maximize profits of the WGC is presented and tested in a case study from Ontario, Canada.

From the extensive study on the proposed WGC model, it is found that the WGC gives three benefits to its participating wind farms.

The first benefit is reduced uncertainty in wind forecasts due to the smoothing effect arising from collective operation of wind farms that are geographically dispersed. Accordingly, the uncertainty related cost of the WGC is lesser than that of wind farms operating independently.

The second benefit is temporal shift of energy. It heavily depends on the market price bandwidth and the cost of storage. Except at very low price bandwidths, the WGC derives considerable benefits by shifting energy from lower priced periods to higher priced periods.

The third benefit is that a WGC is able to offer firm production capacity to the market due to collective operation of wind farms. Accordingly, the WGC receives a capacity credit.

In addition, the sensitivity of the WGC performance to four key parameters is analyzed. These parameters are (a) the uncertainty in wind forecasts, (b) the smoothing effect, (c) the market price bandwidth, and (d) the storage cost. From all the sensitivity analyses, it is very clearly demonstrated that the WGC model consistently performs better than independent operation of wind farms, thus providing a convincing motivation for wind farms to join a WGC. Sensitivity analyses further show that as the parameters such as

uncertainty, smoothing effect, etc. increase, the WGC model becomes more attractive providing improved economic returns.

Chapter 6

General Discussion and Conclusion

6.1 Research Contributions

This thesis addressed three techno-economic challenges in the integration of wind energy into power systems. The main contributions of this research are listed below.

1. Artificial Neural Network Models of Wind Generators for Accurate Three-Phase Unbalanced Power Flow Analyses:

   ANN models of Wind Generators are as accurate as the nonlinear models comprising a nonlinear set of equations. The proposed ANN models of wind generators are considerably faster than the nonlinear models. These new models produce consistent results and significantly reduce the computational time required by power flow analysis algorithms with wind generators.

2. Implementation of ANN Models of Wind Generators in Commercial Software:

   The proposed ANN models of wind generators were implemented in commercial software such as PSS®E and PSS®SINCAL that are widely used by electric utilities. These implementation techniques are of immediate and practical significance for electric utilities wishing to model wind generators in these commercial software programs.

3. Probabilistic Model of Wind Generators for Planning:

   In this work, probabilistic models of wind generators and loads are created and used in power systems analysis algorithms with an innovative method to significantly reduce the probabilistic event space. This method is used for determining probabilistic distributions of voltages.

4. Economic Models for Integration of Wind Energy into Electricity Markets:

   In this work, a Wind Generators Cooperative Model is proposed for competitive integration of wind generators into electricity markets. The method is shown to work well and found to be viable and beneficial in an Ontario (Canada) case study.

6.2 Chapter-Wise Conclusions

Chapter 2

In Chapter 2, a methodology for building ANN models of wind generators was described. Generating sets of epoch is an important task in building ANN models. Use of nonlinear accurate models for building sets of epoch is presented. If nonlinear accurate models are not available, then actually measured input and output data sets of the interested wind generator can be used as epochs. This is an advantage of ANN models which can be used in cases where the accurate model of the wind generator is not available. Once the set of epochs is generated, the back propagation technique can be used for training the ANN. The best ANN configuration is chosen based upon performance indicators. Maximum Absolute Error (MAE) and Average Root Mean Square Error (ARMSE) are suitable measures to judge the accuracy of ANNs. Average Absolute Error (AAE) is suitable for judging the level of training. Details of these performance investigations are given in Chapter 2.

Chapter 3

Chapter 3 describes the implementation of ANN models in power flow analysis algorithm. Two implementations were completed in this study. The first implementation was completed in Matlab for the 37-bus IEEE test system. ANN models are more than ten times faster than nonlinear wind generator models. The execution time of power flow analysis algorithm for the IEEE 37 bus distribution system improved by 40% when, an

ANN model was used instead of a nonlinear wind generator model. Only one wind generator is considered for the study. It is expected that, if many wind generators are in the distribution system the computational speed would increase considerably. The second implementation of the ANN models in PSS®E and PSS®SINCAL was performed. These implementations show the simplicity of ANN model for coding in different programming languages required by those commercial software programs. Further, it proves that simple mathematical operations available in these computer languages are sufficient to implement the proposed ANN models in proprietary commercial power flow analysis software.

Chapter 4

Chapter 4 reported a formulation of probabilistic voltage solution technique for a distribution system. Probabilistic models for wind generators and load are described in detail. In the proposed technique, probability distributions of loads are sectioned into many events where every event has a load value and an associated probability of occurrence. By modeling events with the same probabilities for all load buses, complexity of the problem is simplified considerably. A similar simplification technique is proposed to model the probability distribution of the wind generators. These modeling approximations reduce the size of probabilistic event space and hence reduce the number of power flow solutions required to estimate the probabilistic voltage solution of the distribution system. All the detailed probabilistic models and formulation are given in Chapter 4. Benefit from simplification in the proposed technique has been demonstrated by a case study.

Chapter 5

In Chapter 5, the formulation of a proposed Wind Generators Cooperative model is reported. The WGC model gives three benefits to participating wind farms: 1) it allows

wind generators to minimise uncertainty by spatial smoothing effect, 2) it enables energy arbitrage, and 3) it creates the benefit of capacity credit. Operation of the WGC and mathematical formulation were described in detail. Both costs and benefits of the WGC distributed amongst participating wind farms were proportional to their respective contributions to the costs and benefits, and opportunity costs. A detailed case study considering southern Ontario data is also given in Chapter 5. Ten wind farms have been considered in the case study. According to the results all wind farms get benefits by participating in the WGC. The results of the case study have been verified by four different sensitivity analyses.

6.3 Future Work

ANN Models of Other Renewable Energy Sources: ANN models were built to replace nonlinear models of wind generators. It can easily extendable for other renewable energy sources especially solar PVs connected to distribution systems.

Application of ANN Models in Other Power Systems Studies: As pointed out in this research ANN models are accurate, fast, and consistent in distributions system power flow analysis studies. In this research its application has not been studied in other planning studies, short circuit analysis and transient stability analysis. Such studies may be undertaken using ANN models of wind generators.

Effect of Different Types of Technologies for the Function of WGC: Different types of storage techniques have different characteristics. The optimization problem of Wind Generators Cooperative has been formulated retaining flexibility to accommodate any type of storage technology into the WGC. In Chapter 5, The WGC case study was completed using two pumped hydro stations as energy storage systems. The case study could be extended with other types of storage technologies.

Left Blank Intentionally

Appendices

A 1 Nonlinear Mathematical Model of Type-3 DFIG Wind Generator [30]

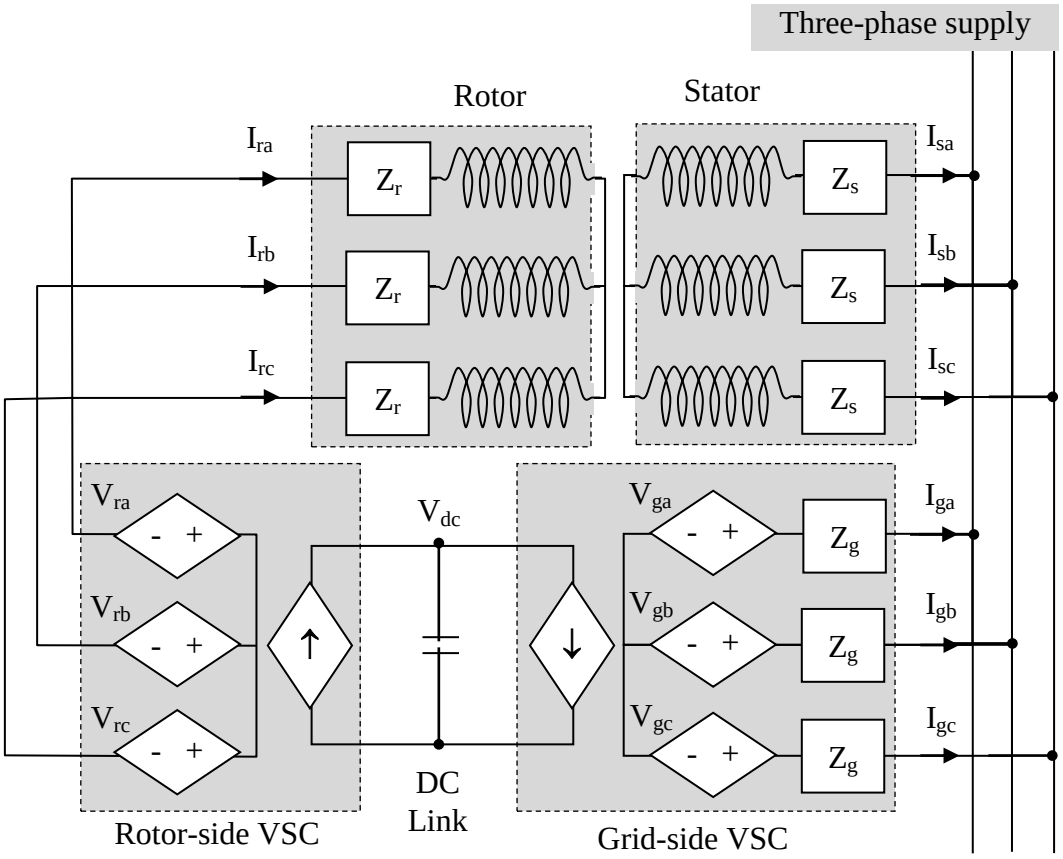

Fig. A1.1. Equivalent Circuit Diagram of Doubly-Fed Induction Generator - Complete Model

Mechanical power of the turbine is given as:

$$P_m = \frac{1}{2} \cdot A \cdot \rho \cdot U^3 \cdot C_p , \qquad (A1.1)$$

where,

$$C_P(\lambda,\beta) = C_1\left(\frac{C_2}{\lambda} - C_3\cdot\beta - C_4\right)\exp\left(\frac{-C_5}{\lambda}\right) + C_6\cdot\lambda \quad . \tag{A1.2}$$

The turbine and the rotor angular speeds are given as:

$$\varpi_t = \frac{\lambda\cdot U}{R_t} \quad , \tag{A1.3}$$

$$\varpi_r = \varpi_t \cdot K_g \quad . \tag{A1.4}$$

Real and reactive power supplies from the grid side converter to the PCC are given as:

$$[P]_{gabc} = \text{real}\left\{[V\angle\delta]_{abc}\cdot\left(\frac{[V\angle\delta]_{abc} - [V\angle\delta]_{gabc}}{[Z]_{gabc}}\right)^*\right\} \quad , \tag{A1.5}$$

$$[Q]_{gabc} = \text{imag}\left\{[V\angle\delta]_{abc}\cdot\left(\frac{[V\angle\delta]_{abc} - [V\angle\delta]_{gabc}}{[Z]_{gabc}}\right)^*\right\} \quad . \tag{A1.6}$$

The induction machine's slip is converted to different symmetrical component networks as below:

$$[\text{slip}]_{012} = \begin{bmatrix} \text{slip}_0 \\ \text{slip}_1 \\ \text{slip}_2 \end{bmatrix} = \begin{bmatrix} 0 \\ \text{slip} \\ 2-\text{slip} \end{bmatrix}. \tag{A1.7}$$

Converted sequence network impedances are:

$$Z_{s\varepsilon} = Z_s, \tag{A1.8}$$

$$Z_{r0} = \text{infinite}, \tag{A1.9}$$

$$Z_{r1} = \frac{\text{real}(Z_r)}{\text{slip}_1} + \text{imag}(Z_r), \tag{A1.10}$$

$$Z_{r2} = \frac{\text{real}(Z_r)}{\text{slip}_2} + \text{imag}(Z_r), \tag{A1.11}$$

$$Z_{m\varepsilon} = Z_m. \tag{A1.12}$$

Induced emf at the stator is written as below:

$$\overline{E}_\varepsilon = \frac{\left(\overline{V}_{s\varepsilon} / Z_{s\varepsilon}\right) + \left(\left(\overline{V}_r / \text{slip}_\varepsilon\right) / Z_{r\varepsilon}\right)}{1/Z_{s\varepsilon} + 1/Z_{r\varepsilon} + 1/Z_{m\varepsilon}} \quad \varepsilon \neq 0. \tag{A1.13}$$

The currents on sequence networks are described from:

$$\bar{I}_{s\varepsilon} = \left(\overline{V}_{s\varepsilon} - \overline{E}_{\varepsilon}\right) / Z_{s\varepsilon}\,, \tag{A1.14}$$

$$\bar{I}_{r\varepsilon} = \left(\overline{V}_{r\varepsilon} / \mathrm{slip}_{\varepsilon} - \overline{E}_{\varepsilon}\right) / Z_{r\varepsilon} \qquad \varepsilon \neq 0\,, \tag{A1.15}$$

$$\bar{I}_{r0} = 0\,. \tag{A1.16}$$

The relationship of real power balance is described as:

$$PL_{\varepsilon} = \left|\bar{I}_{s\varepsilon}\right|^2 \cdot \mathrm{real}(Z_{s\varepsilon}) + \left|\bar{I}_{r\varepsilon}\right|^2 \cdot \mathrm{real}(Z_{r\varepsilon})\,, \tag{A1.17}$$

$$P_{s\varepsilon} = \mathrm{real}\left(\overline{V}_{s\varepsilon} \cdot \bar{I}_{s\varepsilon}^{*}\right), \tag{A1.18}$$

$$P_{r\varepsilon} = \mathrm{real}\left(\overline{V}_{r\varepsilon} \cdot \bar{I}_{r\varepsilon}^{*}\right), \tag{A1.19}$$

and real power balance at any phase:

$$\sum_{\varepsilon}\left(P_{s\varepsilon} + P_{r\varepsilon}\right) = P_m/3 + \sum_{\varepsilon} PL_{\varepsilon}\,. \tag{A1.20}$$

$$[P]_{sabc} = \mathrm{real}\left([V\angle\delta]_{abc} \cdot \left([I\angle\theta]_{sabc}\right)^{*}\right) \tag{A1.21}$$

$$[Q]_{sabc} = \mathrm{imag}\left([V\angle\delta]_{abc} \cdot \left([I\angle\theta]_{sabc}\right)^{*}\right) \tag{A1.22}$$

The real and the reactive power output of the wind generator are:

$$[P]_{abc} = [P]_{sabc} + [P]_{gabc}, \tag{A1.23}$$

$$[Q]_{abc} = [Q]_{sabc} + [Q]_{gabc} = 0. \tag{A1.24}$$

Combining (A1) to (A24), it is possible to form a matrix set of equations as below:

$$0 = F[U, [V]_{abc}, [\delta]_{abc}, [P]_{abc}, [Q]_{abc}]. \tag{A1.25}$$

Equation (A25) may be solved with the knowledge of P_m and $[V\angle\delta]_{abc}$ to determine $[P]_{abc}$ and $[Q]_{abc}$ using Newton- Raphson Technique.

A 2 Nonlinear Mathematical Model of Type-4 PMSG Wind Generator [31]

$$P_m = \frac{1}{2} \cdot A \cdot \rho \cdot U^3 \cdot C_p \tag{A2.1}$$

where,

$$C_p(\lambda, \beta) = C_1\left(\frac{C_2}{\lambda} - C_3 \cdot \beta - C_4\right)\exp\left(-\frac{C_5}{\lambda}\right) + C_6 \cdot \lambda \tag{A2.2}$$

Induced electromotive force:

$$\overline{E}_{ph} = 4.44 \cdot \phi \cdot NT \cdot \frac{\varpi_e}{2\pi} \tag{A2.3}$$

Phase voltage at generator terminal:

$$V_{t\_ph}\angle\varphi_{t\_ph} = \overline{E}_{ph}\angle\varphi_{s\_ph} - I_{s\_ph}\angle\theta_{s\_ph} \cdot (R_s + jX_s) \qquad \forall ph \tag{A2.4}$$

Relationship to the input mechanical power:

$$P_m = \sum_{ph=a,b,c} E_{ph} \cdot I_{s\_ph} \cdot \cos(\varphi_{s\_ph} - \theta_{s\_ph}) \tag{A2.5}$$

Output dc voltage of the rectifier:

$$V_{dcr} = 3/\pi \cdot \sqrt{6} \cdot V_{t\_ph} \quad \forall ph \tag{A2.6}$$

Output dc current of the rectifier:

$$I_{dcr} = \left(\pi/\sqrt{6}\right) \cdot I_{s\_ph} \quad \forall ph \tag{A2.7}$$

Final terminal voltage of the rectifier:

$$V_{dci} = V_{dci} - R_r \cdot I_{dcr} \tag{A2.8}$$

Relationship between ac and dc power:

$$3 \cdot V_{t\_ph} \cdot I_{s\_ph} \cdot \cos\left(\varphi_{t\_ph} - \theta_{s\_ph}\right) = V_{dcr} \cdot I_{dcr} \quad \forall ph \tag{A2.9}$$

Controlled dc voltage after the boost converter:

$$V_{dcb} = \frac{1}{(1-D)} V_{dci} \tag{A2.10}$$

Output current of the boost converter:

$$I_{dcb} = (1-D) \cdot I_{dcr} \tag{A2.11}$$

Output voltage of the boost converter: $V_{dca} = V_{dcb} - R_b \cdot I_{dcb}$ (A2.12)

Line-to-neutral voltage at the terminal of voltage source inverter:

$$V_{a\_ph} = \frac{\sqrt{3}}{2\sqrt{2}} \cdot m_a \cdot V_{dca} \quad \forall ph \tag{A2.13}$$

Output voltage of voltage source inverter:

$$V_{ph}\angle\delta_{ph} = V_{o\_ph}\angle\varphi_{o\_ph} - I_{ph}\angle\theta_{ph} \cdot \left(R_o + jX_o\right) \quad \forall ph \tag{A2.14}$$

Power conversion relationship of the voltage source inverter:

$$\sum_{ph=a,b,c} \left(V_{o\_ph} \cdot I_{ph} \cdot \cos\left(\varphi_{o\_ph} - \theta_{ph}\right)\right) = V_{dca} \cdot I_{dcb} \tag{A2.15}$$

Power output to the grid:

$$P_{ph} + jQ_{ph} = V_{ph}\angle\delta_{ph} \cdot \left(I_{ph}\angle\theta_{ph}\right)^* \quad \forall ph \tag{A2.16}$$

Reactive power output to the grid:

$$\sum_{ph=a,b.c} Q_{ph} = 0 \tag{A2.17}$$

All above equations from (A2.1) to (A2.17) can be written as (A2.18).

$$0 = F\left[U, \left[V\right]_{abc}, \left[\delta\right]_{abc}, \left[P\right]_{abc}, \left[Q\right]_{abc}\right]. \tag{A2.18}$$

A 3 IEEE 37-Bus Test Distribution System Data

Line Segment Data			
Node A	Node B	Length(ft.)	Configuration
701	702	960	722
702	705	400	724
702	713	360	723
702	703	1320	722
703	727	240	724
703	730	600	723
704	714	80	724
704	720	800	723
705	742	320	724
705	712	240	724
706	725	280	724
707	724	760	724
707	722	120	724
708	733	320	723
708	732	320	724
709	731	600	723
709	708	320	723
710	735	200	724
710	736	1280	724
711	741	400	723

Node A	Node B	Length(ft.)	Configuration
711	740	200	724
713	704	520	723
714	718	520	724
720	707	920	724
720	706	600	723
727	744	280	723
730	709	200	723
733	734	560	723
734	737	640	723
734	710	520	724
737	738	400	723
738	711	400	723
744	728	200	724
744	729	280	724
775	709	0	XFM-1
799	701	1850	721

Regulator Data		
Regulator ID:	1	
Line Segment:	799 -701	
Location:	799	
Phases:	A - B -C	
Connection:	AB - CB	
Monitoring Phase:	AB & CB	
Bandwidth:	2.0 volts	
PT Ratio:	40	
Primary CT Rating:	350	
Compensator Settings:	Ph-AB	Ph-CB
R - Setting:	1.5	1.5
X - Setting:	3	3
Voltage Level:	122	122

Underground Cable Configurations			
Config.	Phasing	Cable	Spacing ID
721	A B C	1,000,000 AA, CN	515
722	A B C	500,000 AA, CN	515
723	A B C	2/0 AA, CN	515
724	A B C	#2 AA, CN	515

Spot Loads							
Node	Load	Ph-1	Ph-1	Ph-2	Ph-2	Ph-3	Ph-4
	Model	kW	kVAr	kW	kVAr	kW	kVAr
701	D-PQ	140	70	140	70	350	175
712	D-PQ	0	0	0	0	85	40
713	D-PQ	0	0	0	0	85	40
714	D-I	17	8	21	10	0	0
718	D-Z	85	40	0	0	0	0
720	D-PQ	0	0	0	0	85	40
722	D-I	0	0	140	70	21	10
724	D-Z	0	0	42	21	0	0
725	D-PQ	0	0	42	21	0	0
727	D-PQ	0	0	0	0	42	21
728	D-PQ	42	21	42	21	42	21
729	D-I	42	21	0	0	0	0
730	D-Z	0	0	0	0	85	40
731	D-Z	0	0	85	40	0	0
732	D-PQ	0	0	0	0	42	21
733	D-I	85	40	0	0	0	0
734	D-PQ	0	0	0	0	42	21
735	D-PQ	0	0	0	0	85	40
736	D-Z	0	0	42	21	0	0
737	D-I	140	70	0	0	0	0
738	D-PQ	126	62	0	0	0	0

Node	Load	Ph-1	Ph-1	Ph-2	Ph-2	Ph-3	Ph-4
	Model	kW	kVAr	kW	kVAr	kW	kVAr
740	D-PQ	0	0	0	0	85	40
741	D-I	0	0	0	0	42	21
742	D-Z	8	4	85	40	0	0
744	D-PQ	42	21	0	0	0	0
Total		727	357	639	314	1091	530

A 4 Distributions System Network Component Model

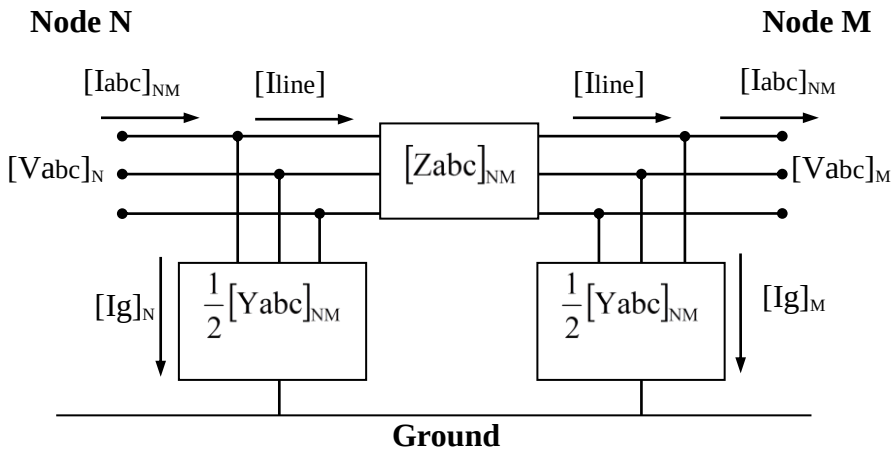

Fig. A4.1. Three-Phase network Component Model

$$[a]_{NM} = [UN] + \frac{1}{2} \cdot [Zabc]_{NM} \cdot [Yabc]_{NM}, \tag{A4.1}$$

$$[b]_{NM} = [Zabc]_{NM}, \tag{A4.2}$$

$$[c]_{NM} = [Yabc]_{NM} + \frac{1}{4} \cdot [Yabc]_{NM} \cdot [Zabc]_{NM} \cdot [Yabc]_{NM}, \tag{A4.3}$$

$$[d]_{NM} = [UN] + \frac{1}{2} \cdot [Yabc]_{NM} \cdot [Zabc]_{NM}, \tag{A4.4}$$

$$[A]_{NM} = [a]_{NM}^{-1}, \tag{A4.5}$$

$$[B]_{NM} = [a]_{NM}^{-1} \cdot [b], \tag{A4.6}$$

$$\begin{bmatrix} [\mathrm{Vabc}]_{N} \\ [\mathrm{Iabc}]_{NM} \end{bmatrix} = \begin{bmatrix} [\mathrm{a}]_{NM} & [\mathrm{b}]_{NM} \\ [\mathrm{c}]_{NM} & [\mathrm{d}]_{NM} \end{bmatrix} \begin{bmatrix} [\mathrm{Vabc}]_{M} \\ [\mathrm{Iabc}]_{MN} \end{bmatrix}, \tag{A4.7}$$

$$[\mathrm{Vabc}]_{M} = [\mathrm{A}] \cdot [\mathrm{Vabc}]_{N} - [\mathrm{B}] \cdot [\mathrm{Iabc}]_{MN}, \tag{A4.8}$$

$$[\mathrm{Zabc}]_{NM} = \begin{bmatrix} z_{11} & z_{12} & z_{13} \\ z_{21} & z_{22} & z_{23} \\ z_{31} & z_{32} & z_{33} \end{bmatrix}, \tag{A4.9}$$

$$[\mathrm{Yabc}]_{NM} = \begin{bmatrix} y_{11} & y_{12} & y_{13} \\ y_{21} & y_{22} & y_{23} \\ y_{31} & y_{32} & y_{33} \end{bmatrix}, \tag{A4.10}$$

A 5 IEEE 70-Bus Distribution System Data

Slack Bus Voltage	Voltage Max	Voltage Min
1.00	1.10	0.90

Bus No.	QG Max	QG Min
70	1000	-1000

Bus No.	PD	QD
1	0	0
2	0	0
3	0	0
4	0	0
5	0	0
6	0.0026	0.0022
7	0.0404	0.03
8	0.075	0.054
9	0.03	0.022
10	0.028	0.019
11	0.145	0.104
12	0.145	0.104
13	0.008	0.005
14	0.008	0.0055
15	-0.5	0

Bus No.	PD	QD
16	0.5455	0.03
17	0.06	0.035
18	0.06	0.035
19	0	0
20	0.001	0.0006
21	0.114	0.081
22	0.0053	0.0035
23	0	0
24	0.028	0.02
25	-0.5	0
26	0.514	0.01
27	0.014	0.01
28	0.026	0.0186
29	0.026	0.0186
30	0	0
31	-0.5	0
32	0.5	0
33	0.014	0.01
34	0.0195	0.014
35	0.006	0.004
36	0.026	0.01855
37	0.026	0.01855

Bus No.	PD	QD
38	0	0
39	0.024	0.017
40	0.024	0.017
41	0.0012	0.001
42	-0.5	0
43	0.506	0.0043
44	0	0
45	0.03922	0.0263
46	0.03922	0.0263
47	0	0
48	0.079	0.0564
49	0.3847	0.2745
50	0.3847	0.2745
51	0.0405	0.0283
52	0.0036	0.0027
53	0.00435	0.0035
54	0.0264	0.019
55	0.024	0.0172
56	0	0
57	0	0
58	0	0
59	0.1	0.072

Bus No.	PD	QD
60	0	0
61	1.244	0.888
62	0.032	0.023
63	-0.5	0
64	0.727	0.162
65	0.059	0.042
66	0.018	0.013
67	0.018	0.013
68	0.028	0.02
69	0.028	0.02
70	0	0

From Bus	To Bus	R (ohm)	X (ohm)
1	70	0.0005	0.0012
2	1	0.0005	0.0012
3	2	0	0
4	3	0.0015	0.0036
5	4	0.0251	0.0294
6	5	0.366	0.1864
7	6	0.3811	0.1941
8	7	0.0922	0.047
9	8	0.0493	0.0251

From Bus	To Bus	R (ohm)	X (ohm)
10	9	0.819	0.2707
11	10	0.1872	0.0619
12	11	0.7114	0.2351
13	12	1.03	0.34
14	13	1.044	0.345
15	14	1.058	0.3496
16	15	0.1966	0.065
17	16	0.3744	0.1238
18	17	0.0047	0.0016
19	18	0.3276	0.1083
20	19	0.2106	0.069
21	20	0.3416	0.1129
22	21	0.014	0.0046
23	22	0.1591	0.0526
24	23	0.3463	0.1145
25	24	0.7488	0.2475
26	25	0.3089	0.1021
27	26	0.1732	0.0572
28	2	0.0044	0.0108
29	28	0.064	0.1565
30	29	0.3978	0.1315
31	30	0.0702	0.0232

From Bus	To Bus	R (ohm)	X (ohm)
32	31	0.351	0.116
33	32	0.839	0.2816
34	33	1.708	0.5646
35	34	1.474	0.4873
36	3	0.0044	0.0108
37	36	0.064	0.1565
38	37	0.1053	0.123
39	38	0.0304	0.0355
40	39	0.0018	0.0021
41	40	0.7283	0.8509
42	41	0.31	0.3623
43	42	0.041	0.0478
44	43	0.0092	0.0116
45	44	0.1089	0.1373
46	45	0.0009	0.0012
47	4	0.0034	0.0084
48	47	0.0851	0.2083
49	48	0.2898	0.7091
50	49	0.0822	0.2011
51	8	0.0928	0.0473
52	51	0.3319	0.1114
53	9	0.174	0.0886

From Bus	To Bus	R (ohm)	X (ohm)
54	53	0.203	0.1034
55	54	0.2842	0.1447
56	55	0.2813	0.1433
57	56	1.59	0.5337
58	57	0.7837	0.263
59	58	0.3042	0.1006
60	59	0.3861	0.1172
61	60	0.5075	0.2585
62	61	0.0974	0.0496
63	62	0.145	0.0738
64	63	0.7105	0.3619
65	64	1.041	0.5302
66	11	0.2012	0.0611
67	66	0.0047	0.0014
68	12	0.7394	0.2444
69	68	0.0047	0.0016

References

[1] E. Lantz, R. Wiser, M. Hand, "The Past and Future Cost of Wind Energy," National Renewable Energy Laboratory, Golden, CO, Tech. Rep. NREL/TP-6A20-53510, May 2012.

[2] World Energy Outlook 2010, International Energy Agency, 75739 Paris Cedex 15, France, [Online]. Available: http://www.worldenergyoutlook.org/publications/weo-2010/

[3] B. Venkatesh, A. Dukpa, and L. Chang, "An accurate voltage solution method for radial distribution systems," Canadian Journal of Electrical and Computer Engineering, vol. 34, pp. 69–74, Oct 2009.

[4] W. H. Kersting, *Distribution System Modeling and Analysis*, Boca Raton CRC Press, 2002.

[5] J. -H. Teng, "A Direct Approach for Distribution System Load Flow Solutions," *IEEE Trans. Power Delivery*, vol. 18, no. 3, pp. 882-887, Jul. 2003.

[6] R. Ranjan, B. Venkatesh, A. Chaturvedi, and D. Das, "Power Flow Solution of Three-Phase Unbalanced Radial Distribution Network," *Electric Power Components and Systems*, vol. 32, Apr. 2004, pp. 421-433.

[7] C.S. Cheng and D. Shirmohammadi, "A Three-Phase Power Flow Method for Real-Time Distribution System Analysis," *IEEE Transactions on Power Systems*, vol. 10, 1995, pp. 671-679.

[8] S. Ghosh and D. Das, "Method for Load-Flow Solution of Radial Distribution Networks," *IEE Proceeding, Generation, Transmission and Distribution*, 1999, pp. 641-648.

[9] E. R. Ramos, A. G. Expósito, and G. Á. Cordero, "Quasi-Coupled Three-Phase Radial Load Flow," *IEEE Trans. Power Systems*, vol. 19, no. 2, pp. 776-781, May 2004.

[10] A. Augugliaro, L. Dusonchet, S. Favuzza, M.G. Ippolito, and E.R. Sanseverino, "A New Backward/Forward Method For Solving Radial Distribution Networks with PV Nodes," *Electric Power Systems Research*, vol. 78, Mar. 2008, pp. 330-336.

[11] A.G. Bhutad, S.V. Kulkarni, and S.A. Khaparde, "Three-phase Load Flow Methods For Radial Distribution Networks," *Conference on Convergent Technologies for Asia-Pacific Region*, Allied Publishers Pvt. Ltd, 2003, pp. 781-785.

[12] H.L. Nguyen, "Newton-Raphson Method in Complex Form," *IEEE Transactions on Power Systems*, vol. 12, 1997, pp. 1355-1359.

[13] J. Arrillaga and B.J. Harker, "Fast-Decoupled Three-Phase Load Flow," *Proceedings of the Institution of Electrical Engineers*, 1978, pp. 734-740.

[14] J.J. Allemong, R.J. Benon, and P.W. Selent, "Multiphase Power Flow Solutions Using EMTP and Newtons Method," *IEEE Transactions on Power Systems*, vol. 8, 1993, pp. 1455-1462.

[15] J.-H. Teng and C.-Y. Chang, "A Novel and Fast Three-Phase Load Flow for Unbalanced Radial Distribution Systems," *IEEE Transactions on Power Systems*, vol. 17, Nov. 2002, pp. 1238-1244.

[16] J.B.V. Subrahmanyam, C. Radhakrishna, and K. Pandukumar, "A Simple and Direct Approach for Unbalanced Radial Distribution System three phase Load Flow Solution," *Research Journal of Applied Science, Engineering and Technology*, vol. 2, 2010, pp. 452-459.

[17] J.-H. Teng, "A Network-Topology-based Three-Phase Load Flow for Distribution Systems," *Proceedings of National Science Council Taiwan*, 2000, pp. 259-264.

[18] J. M. Morales, A. J. Conejo, and J. Perez-Ruiz, "Simulating the Impact of Wind Production on Locational Marginal Prices," *IEEE Trans. Power Systems*, Vol. 26, no. 2, pp. 820-828, May 2011.

[19] K. C. Divya, and P. S. N. Rao, "Models for Wind Turbine Generating Systems and Their Application in Load Flow Studies," *Electric Power Systems Research*, vol. 76, no. 9-10, pp. 844-856, Jun. 2006.

[20] S. Khushalani, J. M. Solanki, and N. N. Schulz, "Development of Three-Phase Unbalanced Power Flow Using PV and PQ Models for Distributed Generation and Study of the Impact of DG Models," *IEEE Trans. Power Systems*, vol. 22, no. 3, pp. 1019-1025, Aug. 2007.

[21] A. E. Feijoo, and J. Cidras, "Modeling of Wind Farms in the Load Flow Analysis," *IEEE Trans. Power System*, vol. 15, no. 1, pp.110-115, Feb. 2000.

[22] A. Fejioo, "On PQ Models for Asynchronous Wind Turbines," *IEEE Trans. Power System*, vol. 24, no. 4, pp. 1890-1891, Nov. 2009.

[23] U. Eminoglu, "Modeling and application of wind turbine generating system (wind generators) to distribution systems," *Renewable Energy*, Vol. 34. no. 11, pp. 2474–2483, Mar. 2009.

[24] J. F. M. Padron, and A. E. F. Lorenzo, "Calculating Steady-State Operating Conditions for Doubly-Fed Induction Generator Wind Turbines," *IEEE Trans. on Power Systems*, vol. 25, no. 2, pp. 922-928, May. 2010.

[25] R. Jayashri, and R. P. K. Devi, "Steady State Analysis of Wind Turbine Generators Interconnected to the Grid," in *Proc. 2006 IEEE Power Engineering Society Power Systems Conf. and Exposition*, pp. 1273-1279.

[26] G. Ofner, O. Koenig, G. Dannerer, and R. Seebacher, “Steady State Modeling of Doubly Fed Induction Generators for Mega Watt Class Wind Turbines,” *in Proc. 2010 XIX International Electrical Machines Conf.*, pp. 1-6.

[27] J. G. Slootweg, H. Polinder, and W. L. Kling, “Representing Wind Turbine Electrical Generating Systems in Fundamental Frequency Simulations,” *IEEE Trans. Energy Conversion and Delivery*, vol. 18, no. 4, pp. 516-524, Dec. 2003.

[28] Babypriya, and R. Anita, “Modeling, Simulation and Analysis of Doubly Fed Induction Generator for Wind Turbines,” *Journal of Electrical Engineering*, vol. 60, no. 2, pp. 79-85, 2009.

[29] Z. Chen, and E. Spooner, “ Grid Interface Options for Variable-Speed Permanent Magnet Generators,” in *Proc. 1998 IEE Electric Power Applications Conf.*, pp. 273-283.

[30] A. Dadhania, "Modeling of Doubly Fed Induction Generators for Distribution System Load Flow Analysis," MAS. Degree Thesis, Dept. Elec. and Comp. Eng., Univ. Ryerson, Toronto, ON, Canada, 2010.

[31] I. S. Wander, "Modeling of Synchronous Generator and Full-Scale Converter for Distribution System Load Flow Analysis," MAS. Degree Thesis, Dept. Elec. and Comp. Eng., Univ. Ryerson, Toronto, Canada, 2011.

[32] S. Li, D. C. Wunsch, E. A. O’Hair, and M. G. Giesselmann, “Using Neural Networks to Estimate Wind Turbine Power Generation,” *IEEE Trans. on Power Systems*, vol. 16, no. 6, pp. 276-282, May. 2001.

[33] K. L. Priddy, and P. E. Keller, *Artificial Neural Networks an Introduction*, Bellingham, Washington USA: SPIE—The International Society for Optical Engineering, *2005. pp. 110-116.*

[34] R. R. Booth, "Power System Simulation Methods Based on Probability Ana1ysis,"*lEEE Trans. Power Apparatus and Systems*, vol. PAS-91, no. 1, pp. 62-69, Jan. 1972.

[35] B. Borkowska, "Probabilistic load flow," *IEEE Trans. Power Apparatus and Systems*, vol. PAS-93, no. 3, pp. 752-759, May. 1974.

[36] G. K. Stefopoulos, A. P. Meliopoulos and G. J. Cokkides, "Probabilistic Power Flow with Non-Conforming Electric Loads," in *Proc. 2004 8th International Conf. on Probabilistic Methods Applied to Power Systems*, pp. 525-531

[37] S. Conti, S. Raiti, "Probabilistic Load Flow for Distribution Systems with Photovoltaic Generators, Part I Theoretical Concepts and Models," in *Proc. ICCEP 2007. International Conf. Clean Electrical Power*, pp. 132-136.

[38] Z. Bie, G. Li, H. Liu, X. Wang and X. Wang, "Studies on Voltage Fluctuation in the Integration of Wind Power Plants Using Probabilistic Load Flow," in *Proc. 2008 IEEE Power and Energy Society General Meeting - Conversion and Delivery of Electrical Energy in the 21st Century*, pp. 1-7. "Probabilistic Load Flow Including Wind Power Generators,"

[39] D. Villanueva, J. L. Pazos and A. Feijóo, "Probabilistic Load Flow Including Wind Power Generators," *IEEE Trans. Power System*, vol. 26, no. 3, pp. 1659-1667

[40] García-González, R. M. Ruiz de la Muela, L. M. Santos, and A. M. González, "Stochastic joint optimization of wind generation and pumped-storage units in an electricity market," *IEEE Trans. Power Syst.*, vol. 23. no. 3, pp. 460-468, May 2008.

[41] A. Dukpa, I. Duggal, B. Venkatesh, and L. Chang, "Optimal participation and risk mitigation of wind generators in an electricity market," *IET Renewable Power Gen.*, vol. 4. no. 2, pp. 165-175, 2010.

[42] U. Focken, M. Lange, K. Monnich, H. Waldl, H. G. Beyer, and A. Luig, "Short-term prediction of the aggregated power output of wind farms-a statistical analysis of the reduction of the prediction error by spatial smoothing effects," *Journal of Wind Engineering and Industrial Aerodynamics*, vol. 90. no. 3, pp. 231-246, Mar. 2002.

[43] P. L, H. Banakar, P. K. Keung, H. G. Far, and B. T. Ooi, "Macromodel of spatial smoothing in wind farms," *IEEE Trans. Energy Convers*, vol. 22, no. 1, pp. 119- 128, Mar. 2007.

[44] Y. Hun, and L. Chang, "A study of the reduction of the regional aggregated wind power forecast error by spatial smoothing effects in the maritime Canada." in *Proc. 2010 IEEE Electric Power and Energy Conf.*, pp. 1-6.

[45] M. Amelin, "Comparison of Capacity Credit Calculation Methods for Conventional Power Plants and Wind Power," *IEEE Trans. Power Syst.*, vol. 24. no. 2, pp. 685-691, May 2009.

[46] L. Gilotte, "Wind Capacity Credit: Accounting for Years of Extreme Risk," in *Proc. 2011 IEEE Trondheim PowerTech Conf.*, pp. 1-4.

[47] E. Baeyens, E.Y. Bitar, P. P. Khargonekar, K. Poolla, "Wind Energy Aggregation: A Coalitional Game Approach," in *Proc. 2011 50th IEEE Conference on Decision and Control and European Control Conf. (CDC-ECC)*, pp. 3000-3007.

[48] J. C. Smith, E. A. DeMeo, B. Parsons and M.R. Milligan, "Wind Power impacts on Electric Power System Operating Costs: Summary and Perspective on Work to Date," Presented at American Wind Energy Association Global Windpower Conf. Chicago, Illinois, 2004.

[49] International Energy Agency. Variability of Wind Power and Other Renewables Management Options and Strategies, Utility Wind Integration Group. [Online]. Available: http://www.uwig.org/ IEA_Report_on_variability.pdf

[50] A. J. Duque, E. D. Castronuovo, I. Sánchez, and J. Usaola, "Optimal operation of a pumped-storage hydro plant that compensates the imbalances of a wind power producer," *Electric Power Systems Research*, vol. 81. no. 9, pp. 1767– 1777, Sep. 2011.

[51] A. K. Varkani, A. Daraeepour, and H. Monsef, "A new self-scheduling strategy for integrated operation of wind and pumped-storage power plants in power markets," *Applied Energy*, vol. 88. no. 12, pp. 5002-5012, Dec. 2011.

[52] S. Papaefthimiou, E. Karamanou, S. Papathanassiou, and M. Papadopoulos, "Operating policies for wind-pumped storage hybrid power stations in island grids," *IET Renewable. Power Gene.*, vol. 3. no. 3, pp. 293-307, Sep. 2009.

[53] S. V. Papaefthymiou, E. G. Karamanou, S. A. Papathanassiou, and M. P. Papadopoulos, "A Wind-Hydro-Pumped Storage Station Leading to High RES Penetration in the Autonomous Island System of Ikaria," *IEEE Trans. Sustainable Energy*, vol. 1. no. 3, pp. 163-172, Oct. 2010.

[54] E. D. Castronuovo, and J. A. Peças Lopes, "On the Optimization of the Daily Operation of a Wind-Hydro Power Plant," *IEEE Trans. Power Syst.*, vol.19, no. 3, pp. 1599-1606, Aug. 2004.

[55] Ontario's Long-Term Energy Plan. Ministry of Energy Ontario, Toronto, ON. [Online]. Available: http://www.energy.gov.on.ca/ en/ltep/

[56] IEEE Power Engineering Society, "Distribution Test feeders", -37 bus feeder, http://ewh.ieee.org/soc/pes/dsacom/testfeeders/index.html

[57] P. Chen, Z. Chen, B. Bak-Jensen, R. Villafáfila and S. Sörensen, "Study of power fluctuation from dispersed generations and loads and its impact on a distribution network through a probabilistic approach," 9th International Conference on Electrical Power Quality and Utilisation, Barcelona, pp. 1 - 5, Oct. 2007.

[58] I. C. da Silva, and et al. “A heuristic constructive algorithm for capacitor placement on distribution systems,” IEEE Transactions on Power Systems, vol. 23, pp. 1619 - 1626, Oct 2008.

[59] B. G. Kumaraswamy, B. K. Keshavan, and S. H Jangamshetti, “A statistical analysis of wind speed data in west central part of Karnataka based on Weibull distribution function,” *Proc. 2009 IEEE Electrical Power & Energy Conference (EPEC),* , pp. 1 - 4, Oct 2009.

[60] Feed-in Tariff Program. (Jul. 2011). FIT rules Version 1.5.1. Ontario Power Authority, ON. [Online]. Available: http://fit.powerauthority.on.ca/sites/default/files/FIT%20Rules%20Version%201%205%201_Program%20Review.pdf.

[61] Independent Electricity System Operator. (2012. Apr.). Hourly wind generator output and hourly nodal price for the 10 zones, IESO, Toronto, ON. [Online]. Available: http://www.ieso.ca/imoweb/marketdata/marketdata.asp

[62] Wind Power Standing Committee. (2012. May). Modeling of Wind Energy, Wind Power Standing Committee, Independent Electricity System Operator, Toronto, ON. [Online]. Available: http://www.ieso.ca/imoweb/pubs/consult/windpower/wpsc-20090616-Modeling.pdf

Glossary of Acronyms and Symbols

A	Area swept by the turbine
AAE	Average absolute error
[a][b][c][d][A][B]	Parameter matrices of a distribution system network component
AGC	Automatic governor control
$ALMP_m$	Average Locational Marginal Price at bus of a wind farm
ANN	Artificial Neural Network
ARMSE	Average root mean square error
β	Blade pitch angle
β_N	Scale parameter of Weibull distribution of wind speed forecast at bus N
$BF_{s,d,t}$	Cooperative bid price for firm power
$BV_{s,d,t,}$	Cooperative variable power bid price
C1....C6	Constants
CA	Total administration cost of the cooperative
Cp	The power coefficient
$CS_{m,s,d,t}$	Share of storage cost component of a wind farm
$CSR_{s,d,t}$	Cost of reserve storage capacity
$CSS_{s,d,t}$	Cost of energy storage
$CST_{s,d,t}$	Total Cost of storage
$CT_{m,s,d,t}$	Transmission related cost share of a wind farm
D	Duty of the boost converter of PMSG
δa, δb, δc or [δ]abc	Angles of three-phase voltage at PCC

DFIG	Doubly-Fed Induction Generator
e	Index to specify epochs
$\overline{E}_0$, $\overline{E}_1$, $\overline{E}_2$	Induced emf phasors at different symmetrical component networks
E_{ph}	Per phase induced electromotive force of the PMSG
ε	Index to denote the symmetrical component network
Er	Derivative of the error power
$E_{t\,(\psi,\Psi)}$	Event relevant to PDF sections m and n and period t of the LDC
η	Leaning rate
f(.)	Sigmoid activation function
FCCG	Full Converter Connected Generator
FΛ(.)	Set of voltage square equations
FP(.)	Set of real power balance equations
FQ(.)	Set of reactive power balance equations
FS(.)	Set of equations for all state variables
γ	Shape parameter of Weibull distribution of wind speed forecast at bus N
HOEP	Hourly Ontario Energy Price
[Iabc]	Three-phase current injection at a distribution system node
I_{dcb}	Output current of the boost converter of PMSG
I_{dcr}	Output dc current of the rectifier of PMSG
IEEE	Institute of Electrical and Electronics Engineers
[Ig]	Three-phase ground current at a distribution system node
i,j	Index to specify the neurons

I_{ph}	Magnitude of the current supplied by the PMSG to the grid
$\bar{I}_{r0}$, $\bar{I}_{r1}$, $\bar{I}_{r2}$	Rotor winding current phasors at different symmetrical component networks
$\bar{I}_{s0}$, $\bar{I}_{s1}$, $\bar{I}_{s2}$	Stator winding current phasors at different symmetrical component networks
I_{s_ph}	Magnitude of generator stator current of PMSG
IT	Index for distribution system power flow iteration
k	Index to specify the layer
Kg	Gear box coefficient
KSM	Smoothing factor used while computing aggregate WGC standard deviation
KWP_h	Water flow rate to power conversion factor (both pumping and generation)
KWR_h	Constant relating variance to Water Reserve Requirement
$\Lambda_{t\,(\psi,\varphi)}$	Represent a vector of voltage squares of all buses (except slack bus) relevant to the even $E_{t\,(m,n)}$
λ	Tip speed ratio
LDC	Load duration curve
LF_t	Load factor at period t
LIT	Ladder Iterative Technique
$LMP_{m,h}$	Locational Marginal Price at bus of a wind farm
m_a	Inverter pulse width modulation index of PMSG
MAE	Maximum absolute error
m, h	wind farm index, hydro storage company index

MVA	Mega Volt Amperes
MW	Mega Watt
MWh	Mega Watt Hour
n	ANN training cycle count
ND	Number of sections of PDF of load
Ne	Number of epochs
nH	Number of hydro storage companies contracted by the WGC
NG	Number of generator buses of the phase equivalent distribution system
NLB	Number of load buses of single phase equivalent distribution system
N,M	Indices for distribution system nodes
nM	Number of wind farms in the WGC
Nout	Number of output neurons in the output layer
ns	Net-stimulus
nS, nDs, nT	Number of seasons, days in season s, hours in a day
NT	Number of coil turns
NW	Number of sections of PDF of wind speed
ωr	Rotor angular speed
ωt	Turbine angular speed
Pa, Pb, Pc or [P]abc	Three-phase wind generator real power output
[Pabc]	Three-phase real power injection at a distribution system node
PCC	Point of common coupling
PCF_s	Cooperative firm power capacity

$PCV_{s,d,t}$	Cooperative bid power
PDF	Probability distribution function
PD_N	Real power demand at bus N of single phase equivalent distribution system
$P\hat{D}_N$	Mean value of load at bus N of single phase equivalent distribution system
$PD_{N\psi}$	Average power demand of PDF section m of load at bus N of single phase equivalent distribution system
$pd_{N\psi}$, pd_{ψ}	Probability of section m of load PDF at bus N
PF	Power factor
[P]gabc	Real power supply form grid side converter to PCC
PG_N	Wind power generation for wind speed U_N at bus N of single phase equivalent distribution system
ph	Index to denote phases of the three-phase system
ϕ	Magnetic flux
φ_{o_ph}	Phase angle of per phase output voltage of the inverter of PMSG
φ_{t_ph}	Phase angle of per phase terminal voltage of the PMSG
PL0, PL1, PL2	Stator and rotor copper losses in sequence networks
$PLoad_{s,d,t}$	Specified maximum percentage of system load
Pm	Rotor mechanical power
PMSG	Permanent Magnet Synchronous Generator
$P_{N\,t\,(\psi,\varphi)}$	Represent a vector of real power injections of all buses (except slack bus) relevant to the even $E_{t\,(\psi,\varphi)}$
Pr0, Pr1, Pr2	Rotor power at different symmetrical component networks

Ps0, Ps1, Ps2	Stator power at different symmetrical component networks
[P]sabc	Real power supply from stator to PCC
pv	Estimated probability of the voltage solution
ψ,ϥ,ϑ	Indices for PDF of sections
$PS_{s,d,t}$	Storage power for water up/down
PSS®E	Power System Simulator for Engineers software
PSS®SINCAL	PSS®SINCAL software
pu	Per unit
PV	Photo Voltaic
PWC_m	Maximum Power capacity of a wind farm
$PW_{m,s,d,t}$	Power output of a wind farm
$Pw_{N\varphi}$,pw_{φ}	Probability of section n of wind speed PDF at bus N
$PWT_{s,d,t}$	Total output power of all wind farms
[Qabc]	Three-phase reactive power injection at a distribution system node
Qa, Qb, Qc or [Q]abc	Three-phase wind generator reactive power output
[Q]gabc	Reactive power supply form grid side converter to PCC
$Q_{N\ t\ (\psi,\varphi)}$	Represent a vector reactive power injections of all buses (except slack bus) relevant to the even $E_{t\ (\psi,\varphi)}$
[Q]sabc	Reactive power supply from stator to PCC
ρ	Density of air
$\rho_N(PD_N)$	Probability density of normal distribution of load PD_N
$\rho_N(U_N)$	Probability density of Weibull distribution of wind speed forecast at bus N
$RVCF_s$	Revenue from market for the WGC through sale of firm power

$RVCV_{s,d,t}$	Revenue from market for the WGC through sale of variable power
$RVGF_{m,s}$	Fixed revenue component of a wind farm
$RVGV_{m,s,d,t}$	Variable revenue component of a wind farm
Rt	Radius of the turbine
rT_m	Transmission system cost rate for a wind farm
$RT_{m,s,d,t}$	Total revenue of a wind farm
rWC_h	Rental for reserving one unit of empty storage capacity
rWS_h	Rental for storing one unit of water for one hour
$\sigma_{m,s,d,t}$	Standard deviation of the output power of a wind farm
σ_N	Standard deviations of load of single phase equivalent distribution system
σ_{PN}	Standard deviations of real power injection of bus N
σ_{QN}	Standard deviations of bus reactive power injection of bus N
σ_{VN}	Standard deviations of voltage solution of bus N
$\sigma_{WGC,s}$	Standard deviation of the aggregate output power of the WGC
slip	Machine slip
$slip_0$, $slip_1$, $slip_2$ or $[slip]_{012}$	Converted symmetrical component slip
SPD_{ψ}	Set of average demands of all buses for the PDF section ψ
$SPG_{\text{Ч}}$	Set of average wind generation for all buses for the PDF section Ч
S_t	Set of state variables
T	Output layer of the Neural Network
TD	Time period of the LDC block
t, d, s	Hour of the day, day of the season, season of the year

θ_{ph}	Phase angle of the current supplied by the PMSG to the grid
θ_{s_ph}	Phase angle of generator stator current of PMSG
U	Wind speed
U_N	Wind speed (m/s) at bus N
$\hat{U}_N$	Mean wind speed at bus N
U_{Nq}	Average wind speed of PDF section n at bus N
Va,Vb,Vc or [V]abc	Magnitudes of three-phase voltage at PCC
[Vabc]	Three-phase distribution system voltage at a node
[VDabc]	Three-phase voltage update vector in distribution system power flow studies
$[V\angle\delta]_{abc}$	Three-phase voltage at PCC
V_{dca}	Final voltage of the boost converter, input voltage to the inverter of PMSG
V_{dcb}	Output voltage of the boost converter of PMSG
V_{dci}	Final voltage of the rectifier, input voltage to the boost converter of PMSG
V_{dcr}	Output dc voltage of the rectifier of PMSG
$V_{N\ t}$	Set of NDxNW voltage values of bus N relevant to the LDC period t
V_{o_ph}	Magnitude of per phase output voltage of the inverter of PMSG
$\overline{V}_{r0}$, $\overline{V}_{r1}$, $\overline{V}_{r2}$	Rotor voltage phasors at different symmetrical component networks
$\overline{V}_{s0}$, $\overline{V}_{s1,}$ $\overline{V}_{s2}$	Stator voltage phasors at different symmetrical component networks

V_{t_ph}	Magnitude of per phase terminal voltage of the PMSG
w	Weights of links
wd	Width of PDF section
WFA_s	Average other water inflow (considering river flow, evaporation and seepage)
$WF_{max,h}$	Maximum water inflow rate limit
$WF_{min,h}$	Maximum water outflow rate limit
$WF_{s,d,t,h}$	Water flow out (negative value for flow in)
WGC	Wind Generators Cooperative
WSI_h	Available stored water at the start of Season #1
$WS_{max,h}$	Maximum capacity of storage company
$WS_{s,d,t,h}$	Storage level
$WSR_{s,h}$	Water storage reserve capacity contribution from storage company
X	Non-normalized output of a neuron
x	Normalized output of a neuron
Y	Non-normalized target output of a neuron
y	Normalized target output of a neuron
[Yabc]	Three-phase shunt admittance matrix between distribution system and the ground in one side of the π model
[YBabc]	Three-phase element matrix of a three-phase Ybus matrix
Ybus	Network admittance matrix
[Zabc]	Three-phase series impedance matrix between two nodes of the distribution system
ξ_N	Variance of wind speed UN

Zg	Lumped impedance of gird side converter
Zm	Magnetizing reactance with respect to stator of the machine
Zm0, Zm1,Zm2 or [Z]m012	Symmetrical Component magnetizing reactance with respect to stator of the machine
Zr0, Zr1, Zr2	Symmetrical component rotor winding impedances
Zs	Stator winding impedance
Zs0, Zs1, Zs2	Symmetrical component stator winding impedances